Atomic Energy Control Board
P.O. Box 1046
Ottawa, Canada
K1P 5S9

Commission de contrôle de l'énergie atomique
C P 1046
Ottawa, Canada
K1P 5S9

INFO-0245

THE EFFECT OF CHANGES IN HUMIDITY ON THE SIZE OF SUBMICRON AEROSOLS

by

C.R. Phillips and A. Khan
University of Toronto

A research report prepared for the
Atomic Energy Control Board
Ottawa, Canada

June 1987

Canada

Research report

87-06480/

SUMMARY

The effect of humidity on inhaled aerosols in the respiratory tract is to cause an increase in particle size of up to several times if the aerosol particle is hygroscopic. The size of inhaled natural atmospheric aerosol increases presumably as a result of its partial hygroscopic nature. Growth is very sensitive to relative humidity in the range 95-100% believed to exist in the respiratory tract. Supersaturation in the respiratory system may occur on inhaling very cold air. Growth is believed to occur on insoluble particles, but the process is poorly understood; the wettability of the surface is believed to be important.

The presence of ionizing radiation and air ions (for example, from uranium and radon/thoron) increases the tendency of water vapour to nucleate. The deposition of particles in the lung is enhanced by high charge density (>10 charges/particle). Radon has been reported to play an important role in the formation of sulphate and nitrate particles in the atmosphere. A detailed overview of the effect of humidity on aerosols is presented in the present work.

Results of experimental measurements made on NaCl (hygroscopic) and kerosene combustion (hydrophobic) aerosols under ambient and humid conditions are reported. Aerosol and activity size distributions were determined simultaneously after allowing attachment of radon progeny to aerosols in a radon chamber. Initial aerosol conditions were 20°C and 35% R.H. Final aerosol conditions were maintained at 37°C and 100% R.H. in order to simulate the conditions inside the respiratory tract. Humidification was achieved by passage of the aerosol through a cylinder of porous, wetted material supported on a wire screen. An average growth

factor of 1.9 ± 0.4 (standard deviation) was observed for the NaCl aerosol and 1.3 ± 0.2 (standard deviation) for the kerosene aerosol. For the activity size distribution, however, the NaCl aerosols were observed to grow by an average factor of only 1.2 ± 0.1 (standard deviation) whereas the kerosene aerosols grew by a factor of 1.3 ± 0.2 (standard deviation). The removal of unattached radon progeny and the small aerosol end of the distribution by deposition on the wire screen cylinder appears to be responsible for the smaller activity size growth factor observed for NaCl aerosols. The kerosene aerosol was affected less, because it was smaller and therefore its deposition in the dry wire screen cylinder was almost the same as its deposition in the humid wire screen cylinder.

DISCLAIMER

The Atomic Energy Control Board is not responsible for the accuracy of the statements made or opinions expressed in this publication and neither the Board nor the authors assume liability with respect to any damage or loss incurred as a result of the use made of the information contained in this publication.

RÉSUMÉ

Sous l'effet de l'humidité régnant dans l'arbre respiratoire, les particules d'aérosols inhalées peuvent grossir et atteindre jusqu'à plusieurs fois leur taille initiale si elles sont hygroscopiques. La taille de l'aérosol atmosphérique naturel inhalé augmentera probablement en raison de sa nature partiellement hygroscopique. L'augmentation de la taille des particules dépend fortement de l'humidité relative quand celle-ci est comprise entre 95 et 100%, comme c'est le cas dans l'arbre respiratoire. Quand l'air inhalé est très froid, on peut atteindre un état de sursaturation. On pense que la taille des particules insolubles peut augmenter sous l'effet de l'humidité, mais le phénomène est mal compris, et l'on suppose que la mouillabilité de la surface est un paramètre important.

La présence de rayonnements ionisants et d'ions dans l'air (provenant par exemple de l'uranium, du radon et du thoron) augmente la tendance de la vapeur d'eau à se fixer sur les noyaux de condensation. La déposition des particules dans le poumon est accrue par la charge électrique des particules (> 10 charges/particule). La littérature indique que le radon joue un rôle important dans la formation de particules de sulfates et nitrates dans l'atmosphère. Une revue détaillée de l'effet de l'humidité sur les aérosols est présentée dans ce rapport.

On présente les résultats des expériences sur des aérosols de NaCl (hygroscopiques) et de combustion du kérosène (hydrophobiques) conduites dans l'ambiance du laboratoire et sous haute humidité relative. La granulométrie des aérosols, en dimension et en activité, a été déterminée simultanément après que l'on ait permis aux descendants du radon de se fixer sur l'aérosol

porteur dans l'enceinte à radon. Les aérosols sont formés initialement dans l'air à 20°C, à une humidité relative de 35%. Les conditions finales sont maintenues à 37°C, à une humidité relative de 100%, afin de simuler les conditions régnant dans l'arbre respiratoire.

L'humidification est réalisée en faisant passer les aérosols dans un cylindre fait de matériau poreux et chargé d'eau, supporté par un treillis métallique. La taille des particules de NaCl est multipliée par 1.9 $\pm$ 0.4 (écart-type), tandis que celle des particules de combustion de kérosène est multipliée par 1.3 $\pm$ 0.2 (écart-type). Le diamètre des particules de NaCl porteuses des descendants du radon n'augmente que d'un facteur 1.2 $\pm$ 0.1 (écart-type) tandis que celui des particules de combustion de kérosène porteuses de descendants du radon augmente d'un facteur de 1.3 $\pm$ 0.2 (écart-type). La collection sur les cylindres poreux de la fraction libre des descendants du radon et des fractions les plus fines de l'aérosol radioactif attaché semble être responsable du faible coefficient de grossissement apparent de l'aérosol de NaCl porteur de descendants du radon. L'aérosol de combustion du kérosène est moins affecté par ce phénomène parce qu'il est plus fin, sa déposition étant presque identique dans chaque cylindre poreux.

TABLE OF CONTENTS

		Page No.
	SUMMARY	
1.	INTRODUCTION	1
2.	NATURE OF AIRBORNE AEROSOLS	3
	2.1 Atmospheric Aerosols	3
	2.2 Diesel Particulates	9
3.	DEPOSITION DYNAMICS OF AEROSOLS IN THE RESPIRATORY TRACT	13
4.	THE INTERACTION OF H_2O WITH AEROSOL PARTICLES AND ITS EFFECT ON RESPIRATORY DEPOSITION	23
	4.1 Hygroscopic Particles	23
	4.2 Non-Hygroscopic Particles	26
	4.3 Deposition of Hygroscopic Particles in the Respiratory System	30
5.	SUPERSATURATION	39
	5.1 Adiabatic Expansion	43
	5.2 Mixing of a Hot Gas with a Cool Gas	47
	5.3 Chemical Reactions to Produce Condensable Species	48
6.	TYPES OF NUCLEATION	49
	6.1 Homogeneous Nucleation	49
	6.2 Heteromolecular Nucleation	59
	6.3 Heterogeneous Nucleation	61
7.	ATMOSPHERIC IONS AND NUCLEATION	66
	7.1 Generation and Behaviour of Ions in the Atmosphere	66
	7.2 Nucleation on Ions	78
8.	BEHAVIOUR OF AEROSOLS IN A HUMID ATMOSPHERE	85
	8.1 Summary of Previous Investigations	85
	8.2 Scope of the Present Investigations	86

		Page No.
9.	MEASUREMENT OF GROWTH FACTOR OF AEROSOL AND ACTIVITY SIZE IN A HUMID ATMOSPHERE	89
	9.1 Experimental Technique	89
	9.2 Aerosol Size Distribution Measurement	93
	9.3 Activity Size Distribution Measurement	97
10.	RESULTS AND DISCUSSION	99
	10.1 Results	99
	10.2 Discussion of Results	99
11.	CONCLUSIONS AND RECOMMENDATIONS	117
	11.1 Conclusions	117
	11.2 Recommendations	118
	REFERENCES	120
	APPENDICES	129
	Appendix A: Aerosol Generation Technique	130
	A.1 Collison Atomizer	130
	A.2 Kerosene Heater	130
	Appendix B: Raw Data	133
	B.1 Activity Size Distribution Data	133
	B.2 Aerosol Size Distribution Data	137
	Appendix C: Experimental Protocol	140

1. INTRODUCTION

The health hazards due to the lung deposition of inhaled airborne particles of various chemical forms have been recognized and studied since the early twentieth century (Ba23, Dr28, Br31). The ultimate health effects of inhaled airborne particles have been demonstrated to be mainly dependent upon their physical and chemical properties. These properties include the shape, size and density of the particles, and govern the mechanics of particle deposition in the respiratory tract; the concentration of particles, which has a linear relationship to the dose imparted to the lungs; and the solubility, chemical reactivity, toxicity and radioactivity of the particles. The average residence time of the particles in the lungs is also an important consideration. Charges carried by particles may result in enhanced deposition in the respiratory tract. The high humidity (<95% R.H.) in the respiratory tract can cause hygroscopic particles to grow in size through absorption of moisture. For such particles, the deposition pattern depends upon their sizes after growth.

Knowledge of the mechanism of deposition of airborne particles in the human respiratory tract provides a basis for making predictions of health hazard. Although the deposition mechanism has been extensively studied, many questions still remain unanswered. An important area in which more studies are required concerns the growth of particles after exposure to the high humidity beyond the pharynx, with particular reference to hygroscopic particles (such as NaCl), hydrophobic particles (such as diesel particulates), and other materials or mixtures of particles with intermediate properties. The role of ionizing radiation from atmospheric radon and thoron progeny as a modifying factor on the sizes

or concentrations of particles is also not well understood. An attempt is made here to illustrate both the well-known and the less well-known aspects of deposition of aerosols in the human respiratory tract.

In order to provide a perspective on the phenomenon of growth of particles in the respiratory tract, the properties of atmospheric aerosols, in general, and diesel particulates, in particular, are discussed briefly. The link between mechanisms of deposition and the resulting deposition efficiencies is then examined.

In order to study the growth of hygroscopic and hydrophobic aerosols in a radon atmosphere, experiments were carried out to measure the aerosol and activity size distributions of NaCl and kerosene aerosols in humid conditions. The results of this experimental study are presented. These results are discussed and conclusions and recommendations for further studies are made.

2. NATURE OF AIRBORNE AEROSOLS

Airborne particulate matter can originate from several sources. The nature of aerosols may vary from place to place depending upon proximity to the ocean, industry or highways. Natural phenomena such as volcanic eruptions and forest or bush fires release large concentrations of airborne particles into the atmosphere. Man's activities create a large variety of aerosols of varying physical and chemical nature. Underground mines, especially when diesel-operated, generally contain higher concentrations of particulate matter than the atmosphere. Both atmospheric and diesel particles are discussed as part of an overview of the physico-chemical nature of particulate matter and its health hazard after deposition in the respiratory tract.

2.1 Atmospheric Aerosols

Atmospheric aerosols are typically mixtures of soluble and insoluble particles and may contain crystals, spheres, aggregates and/or irregular shapes. Atmospheric aerosols are generally diverse and complicated mixtures of different types of particles. In addition to blowing soil and pollen, both of which contribute large quantities of particulate matter to the atmosphere, extra-terrestrial dust and particles produced by atmospheric chemical reactions are significant contributors to the atmosphere's particulate burden. Direct transfer of particles to the air, so-called primary emission, arises from both natural sources and man's activities.

The natural sources of particle production are sea-salt spray,

blowing soil, pollen and particles resulting from natural events such as volcanic eruptions, forest fires and the earth's airborne burden of extraterrestrial dust. Man's activities contribute substantially in the form of industrial emissions, combustion products of coal and petroleum, etc.

Primary emissions may be classified as fine solids (<100 μm), coarse solids (>100 μm), organic compounds, carbon compounds, halogen compounds or radioactive compounds. The compositions of aerosols sampled in three American cities are shown in Table 2.1.

Pollutant gases such as sulphur dioxide, nitrogen oxides and certain reactive hydrocarbon vapours may produce substantial particulate matter as a result of gas-to-particle conversion reactions. Gas phase chemical reactions can lead to formation of condensable species. Reactions involving SO_2, NO, NO_2 and certain organic compounds are especially important. Roberts and Friedlander (Ro75) found the rate of conversion of SO_2 to particulate sulphur in the Los Angeles atmosphere to vary over the range 1 to 13% hr^{-1} and suggest that the SO_2 probably reacts with oxidizing agents generated by ozone-olefin reactions.

Photochemical reactions which are initiated by the absorption of a light photon, hν, occur according to the following generalized scheme

$$NO_2 + h\nu \xrightarrow{1} NO + O$$

$$O + O_2 + M \xrightarrow{2} O_3 + M$$

$$O_3 + NO \xrightarrow{3} NO_2 + O_2$$

$$O + HC \xrightarrow{4} \text{stable products} + \text{radicals}$$

$$O_3 + HC \xrightarrow{5} \text{stable products} + \text{radicals}$$

TABLE 2.1

24-Hour Atmospheric Aerosol Source Breakdown (Ga75)

	Pasadena 9/20/72	Pomona 10/24/72	Riverside 9/20/72
Sea salt	0.7 ± 0.06	5.7 ± 0.6	1.3 ± 0.1
Soil dust	19.8 ± 0.1	15.1 ± 0.5	28.5 ± 0.9
Auto exhaust	5.1 ± 0.15	7.2 ± 0.3	3.9 ± 0.15
Cement dust	1.4 ± 0.15	3.3 ± 0.6	2.3 ± 0.15
Flyash	0.1 ± 0.01	0.2 ± 0.01	0.1 ± 0.01
Diesel exhaust[c]	1.4	1.9	0.9
Tire dust[e]	0.5	0.7	0.4
Industrial and agricultural[c]	4.7	6.6	20.5
Aircraft[c]	1.3	1.8	7.4
SO_4^{2-}[b]	2.9 ± 0.7	19 ± 5	5.9 ± 1.5
NO_3^-[b]	4.9 ± 0.4	36.4 ± 2.7	12.9 ± 1.0
NH_4^+[b]	2.3 ± 0.1	16.3 ± 0.8	5.7 ± 0.3
Organics[d]	29.6	29.3	24.8
Water[b]	12 ± 6	18 ± 9	unknown
Total mass (sum of above)	86.7	161.5	114.6
Measured mass	64 ± 7	180 ± 20	125 ± 14

[a] Values in micrograms per cubic meter. Errors associated with sea salt, soil dust, auto exhaust, cement dust, and flyash are standard errors from the least-squares fit for the chemical element balance; errors associated with SO_4^{2-}, NO_3^-, NH_4^+, water and measured total mass concentrations are analytical errors.

[b] Measured values.

[c] Scaled to auto exhaust based on emission inventory.

[d] Based on a carbon balance.

[e] Assumed 10% of auto exhaust component.

$$\text{Radicals + hydrocarbons} \xrightarrow{6} \text{stable products + radicals}$$

$$\text{radicals + NO} \xrightarrow{7} \text{radicals + } NO_2$$

$$\text{radicals + } NO_2 \xrightarrow{8} \text{stable products}$$

Nitrogen oxides, which are produced in combustion processes and emitted in large quantities into the atmosphere, result in the formation of particulate nitrates. The gas phase oxidation of NO to NO_2 and through the hydroxyl radical to nitric acid is a significant mode of particulate nitrate production. Particulate nitrate is usually present as the ammonium salt in polluted atmospheres. Ammonium salts may form from either gas-phase reaction of nitric acid with ammonia or from reactions in the droplet phase.

Gas phase ozone-olefin reactions also result in the production of particulate organics. Cyclic olefins (which are present in gasoline and in automobile exhaust) and α-pinene (which is produced in significant quantities in forests) react to produce a condensable species. This form of aerosol is believed to constitute a major portion of the total global aerosol burden. Modes of induction of nucleation are discussed in detail later in Section 4.

Tables 2.2 and 2.3 list the sulphur- and nitrogen-based gases and organic vapours generally present in the atmosphere.

The particle size distribution of the atmospheric aerosol can be represented by a multi-modal size-distribution corresponding to the variety of sources from which the various modes originate. The sizes range from molecular clusters of 0.001 μm diameter to fog droplets and dust particles as large as 100 μm diameter. In polluted air, the number

TABLE 2.2

Sulphurous and Nitrogenous Gases known to be in the Lower Atmosphere (Hi84)

Constituent		Concentration range (ppb) Urban	Rural	Origin
Sulphur				
Sulphur dioxide	SO_2	5-500	1-50	Fossil fuel combustion
Hydrogen sulphide	H_2S	1-50	0.1-50	Biogenic, geothermal
Carbony sulphide	COS	0.1	0.1	Biogenic
Dimethyl sulphide	$(CH_3)_2S$	0.1	0.1	Biogenic
Carbonl disulphide	CS_2	0.1	0.1	Biogenic
Methyl mercaptan	CH_3SH	-	~0.1	Biogenic
Nitrogen				
Nitrous oxide	N_2O	300	300	Biogenic
Nitric oxide	NO	10-1000	0.1-100	Fossil fuel combustion
Nitrogen dioxide	NO_2	1-500	0.1-100	Fossil fuel combustion atmospheric oxidation
Nitric acid	HNO_3	0.1-20	0.02-0.3	Atmospheric reactions of NO_2
Ammonia	NH_3	1-80	0.1-10	Biogenic, fuel combustion
Peroxyacetyl nitrate (PAN)	CH_3COONO_3	0.1-60	0.1-1	Atmospheric reaction product

TABLE 2.3

Organic Vapours Identified in Ambient Air (Hi84)

Constituent	Concentration range (ppb)		Origin
	Urban	Rural	
Methanes	20,000	1,000	Biogenic, geogenic
Alkanes (ethane, propane, ...)	100	10	Gasoline, fuels, solvents, etc; partially burned hydrocarbon
Alkene (olefins)	100	10	
Cyclic alkanes	1	0.1	Gasoline, fuels
Aromatics (benzene, toluene, ...)	1	0.1	Gasoline, fuels
Polycyclic aromatics (e.g., benzopyrene)	<0.1	<0.01	Combustion of fuel
Terpenes	0.1	0.1	Biogenic
Aldehydes (formaldehyde, ...)	1-10	0.1-1.0	Biogenic; atmospheric reaction products
Other oxygenates (ketones, alcohols, acids)	<0.1-1.0	<0.1(?)	
Alkynes (acetylene)	1-10	0.1-1.0	Partially burned fuel
Cyclic alkenes	0.1	0.01	Gasoline, fuels

distribution of most of the particles falls in the size range between 0.01 and 0.1 μm. The count median diameter of airborne particles to which radon decay products are attached has been found to be ~0.1 μm; unattached radon progeny atoms have a median of ~0.002 μm (Si78). Concentrations of particles range from 100-1000 particles/cm^3 in areas remote from population to ~10^5 particles/cm^3 in polluted urban atmospheres.

2.2 Diesel Particulates

Although the diesel transportation component of the global particulate burden is only 20%, some special problems are associated with diesel particles. Diesel particles are small and long-lived, are emitted near ground level, and are concentrated in high population areas. Due to their small size, diesel particles are respirable. They may carry heavy metals, SO_2, NO_2, various hydrocarbons and/or carcinogenic compounds adsorbed on their surfaces.

Diesel particles generally exist in the form of clusters or chains formed by aggregates of spherical primary particles. The primary spherical particles are basically combustion-generated soot particles which vary in diameter from 0.01 μm to 0.08 μm, with most being in the 0.015 to 0.03 μm range (Am 82). A typical size distribution of the primary diesel particles (spherules) is shown in Fig. 2.1. The physical processes related to diesel particulate emissions are shown in Fig. 2.2. The particles, chains or clusters can vary widely in chemical nature and phase ranging from all liquid to all solid, with mixtures including carbon, hydrocarbons, sulphate, metals and water. A schematic diagram showing

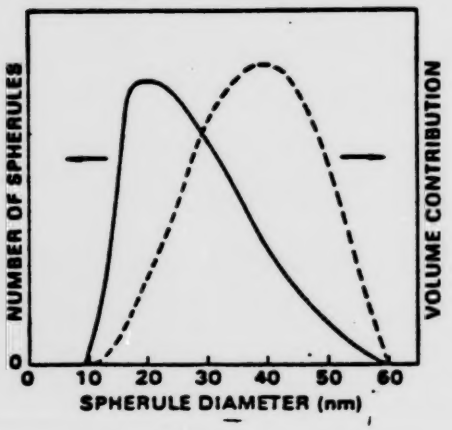

Fig. 2.1. Typical distributions of spherule diameter and volume (Am82).

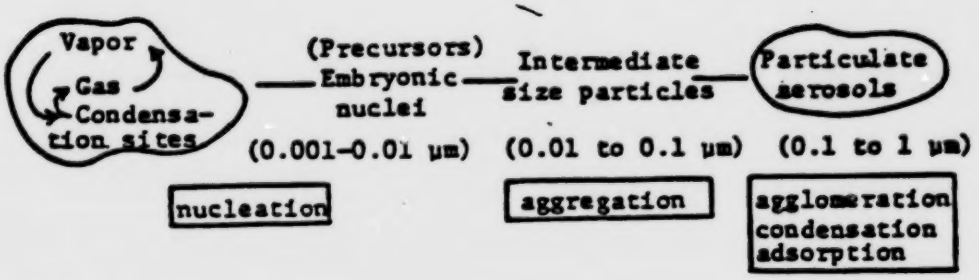

Fig. 2.2. Physical processes related to diesel particulate emissions (Vu76).

Solid/Liquid Particles

Solid Chain Aggregates
(0.01-0.08 m sphere building blocks)

Liquid Sulphate Particles

Liquid Hydrocarbon Particles*

Gaseous Hydrocarbons*

Solid Chain Aggregates with High Molecular Weight Organic Compounds* and/or Inorganic Species such as SO_2, NO_2, H_2SO_4, and sulphates adsorbed on Surface.

* Unburned Hydrocarbons, Oxygenated Hydrocarbons (Ketones, Esters, Organic Acids) and Polynuclear Aromatic Hydrocarbons.

Fig. 2.3. Schematic of basic diesel particles (Vu76).

the nature of the diesel particles is shown in Fig. 2.3. The smallest size spherical diesel particle is about 0.01 μm in diameter. Agglomerates or aggregates of individual spherical diesel particles have been measured and found to follow a lognormal size distribution (Vu76, Ca79). About 90% of the mass of the particulate associated with diesel exhaust is in the form of soot. Soot particles vary in size and hydrocarbon content and may contain trace metals from fuel additives or gases and liquids adsorbed on particle surfaces.

The carbon atoms in a soot particle are arranged in platelets containing hexagonal arrays. The platelets, arranged in typically 2 to 5 layers, form crystallites which are randomly packed to form a soot particle. Soot formation is known to be influenced by fuel additives. Small amounts of SO_2 in the exhaust are oxidized to SO_3 and form sulphuric acid and various metal salts, which appear as particles. NO_x and NH_3 form HNO_3 by several kinetic schemes and can create a variety of nitrate-based particles. Metal oxides are known to be strong catalysts especially in sulphate reactions. These aspects of atmospheric chemistry have been summarized by Fennelly (Fe75). Hydrocarbon vapours form a variety of organic molecules by photochemical means. $HC/NO_x/SO_2$ systems produce sulphuric acid droplets which contain carbonaceous material if heavier hydrocarbons are present. The relative importance of each of the chemical reaction mechanisms mentioned above varies greatly according to local conditions.

3. DEPOSITION DYNAMICS OF AEROSOLS IN THE RESPIRATORY TRACT

Knowledge of deposition dynamics of aerosols in the respiratory tract is necessary in order to understand the role of humidity on aerosol retention in the lung. A detailed discussion of the deposition pattern in different regions of the lung is not included here. However, since a reference to different parts of the respiratory system is required occasionally, a representation of the human respiratory system is shown in Fig. 3.1.

Deposition of particles in the lung is governed both by the nature of the particle and by the anatomy of the lung. Two of the most important characteristics of the particle pertaining to its ultimate health hazard are its size and its chemical and/or radionuclide nature.

The air flow through the respiratory tract can be described by the Reynolds number, Re, in a manner similar to that for airflow through a conduit:

$$Re = \frac{UD}{\nu} \qquad (1)$$

where U is the average flow velocity, D is the airway diameter and ν is the kinematic viscosity of air. For Re <2300, viscous effects dominate the flow and the flow pattern is laminar and orderly. As Re increases, inertial effects become significant, and the flow pattern eventually becomes turbulent with convective mixing of the air in eddies. Since the kinematic viscosity, ν, is a constant for air, the Reynolds number depends only on the airway diameter and the flow velocity. Peak flow rate through the lungs is approximately 500 ml/sec for a resting breathing rate of 15 breaths per minute and a tidal volume of 600 ml. At this flow rate, the Reynolds number in the trachea is about 2000 and

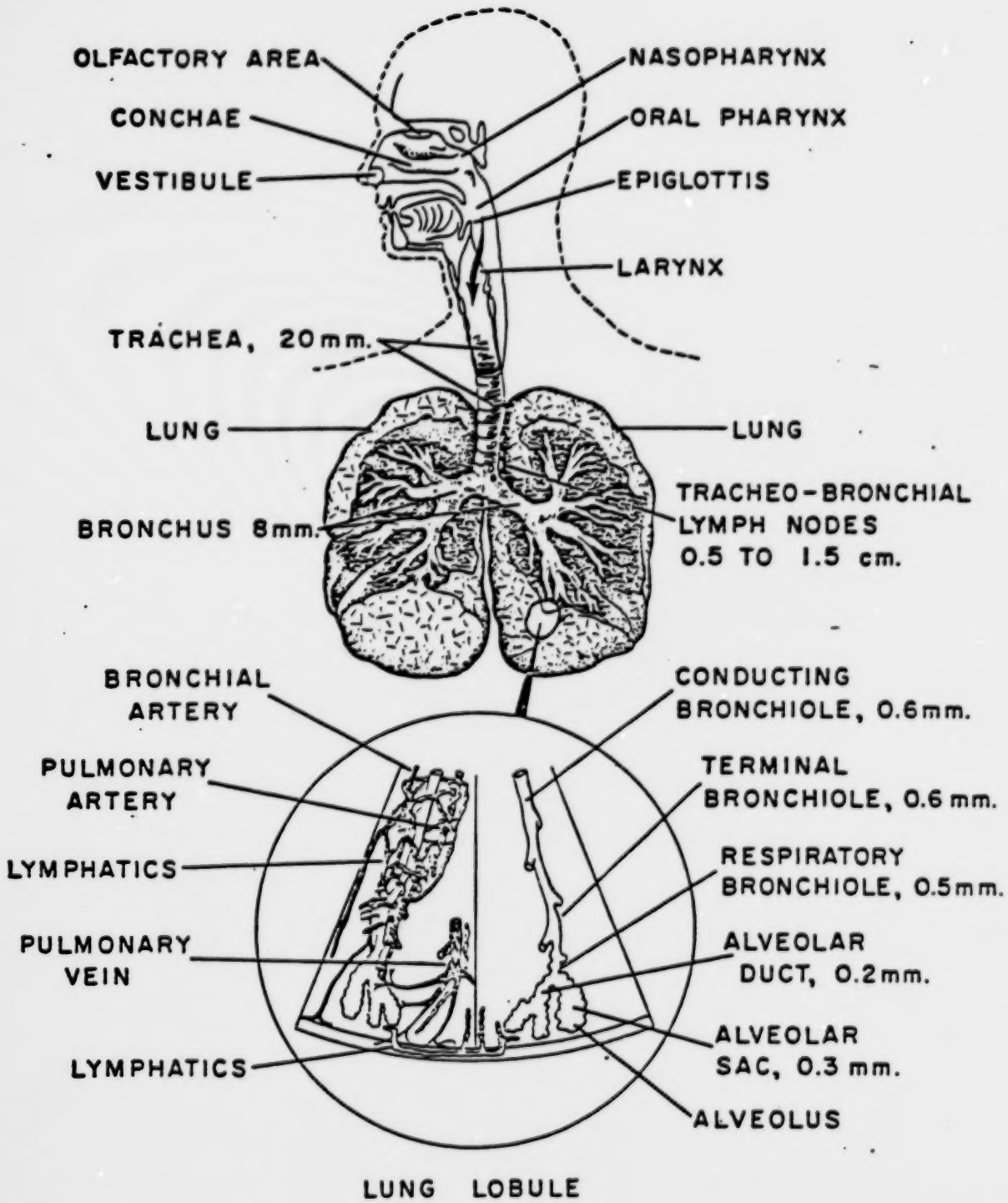

Fig. 3.1. The human respiratory system.

falls below 100 by the eighth generation. In some of the larger airways, the flow is, therefore, turbulent while in the smaller pulmonary airways it is always laminar. However, even in those regions where flow is laminar, the velocity profiles are not parabolic because most of the smaller airways are only three diameters long and the flow normally requires many tube diameters to develop its parabolic profile.

The size of the particle, together with its flow velocity, determines the region where deposition is most likely to occur. For an aerosol particle of diameter d_p smaller than the mean free path, λ, of air molecules (0.065 μm), the force exerted by air on the moving particle is proportional to the product of velocity and d_p. With increasing particle size, the drag force, F_d, or the resistance of air to the relative motion of the particle, increases according to Stoke's Law

$$F_d = 3\pi\eta d_p V \qquad (2)$$

where η is the viscosity of the air and V is the particle-fluid relative velocity.

Although corrections to Stokes Law may be needed for increasing particle size or velocity, for example, when an abrupt change in airflow direction occurs (such as at airway bifurcations), Stokes Law provides a useful guide to particle/air interactions for many practical lung conditions. For particles smaller than the mean free path, the Cunningham correction term (see below) may be needed.

Processes which control deposition efficiency in each region of the respiratory tract have been studied and reviewed in detail by Lipmann (Li77), Lipmann and Altshuller (Li75) and Lipmann et al (Li80, Li83). A brief description of the five mechanisms which play a significant role in particle deposition in the respiratory tract follows.

a) Gravitational Sedimentation:

Sedimentation under the force of gravity is an important mechanism for deposition in the smaller bronchi, the bronchioles and the alveolar spaces where both the air velocity and the airway dimensions are small. Particles larger than about 0.1 μm suspended in a gas settle slowly under the influence of gravity. The drag force F_d on a falling spherical particle is given by Stokes law as:

$$F_d = 3\pi\eta d_p V \tag{3}$$

The gravitational force, F_g, is given by

$$F_g = \frac{\pi d_p^3}{6} (\rho_p - \rho_a)g \tag{4}$$

where ρ_p is the particle density, ρ_a is the air density and g is the gravitational constant.

At the terminal settling velocity, both the drag force and the gravitational force are equal because the particle is no longer accelerating. On equating expressions (3) and (4) and solving for the terminal settling velocity, V_t, the Stokes terminal settling velocity is obtained:

$$V_t = \frac{g d_p^2}{18\eta} (\rho_p - \rho_a) \tag{5}$$

This relationship holds for particles with diameter d_p between 1 and 40 μm. For smaller particles, the Cunningham slip correction factor should be applied to obtain

$$V_t(\text{actual}) = V_t\left(1 + \frac{2A\lambda}{d_p}\right) \tag{6}$$

where λ is the mean free path of air molecules (about 0.065 μm in air under normal conditions) and

$$A = 1.26 + 0.4\, e^{-1.1 d_p/2\lambda} \qquad (7)$$

When the terminal settling velocity of the particles falls below ~ 0.001 cm/s (V_t for a unit density sphere of ~ 0.5 μm), diffusion becomes more important than sedimentation.

b) Inertial Impaction

The momentum of a large particle causes it to resist changes in its direction in its tortuous passage through the nose, mouth and the branching airways of the lung. Some particles, especially those along the centre line of the air stream, collide with the mucous-lined walls. The highest density of deposition due to inertial impaction is at or near the leading edge of the bifurcation.

If a particle is moving with a speed V in the centre of an airway in which the airstream changes direction by an angle θ, the particle experiences a lateral displacement, L, across the streamlines of

$$L = \frac{V_t V \sin \theta}{g} \qquad (8)$$

where V_t is the terminal velocity of the particle. The proportion of particles initially travelling towards an obstacle of diameter D which will actually strike it is a function of the Stokes' number

$$St = \frac{\rho_p d_p^2 V}{18 \eta D} \qquad (9)$$

The tendency for inertial impaction in airways can be computed from its Stokes number (Ch78).

c) Diffusion:

Constant bombardment of airborne particles by surrounding gas molecules imparts a random motion to the particles called Brownian

motion. Brownian motion causes the particles to be displaced from one region of a gas volume to another. This random displacement of particles increases with decreasing particle size and becomes an effective mechanism of deposition in the lung as the root mean square of the displacement approaches the size of the air sacs in the alveoli. The root mean square displacement, δ, after a time interval, t, can be expressed as

$$\delta = \sqrt{6 D_p t} \tag{10}$$

where D_p is the diffusivity of the particle, inversely proportional to its diameter, d_p, but independent of its density. The diffusivity can be expressed as:

$$D_p = \frac{kT}{3 \pi \eta d_p} \tag{11}$$

where k is the Boltzmann constant and T is the absolute temperature. On substituting eqn. (11) into eqn. (10), the root mean square displacement becomes:

$$\delta = \left(\frac{2kTt}{\pi \eta d_p}\right)^{1/2} \tag{12}$$

Equation (12) shows that particle diameter and the residence time in the airways are the only important variables affecting diffusional deposition.

For radon and thoron progeny atoms attached to small particles, diffusional deposition is high in the nasopharynx passage and in large airways such as the trachea. In general, diffusional deposition is important in small airways and alveoli and at airway bifurcations for particles with diameter below 0.5 μm. For particles of ~0.5 μm both diffusion and inertial impaction are minimal resulting in negligible deposi-

tion in the respiratory system. Figure 3.2 demonstrates the shape of the lung deposition efficiency curve for airborne particles.

d) Interception:

When a particle is in such close proximity to a surface that its edge contacts the surface, the particle is said to be intercepted by the surface. Interception is generally due to the particle's shape, orientation or rotation rather than its inertia when the particle trajectory is close to a surface. The interception mechanism is particularly important for fibrous particles having a large length to diameter ratio. Straight fibres have a greater chance of penetrating the alveoli than curved fibres because the former assume a more parallel orientation to flow streamlines.

A schematic representation of the four mechanisms of particle deposition in the lung is given in Fig. 3.3.

e) Deposition of Charged Particles:

The presence of a charge on a particle may affect its deposition efficiency in the respiratory tract because of the image charges induced by the particles on the electro-conductive epithelial tissue of the airway walls. An induced image charge of opposite polarity attracts the particle resulting in its deposition on the airway wall (Fu65). This mechanism has been confirmed experimentally by Chan et al (Ch78a), using models of casts of human airways, and by Melandri et al (Me77), using human subjects. Theoretical analysis of the image-force effect on fine particle deposition in the respiratory system has been carried out by Brock and Marlow (Br 75) who concluded that deposition due to particle charge should not be neglected when the net number of charges of either

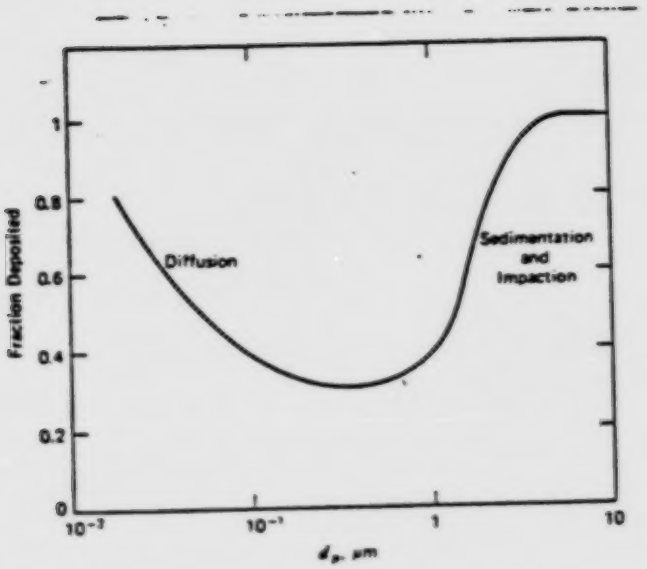

Fig. 3.2. Form of the efficiency curve for particle deposition in the lung. Particles in the size range between 0.1 and 1 μm are too large to diffuse rapidly or deposit because of inertial effects (Fr77).

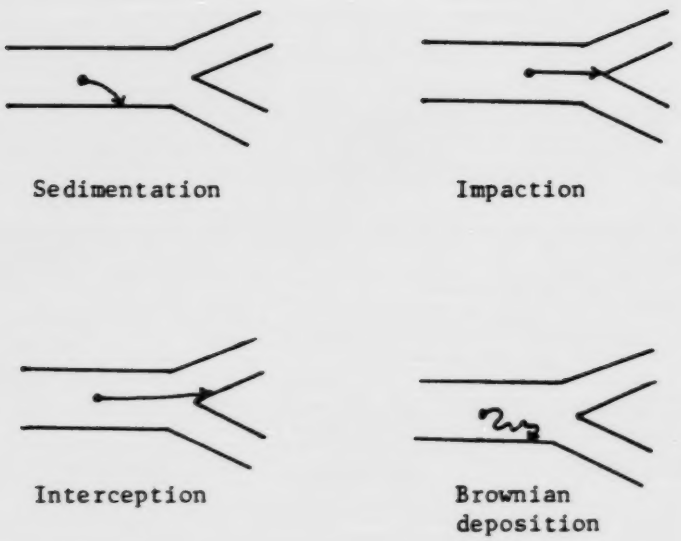

Fig. 3.3. Schematic representation of the four mechanisms for the removal of uncharged inhaled aerosols in the respiratory tract airways.

sign per particle exceeds 10. Chan et al. (Ch78a) found that for particles with mass median aerodynamic diameters of 2-7 μm and for particle charge levels of 360-1100 negative charges per particle, deposition was enhanced in the trachea, especially at (low) steady flow rates of 15 and 30 litres/minute. Chan et al. proposed that at these charge levels deposition be correlated with the parameter

$$\frac{CQ^2}{d_p U}$$

where C is the Cunningham slip correction factor and Q is the charge per particle. Chan et al.'s work verifies that the charge effect may be important for submicron particles.

Melandri et al (Me 77) demonstrated that the effect of unipolar charging of 30-110 elemental charges per particle for 0.3-1.1 μm diameter particles at an inhalation flow rate of 24 L/min was to increase deposition for mouth breathing by 15-30%.

Deposition of hygroscopic particles is another important aspect of lung deposition and is discussed separately in the next section.

4. THE INTERACTION OF H_2O WITH AEROSOL PARTICLES AND ITS EFFECT ON RESPIRATORY DEPOSITION

As a result of uptake of water vapour from the interior of the respiratory airways, a particle which is soluble may grow in size in a fraction of a second to a large equilibrium diameter (Me73). This growth process may be important in respiratory deposition because, after undergoing growth in the mouth and the upper region of the respiratory tract, the particle deposits according to its final diameter (Bl83). Deposition is governed by the mechanism which is dominant in the particular size range. As previously discussed in Section 3, each deposition mechanism is significant in a specific size range and leads to deposition at specific preferred sites. The final size of an inhaled particle is significant in determining the deposition pattern of aerosols in the lung.

4.1. Hygroscopic Particles

Any increase in particle size after exposure to a humid atmosphere depends largely on the solubility of the particle in water. For this reason, most of the studies carried out in this area have been related to hygroscopic particles such as NaCl, present in ocean environments.

Cooper et al (Co73) concluded that at a phase change the volume of a hygroscopic particle increases to approximately $1/(1 - f_{RH})$ times its original volume, where f_{RH} is the fractional relative humidity. Depending upon the particle size (smaller particles of NaCl change phase at lower humidities), Cooper et al's relationship predicts a volume increase of four-fold or less because the majority of the NaCl particles change phase at 75% R.H. Cinkotai (Ci71) theoretically computed the

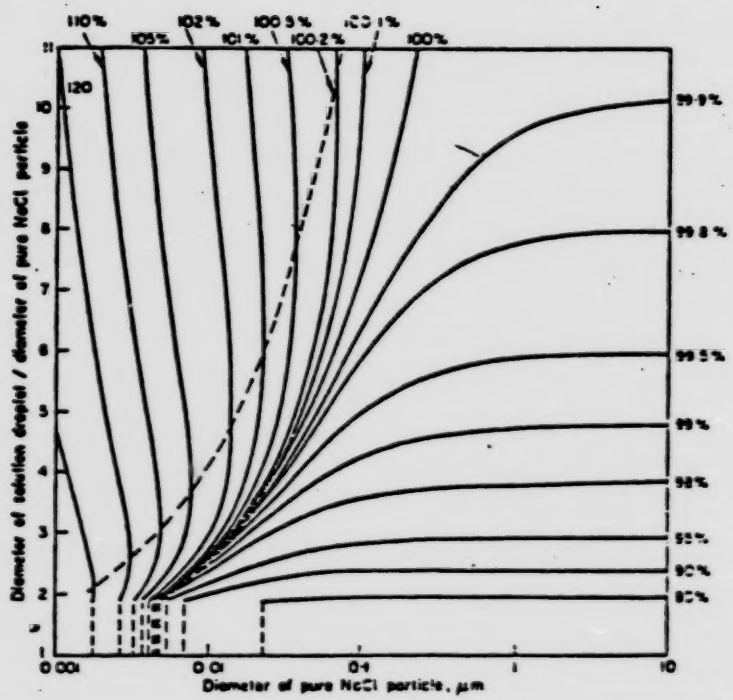

Fig. 4.1. The ratio of the diameter of NaCl solution droplet to the diameter of the NaCl particle from which the droplet has been formed at various levels of relative humidities (Ci71).

ratios of the diameter of an NaCl solution droplet to the diameter of the NaCl particles from which the droplets had grown at various humidities. His work showed that the diameter of a NaCl solution droplet of 0.01 μm diameter grows by a factor of 2.25 at 93% R.H. and much more between 99 and 100% R.H. (36°C temperature).

According to Reist (Re84) the injection of soluble particles into humid air results in the almost immediate generation of stable droplets of a much larger size. Reist found that at 100% R.H. the particle size of NaCl particles of $\sim 10^{-16}$ g mass increased about five-fold and of NaCl particles of $\sim 10^{-13}$ g mass, about 10-fold. The masses refer to the amount of NaCl contained in a droplet. Dautrebande and Walkenhorst (Da61) observed a 6-7 fold increase in NaCl particle diameters at a relative humidity of 99.8%. Later, Dautrebande and Walkenhorst (Da64) concluded that NaCl particles, which exist in air as fine crystals below 76% relative humidity, become droplets above 90% R.H. Above 95% R.H. the increase in the volume of NaCl droplets was found to be particularly marked. According to calculations by Zebel (Ze56), NaCl particles of radius 0.1 μm grow by a factor of 5 at 99.9% R.H. and by a factor of 7 at 99.8% R.H. In the range of relative humidity 99-100%, the growth of NaCl particles seems to be extremely sensitive to slight changes in humidity, a result confirmed theoretically by Cinkotai (Ci71), as shown in Fig. 4.1.

Figure 4.1 also demonstrates that the uptake of water by pure NaCl particles begins only above a certain threshold value of relative humidity. This threshold is reached when the vapour pressure of water over a droplet saturated with NaCl just equals the ambient vapour pressure that

corresponds to the relative humidity. Cinkotai (Ci71) developed the following equation to calculate the threshold value of relative humidity, $R.H._t$, for a given NaCl particle:

$$R.H._t = 76\, e^{1.19 \times 10^{-7}/D_o} \qquad (13)$$

where D_o is the particle diameter.

Porstendörfer (Po71) reported an experimentally obtained growth factor of 3 for NaCl particles of 0.06 μm at 100% R.H. (20-22°C), in contrast to a factor in the range 5-7 at close to 100% R.H., as reported by other workers (Ze56, Da61). Ferron (Fe77) lists the various parameters which may affect the water vapour concentration at the particle surface as being the temperature, the equivalent diameter (diameter of a sphere of equal volume), and the solute concentration. The discrepancies in the growth factor at 100% R.H. reported by various workers may be due to the fact that not all of the above parameters were identical in the reported investigations. Ferron (Fe77) performed detailed calculations on the growth of soluble aerosol particles as a function of humidity for 12 salts. His results are outlined in Table 4.1.

Bell and Ho (Be81) obtained experimental data on the growth rate of NaCl and found a growth factor of 3-4.5 at 95% R.H. (36-38°C). Bell and Ho reported that the rate of growth of particles, among other factors, depends also on the initial rate of mixing of dry aerosol with humid air, and increases as the Reynolds number increases from 1000 to 3000.

4.2 Non-Hygroscopic Particles

Particles of many materials other than hygroscopic salts have also

TABLE 4.1

Characteristic Properties of Some Salts.
The increase of the aerodynamic diameter ① of 1 μm particles in the lung (D_1) and the reciprocal of the weight concentration of salt for that particle in the lung (g_s^{-1}) are presented. g_s^{-1} is the factor by which the mass of a dry particle in the lung is increased (Fe77)

Salt	Molecular weight	Density (g/cm^3)	Solubility	i ②	j ③	D_1 (μm)	g_s^{-1}
$AlCl_3$	133.4	2.4	0.7	4	0	3.8	36.1
$CoCl_2 \cdot H_2O$	165.87	2.477	0.91	3	2	3.2	58.3
$CoCl_2 \cdot 6H_2O$	237.93	1.924	1.2	3	6	3.0	40.4
KNO_3	101.11	2.11	0.39	2	0	3.4	64.4
$MgCl_2$	95.22	2.32	0.56	3	0	3.9	102
NaCl	58.44	2.165	0.37	2	0	4.1	113
$NaNO_3$	84.99	2.261	1.0	2	0	3.6	76.8
NaOH	40.00	2.130	1.0	2	0	4.7	166
$Ni(OH_3)_2 \cdot 6H_2O$	290.81	2.05	3.0	3	6	2.8	32.9
$Pb(NO_3)_2$	331.20	4.53	0.61	2	0	1.9	18.9
$UO_2(NO_3)_2 \cdot 6H_2O$	502.13	2.807	3.1	3	6	2.1	18.8
$ZnSO_4 \cdot 7H_2O$	287.54	1.957	1.0	1	7	1.9	10.9

① diameter of a fictitious sphere of unit density (1 g/cm^3) that has the same terminal setting velocity as the particle.

② number of ions into which a salt molecule dissociates in H_2O.

③ number of H_2O molecules per salt molecule.

been studied for their interaction with water. Porstendörfer (Po71) studied aerosols of SiO_2 and latex, cigarette smoke and atmospheric aerosols. While SiO_2 and latex are hydrophobic materials, cigarette smoke and atmospheric aerosols may contain soluble components in non-negligible proportions. Porstendörfer's results are summarized in Table 4.2.

Although latex particles are not hygroscopic, Langer and Liebermann (La60) found that the size of latex particles increased with increasing humidity. This result was interpreted by Porstendörfer (Po71) to be due to deposits of the suspension solution remaining on the surface of the latex particles. The growth factor of 1.55 for cigarette smoke and 2 for atmospheric aerosols suggests the presence of water-soluble components in both types of aerosols. Cinkotai (Ci68) found the change in size of cigarette smoke particles (4-10 μm radius) to be a factor of 1.3-1.5 at a relative humidity of 99%, a result in agreement with Porstendorfer's work. However, growth of particles may not be due solely to solubility in water. Yoshida et al (Yo 76) used hydrophobic materials such as dioctyl phthalate and carbon black and found growth of 4-8 times in a supersaturated atmosphere created by continuously mixing hot saturated air (78-81°C) with cold air (19-28°C) in an insulated chamber. Yoshida et al postulated that the growth of such particles was caused by the instability of the supersaturated atmosphere. The rate of growth of aerosol particles was found to be very rapid; growth was complete within 1 second. Although on a theoretical basis the width of the size distribution is generally expected to become narrower after growth, Yoshida et al (Yo76) did not observe any change in the width of the size distribution.

Atmospheric aerosols were studied by Sinclair et al. (Si74) who

TABLE 4.2

Experimentally Observed Particle Enlargement at Higher Relative Humidity; Growth time > 1.5 sec (Po71)

Aerosol	Relative humidity, F (%) (Temp. 20-22°C)	Particle concentration (#/cm^3(x 10^4)	Particle radius (μm)		Observed av. radius at F % R.H.	observed av. radius at 40-50% R.H.
NaCl	100	5.4	0.06		2.9	
		5.0			2.8	
		3.0			2.9	3.0
		4.6			3.04	
		1.8			3.55	
SiO_2	100	5.4	0.12		0.96	
		5.4			0.95	0.98
		5.4			1.02	
latex	100	4.0	0.05		1.29	1.35
		4.8			1.41	
cigarette smoke	100	4.6	0.011		1.5	
		4.75	0.012	0.011	1.52	1.55
		4.2	0.016		1.64	
atmospheric* aerosols	100	1.1	0.04		2.25	
		2.2	0.023		1.78	
		3.5	0.02		1.77	
		1.9	0.026		1.39	
		1.0	0.033	0.028	3.0	2.0
		1.0	0.035		2.09	
		2.2	0.027		2.11	
		1.9	0.037		2.0	
		3.1	0.02		1.75	
		3.4	0.018		2.12	

* individual measurements were made on different days

found the ratio of the number median diameters at 98 and 57% R.H. to be 1.38 - 1.45. These results were observed to be in accordance with the following equation derived by Kasten (Ka69) for the increase in particle size of natural aerosols with humidity:

$$\frac{d(R.H.)}{d(o)} = (1 - R.H.)^{-1/K} \qquad (14)$$

where d(R.H.) = particle diameter at a given relative humidity, R.H., and d(o) = particle diameter at zero relative humidity, i.e. diameter of dry aerosol. In Sinclair et al.'s work, the value of K was found to be 4 on the average but K was found to increase (from 2.5 - 5) with increasing humidity (29-98 % R.H.) for a size distribution with a number median diameter of 0.018 μm and a geometric standard deviation of 2. Results of these and other investigations are summarized in Table 4.3. [The results of the present study are compared in Table 10.1 with the studies in Tables 4.2 and 4.3.]

4.3 Deposition of Hygroscopic Particles in the Respiratory System

Although there is some evidence that hydrophobic particles can grow under appropriate conditions of supersaturation (Yo76), such growth has not been established to be the case under conditions prevailing in the respiratory tract. The discussion in this section is therefore limited to the respiratory deposition of hygroscopic particles or mixtures containing one or more hygroscopic components (such as the atmospheric aerosol). For insoluble particles, deposition is assumed to occur in accordance with the Stokes-equivalent drag diameter, which is the diameter of the inhaled particles considered to remain unaltered till deposition takes place. For hygroscopic particles, deposition as a

TABLE 4.3

Summary of Investigations on Growth of Particles in a Humid Atmosphere

Reference	Aerosol material	R.H. (%) (Temp °C)		Growth factor	Particle radius (μm)	Residence time (s) (breathing frequency/ min)
		Initial	Final			
Ze56[1]	NaCl	NA	99.9 (-)	5	0.1	0.075
			99.8 (-)	7		
Da61[2]	NaCl	NA	99.8 (-)	6-7	NA	NA
Ju67[1]	atmospheric aerosols	NA	100 (36)	2	0.03-10	NA
C168[2]	cigarette smoke	NA	99 (-)	1.3-1.5	4-10	NA
Ge69[2]	radon progeny attached to atmospheric aerosols	35-40 (21)	95-100 (35)	~ 2	0.02-0.045	(8-20)
W169,73[2]	mixtures of salts and acids, maritime aerosols, av. continental aerosols	NA	70-100	2-6[3]	NA	NA

cont'd.....

TABLE 4.3 (cont'd)

Reference	Aerosol material	R.H. (%) (Temp °C)		Growth factor	Particle radius (μm)	Residence time (s) (breathing frequency/ min)
		Initial	Final			
Ci71[1]	NaCl	NG	93 (36)	2.25	0.005	NG
			99-100 (36)	>5	0.005	
Si74[2]	atmospheric aerosols	29-30 (NG)	98 (ambient)	1.38-1.45	0.01-0.04	NG
Be81[2]	NaCl	NG	95 (34-38)	3-4.5	1-3	(0.05-1)
Tu84[2]	NaCl	NG	98-99 (32-33)	3.5-4.5	0.06-0.1	(10, 15)

[1] theoretical results

[2] experimental results

[3] mass increase

NA not available

NG not given

function of particle size in inhaled air is complicated by the growth of the particles in the moist air to an unknown final diameter. In this case, deposition may initially occur as a function of the thermodynamic diameter (diameter of a fictitious sphere with the same diffusional mobility as the particle) and, after the particle has grown larger than about 0.2 μm, deposition may occur as a function (entirely or partly) of the aerodynamic diameter. A further complication arises due to the diverse chemical properties of the ambient hygroscopic aerosol, which may result in different growth characteristics and therefore different deposition efficiencies for particles of different properties (Fe77).

Growth of particles is affected by the actual relative humidity in the respiratory tract, estimates of which vary. Arguments have been presented in favour of 90-95% R.H. based on the measurements of Derry et al. (De67) in the trachea and large airways of anaesthesized human subjects. Bell and Ho (Be81) postulate that complete mixing of the inhaled air with saturated lung air does not occur. Even if complete mixing were to take place, Bell and Ho reason that volume dilution considerations predict that the relative humidity of the mixed air would be significantly less than 99-100%, perhaps of the order of 95%. Ferron (Fe77) theoretically estimated the relative humidity in the respiratory tract to be 96-100%. Other authors have used the 99-100% R.H. range without being more specific. It should be noted, however, that based upon Cinkotai's arguments (Ci77), growth of hygroscopic particles is very sensitive to even a slight change in relative humidity in the 98-100% range. Deposition data for hygroscopic aerosols discussed in this section should be interpreted in terms of the above limitations.

Theoretical studies of enhanced deposition of hygroscopic aerosols have been conducted by Martonen (Ma82), Ferron and Hornik (Fe84) and Xu and Yu (Xu84). Martonen (Ma82) calculated the deposition of both non-hygroscopic and hygroscopic particles in airways using the lung structure model of Weibel (We63). He concluded that the effect of hygroscopic particle growth is mainly on the total tracheobronchial deposition rather than on the distribution within the tracheobronchial generations. The results of Martonen are summarized in Table 4.4.

Ferron and Hornik (Fe84) used different humidity profiles for different regions of the respiratory tract and found enhanced deposition in the tracheobronchial and pulmonary region for hygroscopic particles in the size range 0.3 to 3.0 μm. However, results using different humidity profiles were found to be similar to those for a constant relative humidity of 99.5% at 37°C. The deposition probability of particles in the size range 0.3-10 μm was found to be important for the enhanced lung deposition of growing particles.

Xu and Yu (Xu84) compared their theoretically calculated data for NaCl deposition in the lung with the experimental data of Tu and Knutson (Tu84) and found good agreement. A plot of the calculated data of the former authors for both NaCl and non-hygroscopic particles is shown in Fig. 4.2. Xu and Yu found that the minimum deposition for NaCl occurs at 0.08 μm initial diameter, which is smaller by a factor of 6 to 7 than the usual value of 0.5 μm for non-hygroscopic particles. This result leads to the conclusion that an NaCl particle grows 6-7 times its initial size in the airways during a respiratory cycle. It was also found by Xu and Yu that for NaCl particles of initial diameter >0.2 μm, deposition was

TABLE 4.4

Deposition of Nonhygroscopic and Hygroscopic (NaCl) Aerosol Particles in the Conducting Airways: Modelling Calculations by Martonen (Ma82)

	Nonhygroscopic particles	NaCl Particles (a) Experimental growth rate	NaCl Particles (b) Theoretical growth rate
*Particle size on inhalation (μm)	3.0	3.0	3.0
*Particle size at terminal bronchioles (μm)	3.0	4.2	5.2
Total tracheobronchial deposition (% of particles entering trachea)	19	29	47
% of tracheobronchial deposition in generations			
0.6	38.4	37.1	40.0
7-10	24.6	24.4	24.5
11-16	37.0	38.5	35.5

Inspiratory flow rate = 40 L min^{-1}
*Aerodynamic diameters

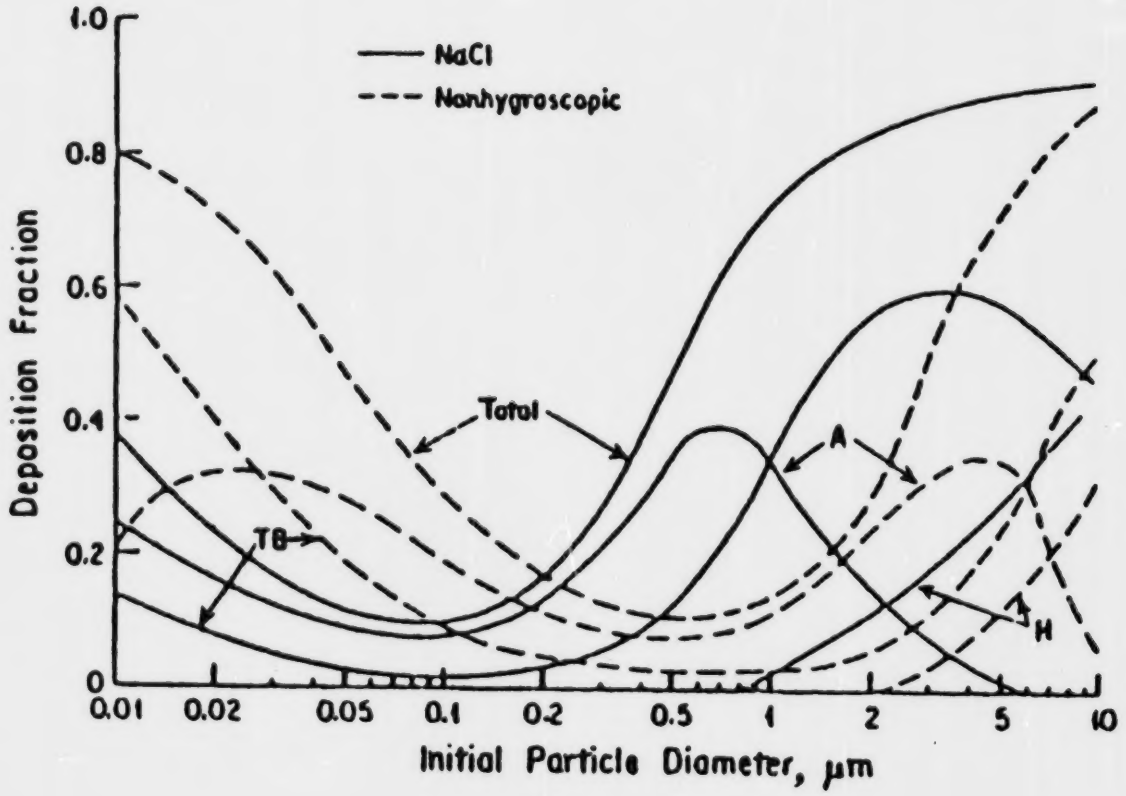

Fig. 4.2. Calculated total and regional deposition of NaCl and non-hygroscopic particles. H: head deposition, TB: tracheo-bronchian deposition, A: Alveolar deposition (Xu84).

greater than for similar non-hygroscopic particles; deposition was less if the initial particle diameter of NaCl was less than 0.2 μm.

Experimental data on respiratory deposition of hygroscopic particles were obtained by Stuart (St73), Bell et al (Be78), Scherer et al (Sc79) and Tu and Knutson (Tu84). All of these investigators confirmed that deposition was enhanced by the hygroscopic nature of the particles. Tu and Knutson (Tu84) compared their experimental data on total deposition from NaCl with hydrophobic kerosene combustion products in the size range 0.03 to 0.4 μm. Hygroscopic particles were found to show minimum deposition in the size range 0.06 to 0.09 μm. The theoretical results of Yeh and Schum (Ye80) for 750 cm^3 tidal volume agreed well with the kerosene aerosol data. Comparison is shown in Fig. 4.3. George and Breslin (Ge69) found that total respiratory deposition decreased from 50 to 30% as the particle diameter of attached radon progeny increased from about 0.01 to 0.08 μm. Based upon this result and experimental observations, Sinclair et al (Si74) concluded that the total respiratory deposition of small hygroscopic particles would decrease during periods of high humidity.

In summary, deposition of hygroscopic particles depends strongly upon the initial particle size which, after undergoing growth, results in a higher or lower deposition, depending upon ultimate size. The minimum in deposition occurs at about 0.5 μm ultimate size, as indicated earlier.

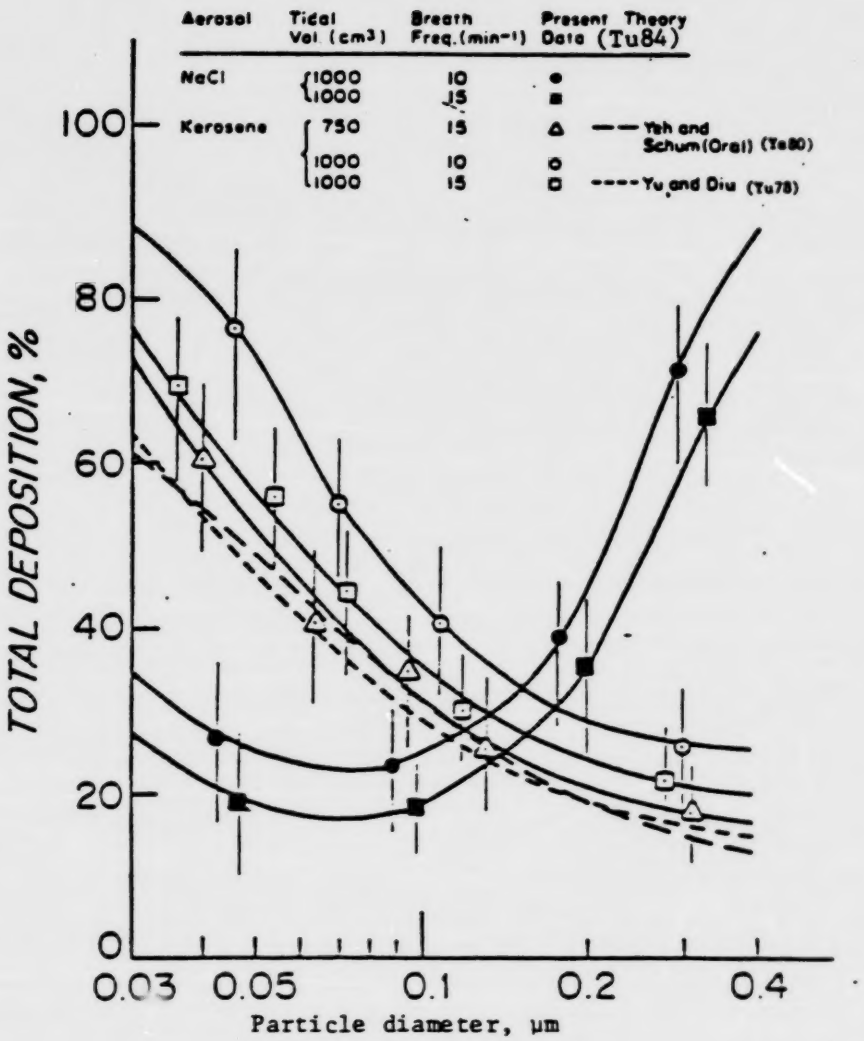

Fig. 4.3. Total deposition for nasal breathing of kerosene and NaCl particles (Tu84).

5. SUPERSATURATION

Since supersaturated vapor is a prerequisite for almost all types of nucleation, an understanding of the term supersaturation and how supersaturation can be produced is important. The degree of saturation can be defined in terms of the saturation vapor pressure, P_s, and the actual partial pressure of vapour, P, and expressed as the saturation ratio, S, where

$$S = \frac{P}{P_s} \tag{15}$$

A vapour is unsaturated for $S < 1$, saturated for $S = 1$, and supersaturated for $S > 1$. The saturation vapour pressure, P_s, is the pressure required to maintain a vapour in mass equilibrium with the condensed vapor at a specified temperature. It is a property of a material, liquid or solid, and is fixed at a given temperature. When $P_s = P$, evaporation from the surface of a liquid just equals condensation on that surface, resulting in mass transfer equilibrium at the surface. The amount of supersaturation refers to that portion of the saturation ratio, S, which is in excess of 1.0. For example, a supersaturation of 6% corresponds to a saturation ratio of 1.06, which corresponds to a relative humidity of 106% at the specified temperature. The supersaturation is therefore given by $(P - P_s)/P_s$.

In order to examine how an initially unsaturated vapor attains a condition of supersaturation, it is helpful to study the usual form of the vapor pressure-temperature (P, T) diagram as shown in Fig. 5.1.

In Fig. 5.1, vapour and liquid co-exist in equilibrium along the

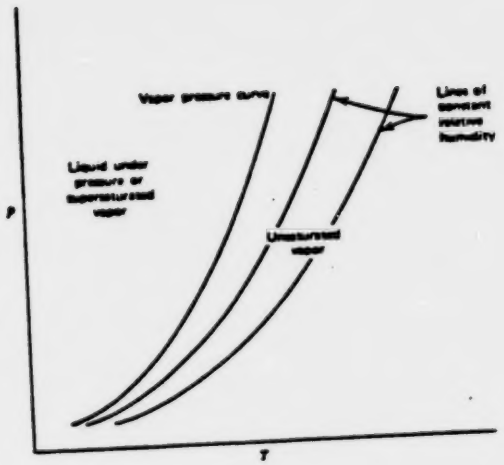

Fig. 5.1. Typical form of the vapour pressure curve with lines of constant relative humidity (Fr77).

vapor pressure curve whereas the region to the right of the curve represents unsaturated vapour and the region to its left represents supersaturated vapour. The slope of the vapour pressure curve is given by

$$\frac{dP_s}{dT} = \frac{\Delta H P_s}{RT^2} \qquad (16)$$

which is the Clausius-Clapeyron equation. In eqn. (16), ΔH is the molar heat of vaporization, R is the gas constant (8.3×10^7 ergs/mole °K) and T is the temperature in °K.

Integration of eqn. (16), treating ΔH as a constant (the heat of vaporization is approximately constant over a wide range of temperature), gives:

$$\ln P_s = -\frac{\Delta H}{RT} + \text{const.} \qquad (17)$$

Reist (Re84) has expressed the above equation as

$$\ln P_s = A - \frac{B}{T} \qquad (18)$$

where the constants A and B at T = 20°C are listed in Table 5.1.

Hinds (Hi82) gives the following general expression for the saturation vapor pressure of water in mm Hg at a temperature T°C:

$$\log_{10} P_s = 8.11 - \frac{1750}{T + 235} \qquad (19)$$

From the above equation, it can be seen that an ambient temperature change of 10°C changes P_s by a factor of about two. Thus the conditions of supersaturation can vary enormously for small changes in the ambient temperature. This result has important implications with respect to supersaturation in working environments in which the temperature may vary from well below freezing to warm or hot. In cold conditions, much higher supersaturation is possible compared to hot

TABLE 5.1

Values of the Constants A and B for Various Liquids, T = 20°C (Re84)

Liquid	A	B
Bromine	18.47	3915
Water	21.18	5367
Iodine	22.96	7155
Uranium hexafloride	22.95	5344
Acetone	18.51	3906
Benzene	20.60	4759
Bromobenzene	19.44	5364
Decane	19.67	5694
Diethylether	17.97	3488
Ethanol	21.24	5200
n-Hexane	18.09	3896
Methyl iodide	17.54	3439
Naphthalene	25.87	8423
n-Octane	23.98	6537

conditions, and particle growth would be much more rapid.

For condensation to occur, any path on the (P, T) diagram leading from the unsaturated state to the supersaturated state can be adopted. The two paths which are most common are reversible adiabatic expansion and mixing with cooler air at a lower particle concentration. These two processes, which lead to the formation of aerosol composed of small liquid droplets, are discussed in the following sections.

5.1 Adiabatic Expansion

Cooling by adiabatic expansion is a procedure for producing a uniform supersaturation throughout a vapor without having to establish temperature gradients. No heat input is allowed from the surroundings in this process, which consists of rapid expansion in an insulated chamber by means of a piston displacement, or expansion of a gas at a nozzle exit. Adiabatic expansion takes place in nature when large masses of humid air rise by buoyancy and expand adiabatically with the decrease in pressure resulting in formation of clouds. No significant heat transfer from the surroundings takes place in this case because the mass of air is very large. For a reversible adiabatic expansion, the conditions along the path on a (P, T) diagram are related by the equation

$$\frac{P_2}{P_1} = \left(\frac{T_2}{T_1}\right)^{\gamma/\gamma-1} \tag{19}$$

where P and T represent the total pressure and temperature, respectively; the subscripts 1 and 2 refer to before and after the expansion; γ is the ratio of specific heat at constant pressure to specific at constant volume. The path of the expansion process is shown in Fig. 5.2. As

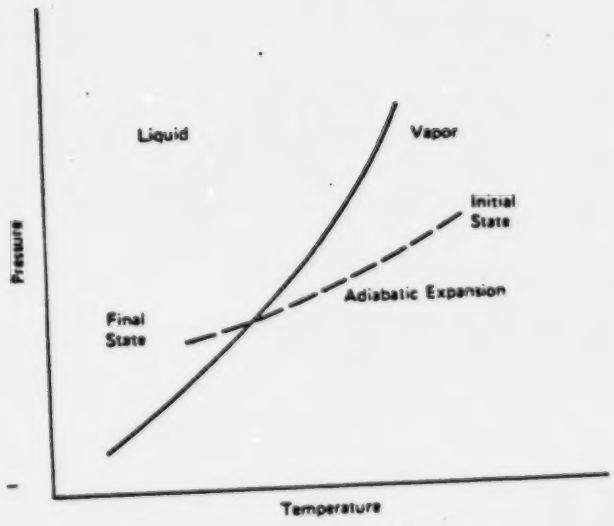

Fig. 5.2. Reversible, adiabatic expansion from an initially unsaturated state carries the vapour across the saturation curve into a region where the stable state is a liquid (Fr77).

seen in Fig. 5.2, both the temperature and the pressure of an initially unsaturated gas decrease up to the point of condensation.

In a very early study of condensation, Coulier (Co75) in 1875 enclosed air in a flask together with water and produced supersaturation by compressing a hollow india-rubber ball connected to the flask and then suddenly releasing it. He observed dense condensation following a small expansion in fresh unfiltered air. Unaware of Coulier's work, Aitken (Ai80) also produced supersaturation, sometime during the same period as Coulier, by using an expansion method similar to Coulier's. Aitken further showed that condensation takes place on certain dust nuclei for an expansion ratio (water vapour in air) as low as 1.004, while other nuclei required an expansion ratio as great as 1.02. This dilemma was resolved by Wilson (Wi97, 99) in his famous cloud chamber experiments in which he distinguished two critical values of supersaturation corresponding to onset limits of effectiveness of different nuclei. The lower limit, at roughly four-fold supersaturation of water vapour in air, was demonstrated to involve gaseous ions as nuclei on which condensation takes place, while the upper limit, at about eight-fold supersaturation, was found to involve uncharged aggregates of molecules. This aspect of nucleation is discussed further in Section 7.

More recent studies of condensation by adiabatic expansion have been carried out by Wegener and Pouring (We64) in converging-diverging nozzles. In these experiments, air and water were expanded through a nozzle as shown in Fig. 5.3. With isentropic drop of pressure and temperature, saturation was attained in the section upstream of the throat where cooling rates of 10^5 to 10^6 °C/sec could be achieved.

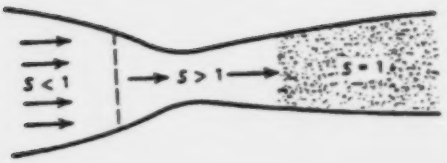

Fig. 5.3. Adiabatic expansion in a converging-diverging nozzle.

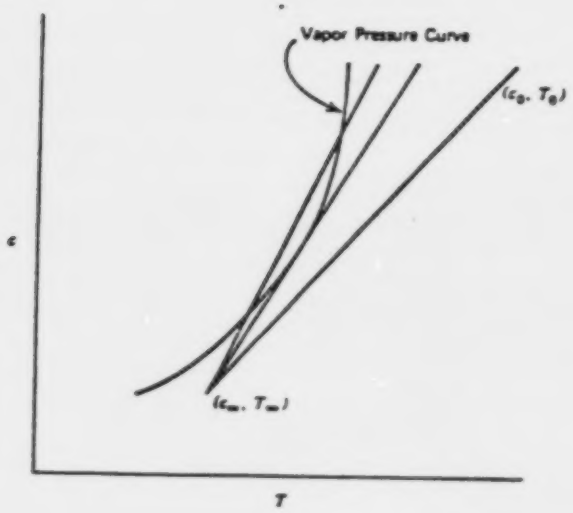

Fig. 5.4. Air-vapour mixtures at three different source conditions (c_0,T_0) mixing with air of the same ambient conditions (c_∞,T_∞). No condensation occurs for the source on the right while condensation can occur, depending on availability of nuclei and mixing rates, for the one on the left. The middle line shows a limiting situation. Case of the Lewis number = $\kappa/\rho C_p D = 1$ (Fr77).

Nuclei generated in the gas grew to a sufficiently large size and formed visible fog at some point in the diverging section.

5.2 Mixing of a Hot Gas with a Cool Gas

The most commonly observed example of condensation by mixing is the appearance of exhaled breath as fog in winter. When exhaled air, which is saturated at body temperature on its way out from the lungs, mixes with the cold ambient air at sub-freezing temperature, the resulting temperature drop in the exhaled air promotes condensation. Condensation is discouraged by dilution, and the relative rates of cooling and dilution during mixing determine whether saturation conditions are reached. In the case of a hot jet of a condensable vapour-air mixture mixing with air at lower temperature, the temperature distribution, for constant C_p (heat capacity at constant pressure) is given by

$$\frac{C - C_\infty}{C_o - C_\infty} = \frac{T - T_\infty}{T_o - T_\infty} \qquad (19)$$

where C, the mass fraction of the diffusing species (g/g of gas) is equal to C_o at the source and C_∞ in the ambient air. Similarly the temperature is T_o at the source and T_∞ in the ambient air. Equation (19) holds provided $K/\rho C_p D = 1$, where K is the thermal conductivity and D is the diffusion co-efficient. The dimensionless group $K/\rho C_p D$ is called the Lewis number and is generally close to unity for gas mixtures.

For the general case of Lewis No. $\neq 1$, the relationship between concentration and temperature depends on the flow field; for the special case of Lewis No. $= 1$ the relationship is independent of the nature of

the flow in regions in which condensation has not yet occurred.

Equation (19) suggests that the plot of the mass fraction-temperature relationship is a straight line determined by conditions at the source and in the ambient atmosphere. From Fig. 5.4 the limits placed on condensation that must exist at the source can be observed. For condensation to occur, the mixing line must be at least tangent to the vapour pressure curve.

5.3 Chemical Reactions to Produce Condensable Species

Gas phase chemical reactions can also produce condensable species. Gas phase reactions are of special interest in air pollution. In the atmosphere, reactions involving SO_2, NO-NO_2 and certain organic compounds are important. If the product of such reaction is only a single condensable species, it can condense by homogeneous nucleation in the absence of existing particles. However, sometimes two or more condensable species may be produced. Heteromolecular nucleation can then take place at partial pressures much lower than those required for nucleation of the pure vapours if the two condensable species strongly interact (e.g. as in the water vapour-sulphuric acid system). Both homogeneous and heteromolecular types of nucleation are discussed in the next section. In general, chemical reactions leading to the formation of condensable species are poorly understood.

6. TYPES OF NUCLEATION

Nucleation can be initiated by different mechanisms in the presence or absence of particles. In the absence of particles in a condensable vapor, particles can be formed by homogeneous nucleation on molecular clusters in a supersaturated vapor. In a multicomponent system, heteromolecular nucleation may give rise to formation of mixed particles. Heterogeneous condensation can occur on existing particles or ions. These three mechanisms of nucleation are discussed in the following sections.

6.1 Homogeneous Nucleation

Before discussing homogeneous nucleation, which occurs with molecular clusters, the Kelvin effect must be understood. The Kelvin effect sets a lower limit on the particle size of a polydisperse aerosol that can serve as a condensation nucleus. Since there are fewer molecules in the layers adjacent to the surface in a small droplet as compared to a plane surface, the energy necessary to separate a molecule from the attractive energy of its neighbours is smaller than for a plane surface. Thus molecules on the surface of a small drop can escape into the vapour phase more easily than from a plane surface and the vapour pressure over a drop is greater than that over a plane surface. This result is called the Kelvin effect. For a drop of diameter, d_p, the Kelvin relationship is

$$\ln \frac{P_d}{P_s} = \frac{4 \sigma \bar{V}_m}{d_p kT} \qquad (21)$$

in which P_d is the equilibrium vapour pressure of the drop, which depends

on its radius of curvature; P_s is the saturation vapour pressure; V_m is the volume per molecule (molecular volume) of the liquid; σ is the surface tension; k is the Boltzmann constant.

Condensation may take place when $S = \frac{P_d}{P_s} > 1$. From eqn. (21), it can be observed that a supersaturation ratio greater than unity is expected for small droplets at equilibrium with a condensable vapour. The logarithm of the supersaturation ratio is inversely proportional to the particle diameter and directly proportional to the product of the surface tension and the molecular volume of the liquid.

If a droplet is composed of mixtures of constituents, the equilibrium vapour pressure relations become more complicated. In case of a solvent, its vapour pressure over a droplet containing a non-volatile solute is given by the Kelvin relation as

$$\ln \frac{P_{Ad}}{P_{As}} = \frac{4 \sigma \bar{V}_A}{d_p kT} - \frac{6 n_B \bar{V}_B}{\pi d_p^3} \qquad (22)$$

where the volume of the droplet is

$$\frac{\pi d_p^3}{6} = n_A \bar{V}_A + n_B \bar{V}_B \qquad (23)$$

In the above equations, P_{Ad} is the vapour pressure of the pure solvent at temperature T, V_A and V_B are the molar volumes of the solvent and solute, respectively, and n_B is the number of moles of solute. Equation (22) is sometimes referred as Kohler's equation. Both Kelvin's relation and Kohler's equation are plotted in Fig. 6.1. It is demonstrated clearly from this figure that the radius of curvature influence is strongest at large particle size whereas the vapour pressure reducing effect of the solute dominates at small particle size.

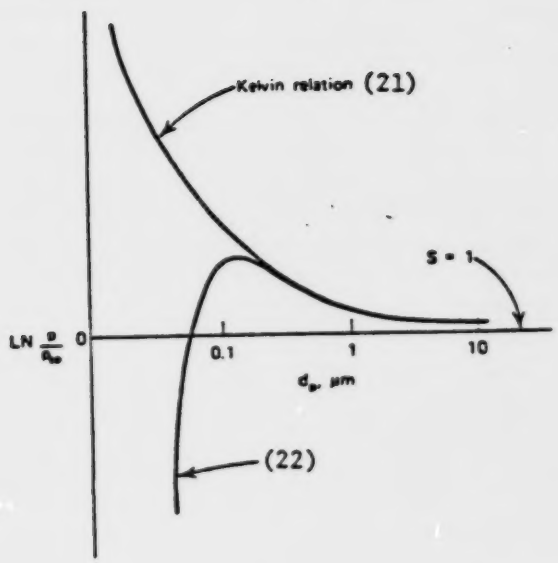

Fig. 6.1. Equilibrium vapour pressure curves for droplets composed of solvent alone (Kelvin relation) and of a solvent with a fixed mass of non-volatile solute (Kohler's equation) (Fr77)

If the value of S associated with a drop of a given diameter produces a point lying to the right of the curve in Fig. 6.2, the drop will grow, whereas if the point lies to the left of this curve the drop will evaporate. It can be seen that for $S < 1$ a pure liquid drop will always evaporate. Even with supersaturation, droplets smaller than a critical size will also evaporate. The maximum sustainable supersaturation corresponds to a particle of diameter of about 0.2 μm in the case of a mixture of constituents (Kohler's eqn., Fig. 6.1).

In the process of homogeneous nucleation, initially random accumulation of molecular clusters takes place in a supersaturated atmosphere as the vapour becomes increasingly supersaturated. Such tiny clusters have been found to exist experimentally (Mi56, Mi67, Ca79). Molecular clusters can be formed even in unsaturated vapour due to the attractive forces between molecules, such as van der Waals forces. The clusters are formed continuously but are unstable and continuously disintegrate. In supersaturated vapour, the number concentration of clusters formed can be so large that the clusters collide with one another frequently and form agglomerates. Once such an agglomerate exceeds a certain critical nucleus size, even momentarily, it becomes stable and grows by condensation to form a larger particle. This process of homogeneous nucleation is also called self-nucleation because the nuclei are generated by the vapour itself. The supersaturation required for particle formation by this process for a given vapour and temperature is called the critical saturation ratio. Figure 6.3 demonstrates that homogeneous nucleation only takes place at a well-defined critical saturation ratio. For pure

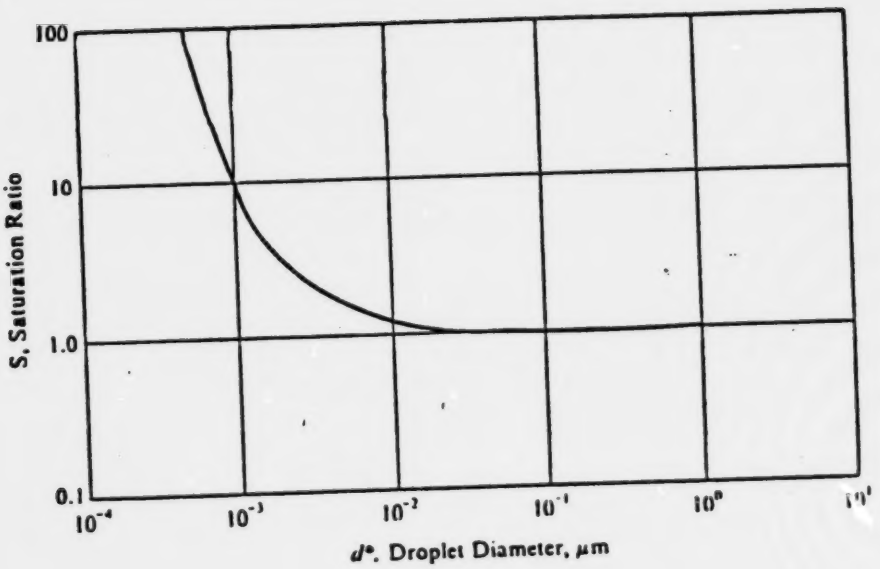

Fig. 6.2. This figure demonstrates the Kelvin relationship in greater detail (Re84).

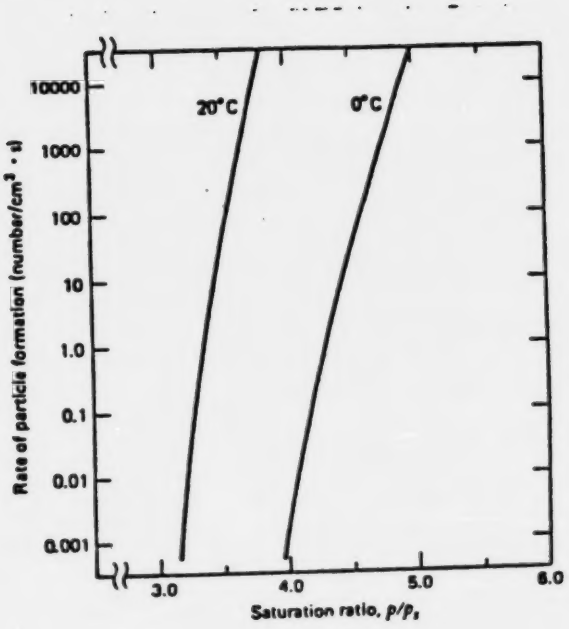

Fig. 6.3. Particle formation rate for homogeneous nucleation versus saturation ratio at 20 and 0°C (Hi82).

water vapour at 20°C, particles are spontaneously formed when the saturation ratio exceeds 3.5. This ratio corresponds to a Kelvin diameter of 0.0017 μm, the diameter of molecular cluster agglomerates consisting of 90 water molecules. A large number concentration of submicron particles is generally formed with a narrow but not monodisperse size distribution.

The theory of formation of clusters begins with consideration of the equilibrium between agglomerates of different size in a pure vapour. The reactions can be written as

$$e_{g-1} + e_1 \longrightarrow e_g \tag{24}$$

where e_1 represents a single molecule and e_g is a cluster or embryo of g molecules. The rate of formation of e_g by condensation of e_1 on e_{g-1} is equal to the rate of loss of e_g by evaporation. The equilibrium relationship can be written as

$$\beta S_{g-1} n_{g-1} = \alpha_g S_g n_g \tag{25}$$

where β is the flux of single molecules (molecules per unit time per unit area) condensing on clusters containing g-1 molecules each, S_{g-1} is the effective area for condensation of the clusters, n_g is the concentration of clusters containing g molecules each, α_g is the evaporative flux from clusters containing g molecules each and S_g is the effective area of evaporation.

The condensation area can be assumed to be approximately equal to the evaporation area. The flux of condensing single molecules, β, can be obtained from the kinetic theory of gases as

$$\beta = \frac{P_1}{(2\pi m kT)^{1/2}} \tag{26}$$

where P_1 is the partial pressure of the single molecule and m is the

molecular mass. All molecules striking the surface of the nucleus are assumed to stick.

From the Kelvin equation (21)

$$P_d = P_s \exp\left(\frac{4\sigma V_m}{d_p kT}\right) \tag{27}$$

From eqn. (27), the evaporative flux is

$$\alpha_g = \frac{P_d}{(2\pi m kT)^{1/2}} = \frac{P_s}{(2\pi m kT)^{1/2}} \cdot \exp\left(\frac{4\sigma V_m}{d_p kT}\right) \tag{28}$$

Substituting from eqns. (26) and (28) into eqn. (25) with $S_{g-1} = S_g$ gives:

$$\frac{n_{g-1}}{n_g} = \frac{\alpha_g}{\beta} = \frac{P_s}{P_1} \exp\left(\frac{4\sigma V_m}{d_p kT}\right) \tag{29}$$

However, P_1/P_s is the saturation ratio, S, and the diameter, d_p, of a cluster of g molecules can be expressed in terms of the volume of g molecules, gV_m as

$$d_p = \left(\frac{6 V_m g}{\pi}\right)^{1/3}$$

With these substitutions eqn. (29) becomes

$$\frac{n_{g-1}}{n_g} = \frac{1}{S} \exp\left(\frac{2\sigma V_m \left(\frac{4}{3}\pi/V_m\right)^{1/3}}{g^{1/3} KT}\right) \tag{30}$$

Multiplying eqns. of form (30) for successively smaller values of g down to g = 2 gives

$$\frac{n_1}{n_2} \cdot \frac{n_2}{n_3} \cdot \frac{n_3}{n_4} \cdots\cdots \frac{n_{g-2}}{n_{g-1}} \cdot \frac{n_{g-1}}{n_g} = \frac{n_1}{n_g} = \frac{1}{S^{g-1}} \cdot$$

$$\exp\left(\frac{2\sigma V_m \left(\frac{4}{3}\pi/V_m\right)^{1/3}}{KT} \sum_{g=2}^{g} g^{-1/3}\right) \tag{31}$$

For larger values of g

$$\sum_{g=2}^{g} g^{-1/3} \approx \int_{0}^{g} \frac{dg}{g^{1/3}} = \frac{3}{2} g^{2/3} \qquad (32)$$

Thus for $n_s = P_s/kT$ the equilibrium distribution of nuclei is given by

$$n_g = n_s s^g \exp\left(\frac{-3\sigma V_m \left(\frac{4}{3}\pi V_m\right)^{1/3} g^{2/3}}{kT}\right) \qquad (33)$$

Since the approximation (32) holds only for sufficiently large values of g, eqn. (33) leads to considerable error for small g, that is, for few molecules in a cluster.

A plot of eqn. (33) is shown in Fig. 6.4 for saturation ratios greater and smaller than unity. For $S < 1$, that is, an unsaturated gas, the concentration of clusters n_g is a monotonically decreasing function of g, the number of molecules in a cluster. For $S > 1$, that is, a supersaturated gas, n_g is smallest at a cluster size d_p^* given by differentiation of eqn.(33) with respect to g and setting the derivative equal to zero:

$$d_p^* = \frac{4\sigma V_m}{kT \ln S} \qquad (34)$$

The value of the critical nucleus size in eqn. (34) is important in determining whether evaporation or growth will take place. Nuclei smaller than d_p^* tend to evaporate while nuclei of critical size d_p^* or greater tend to grow. The number of nuclei of critical size d_p^* is given by

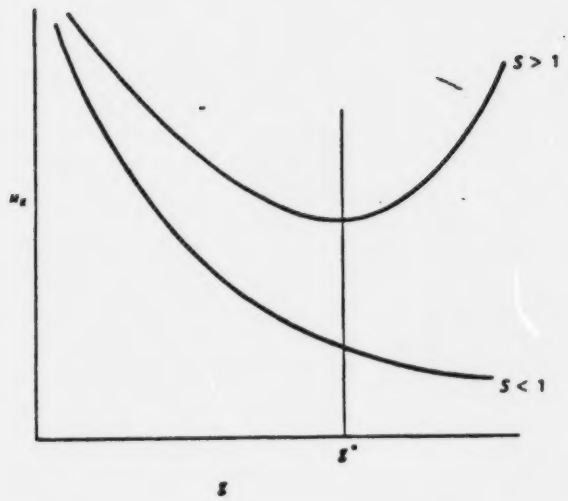

Fig. 6.4. Discrete size distribution at equilibrium for clusters formed by homogeneous nucleation. For S > 1, an infinite mass of material must be present in the cluster phase at equilibrium (Fr77).

$$n_g^* = n_1 \exp\left(\frac{-16\,\pi\,\sigma^3\,V_m^2}{3(kT)^3(\ln S)^2}\right) \qquad (35)$$

In the above equation, the exponential term essentially represents the ratio of the free energy of formation of the critical-sized droplet ΔG^* and kT.

6.2 Heteromolecular Nucleation

In many situations nucleation takes place in a multicomponent system where one or more components are supersaturated. This form of nucleation is described as heteromolecular nucleation. The theory for heteromolecular nucleation is complicated and was worked out in a generalized way for nucleation in a binary vapor mixture by Reiss (Re50). In heteromolecular nucleation, the free energy, ΔG, of the critical embryo is that required to form a droplet having a size and composition such that it is in equilibrium with the surrounding gas phase. Reiss (Re50) showed that in a three-dimensional diagram system of ΔG versus the number of moles of components A and B, there exists a saddle point which is the barrier that the embryo must overcome in order to grow and stabilize during the process of nucleation.

Calculations by Mirabel and Katz (Mi74) for the sulphuric acid-water vapor system and the nitric acid-water vapor system are shown in Fig. 6.5. The activity of the acid in the vapor is plotted as a function of the relative humidity for nucleation of 1 embryo/cm^3 s. The figure shows that the activity for nucleation decreases with humidity and that sulphuric acid will nucleate at much lower activities than nitric acid. It should also be noted that in heteromolecular nucleation, because of the two condensable vapors present, nuclei will be produced at much lower

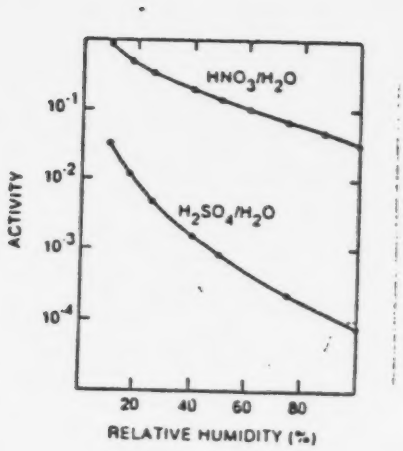

Fig. 6.5. Activity of the acid in the vapour phase needed to achieve a nucleation rate of 1 nucleus/cm^3 sec as a function of relative humidity for $H_2SO_4 + H_2O$ and $HNO_3 + H_2O$ at 25°C (Mi74).

activities than for pure vapours.

6.3 Heterogeneous Nucleation

Nucleation on foreign nuclei present in a condensable vapour system is described as heterogeneous nucleation. The foreign nuclei may consist of ions or particles (soluble or insoluble). Nucleation on ions is treated separately in Section 7. In this section, nucleation on both soluble and insoluble particles is discussed.

Assuming that a particle behaves like a pure drop of the condensing species (vapour molecule), the growth rate of particles by heterogeneous condensation can be estimated from the following considerations. The growth rate is governed by the rate of random molecular collisions when the particle size is less than the gas mean free path, which is likely to be the case when a particle first starts to grow. The rate of arrival, Z_{in}, of vapour molecules per unit area of the particle surface is then given by

$$Z_{in} = \frac{P}{(2\pi\, m\, kT)^{1/2}} \tag{36}$$

where P is the partial vapor pressure.

The net rate of arrival of molecules at the particle surface area of the particle surface, n_Z , is $(Z_{in}-Z_{out})\, A_s$, where A_s is the surface area of the particle. Z_{out} is the rate of loss of the vapor molecules per unit area of the particle surface given by

$$Z_{out} = \frac{P_d}{(2\pi\, m\, kT)^{1/2}} \tag{37}$$

where P_d is the partial vapour pressure at the particle surface. Therefore,

$$n_Z = \frac{\pi d_p^2 (P - P_d)}{(2 \pi mkT)^{1/2}} \tag{38}$$

The rate of change of particle volume is

$$\frac{dV}{dt} = n_Z V_m \tag{39}$$

where $V_m = \frac{M}{\rho_p N_a}$, M being the molecular weight of the material of which the particle us composed, ρ_p its density and N_a Avogadro's number. Substitution of $V = \pi/6\ d_p^3$ into eqn. (39) gives

$$\frac{\pi}{6} \frac{d}{dt} (d_p^3) = n_Z V_m = \frac{\pi d_p^2 (P - P_d)}{(2\pi mKT)^{1/2}} \cdot \frac{M}{\rho_p N_A} \tag{40}$$

Simplifying the above equation gives

$$\frac{d(d_p)}{dt} = \frac{2 M (P - P_d)}{\rho_p N_a (2\pi m kT)^{1/2}} \tag{41}$$

Equation (41) gives the rate of growth of particles of size less than the gas mean free path. It is noteworthy that the growth rate in this case is independent of the particle size.

For particles larger than the gas mean free path, growth depends upon the rate of diffusion of molecules to the particle surface. The rate of collision of vapor molecules with a particle of diameter d_p can then be expressed similarly to the coagulation rate expression as

$$n_Z = 2\pi d_p D_V N \tag{42}$$

where D_V is the diffusion coefficient of a vapour molecule. The diffusion coefficient of the particle is negligible compared to D_v. In eqn. (42), N is the net concentration of vapour molecules and can be expressed in terms of partial pressures as

$$N = \frac{P - P_s}{kT} \tag{43}$$

In eqn. (43) the vapour pressure, P_s, at the temperature of the particle now replaces P_d used in eqn. (41), because of a negligible Kelvin effect. Following the procedure used for the case of particles smaller than the gas mean free path, the rate of particle growth becomes

$$\frac{d(d_p)}{dt} = \frac{4 D_v M(P - P_s)}{RT \rho_p d_p} \tag{44}$$

The above equation gives the rate of growth of particles for particles larger than the gas mean free path and shows that the rate is inversely proportional to the particle size. This means that the rate of growth is rapid for small particles but as particles grow larger their growth slows down.

For a soluble particle, condensed-phase formation is complicated by the dissolution process. Considering for example water vapor condensation, a small dry hygroscopic particle will remain solid up to a certain characteristic relative humidity less than 100% at which it dissolves in water to form a saturated solution. Table 6.1 gives the relative humidities for dissolution of large crystals of different salts.

The humidity values given in Table 6.1 will vary with crystal size due to the Kelvin effect. The size of the droplet formed on dissolution of the salt crystal depends on the solubility. For the same mass concentration, salts that absorb more water form more dilute solutions and larger droplets than salts which absorb less water to form concentrated solutions and therefore smaller droplets. Sodium chloride is an example of the former kind and ammonium salts are examples of the latter kind.

TABLE 6.1

Relative Humidity and Concentration for Saturated Solutions at 20°C (Fr77)

Salt	Relative Humidity (%)	Solubility (g/100 g H_2O)
$(NH_4)_2SO_4$	81	75.4
NaCl	75.7	36
NH_4NO_3	62 (25°C)	192
$CaCl_2.6H_2O$	32	74.5

Insoluble nuclei can be classified into those which are easily wetted and those which are not. Particles with easily wettable surfaces can rapidly take on the appearance of a droplet and may be considered as pure drop nuclei. The Kelvin equation can be used in this case with a lower limit on nucleus size in order to predict droplet growth or evaporation. However, if the particle surfaces are not wettable, condensation is much more difficult because the condensing liquid tends to pull into small spheres on the particle surface. A liquid coating is only formed when the entire surface is covered with these spheres. Condensation on such particles can therefore only be achieved at high supersaturation. The role of insoluble nuclei in the condensation process is not been fully understood to date and more work is required in this area.

In general, the extremely high supersaturation required for homogeneous nucleation is not necessary for heterogeneous nucleation since condensation of a vapor takes place in the presence of small particles. These particles (condensation nuclei) can range in size from near molecular dimension to particles greater than 1 μm. The concentrations of these nuclei, the sources of which were discussed in section 2.1, can range from 100 particles/cm^3 to > 10^6 particles/cm^3 in the atmosphere. However, only a small fraction of the aerosol enters into the condensation process. The largest and most soluble nuclei are activated first followed by smaller and less soluble nuclei. The degree of supersaturation present in the atmosphere and the rate of cooling of air are the important factors in the process of condensation.

7. ATMOSPHERIC IONS AND NUCLEATION

Atmospheric ions have always formed an important part of studies on the atmospheric environment. Atmospheric ions control the electrical properties of the atmosphere and may also play a role in aerosol formation and trace gas processes. Their interactions with atmospheric molecules, atoms, electrons and ions involve large collision cross-sections, and result in increased chemical reactivity and greater molecular cluster formation through electrostatic bonding.

The nucleation process can be facilitated by the presence of ions. Wilson (Wi97) demonstrated in his original cloud chamber experiments that the supersaturation required for the initiation of nucleation is considerably reduced in the presence of ions in a supersaturated system. This reduction means that the growth and subsequent deposition of particles in the respiratory tract may be affected by the presence of ions in the atmosphere. The sources and abundance of ions in the atmosphere and their growth in humid air are discussed in the following sections.

7.1 Generation and Behaviour of Ions in the Atmosphere

An ion is generated when a particle of sufficient kinetic energy collides with a gas molecule or an atom and dislodges an electron from its outer electron shell. The colliding particle can belong to any of the following four ionizing agents in the atmosphere: corpuscular radiation (α- or β-rays of radioactive origin); electromagnetic radiation (γ-rays of radioactive origin or shortwave ultraviolet radiation); cosmic radiation; and ions or electrons which have acquired sufficient energy for impact ionization in strong electric fields.

Ionization occurs easily in atoms of low ionization potential (the energy required to remove an electron from the outer shell). The ionization potentials of some gaseous constituents of the atmosphere (for clean air) are listed in Table 7.1. Neither the positive molecular ion nor the electron are stable in air at atmospheric pressure. The electron attaches to a neutral molecule in less than 1 μsec, with preference for oxygen and water molecules. The tendency of electrons to attach to different types of molecules is determined by the electron affinity of the molecules. Free electrons are, however, present in the higher levels of the atmosphere where the pressure is lower. Ion formation in the atmosphere is schematically represented in Fig. 7.1.

Molecular ions tend to enlarge by attaching to neutral molecules to form clusters. These clusters are held together by electrostatic forces between the central ionized molecule and the neutral (polar) molecules. The electrostatic bond becomes weaker with increasing cluster size. Cluster size has been found to be inversely proportional to the absolute temperature. The mobility (that is, the coefficient of proportionality between the migration velocity in the electric field and the electric field intensity) of negative ions is generally 30-40% higher than that of positive ions (Is71). Mobility increases with increasing temperature and decreases with increasing pressure. In air-vapour mixtures, the mobility decreases in a disproportionate manner when approaching the saturation point of the vapour. Negative ions react strongly in air-vapour mixtures. The formation of negative complexes is affected appreciably by the presence of water vapour. Siksna (Si69) has discussed the role of water in the production of ions in atmospheric air. In humid air, pri-

TABLE 7.1

Ionization Potentials of Atmospheric Constituents in U.S. Standard Atmosphere - from (Mo69)

Neutral gas (in order by decreasing ionization potential)	I.P. (eV)	Concentration (molecules cm^{-3})
He	24.46	1.41×10^{14}
Ne	21.47	4.89×10^{14}
A	15.68	2.51×10^{17}
H_2	15.6	1.34×10^{13}
N_2	15.51	2.10×10^{19}
CH_4	14.5	5.39×10^{13}
CO	14.1	5.39×10^{13}
CO_2	13.7	8.45×10^{15}
Kr	13.93	3.07×10^{13}
(O	13.61	7.15×10^{4})†
SO_2	13.1	2.69×10^{13}
N_2O	12.9	1.35×10^{13}
(H_2O	12.59	5.3×10^{17})*
Xe	12.08	2.34×10^{12}
O_2	12.07	5.63×10^{18}
NH_3	11.2	5.39×10^{12}
NO_2	11.0	5.39×10^{11}
O_3	11.7	1.35×10^{12}†
(H_3O	7.5	--)
I_2	9.7	2.69×10^{11}
NO	9.25	6.72×10^{11}

Values in brackets are not listed in the U.S. Standard Atmosphere.

* Assuming a relative humidity of 63% at 25°C.

† Without regarding production of O and O_3 respectively by means of photochemical reactions in polluted atmospheres.

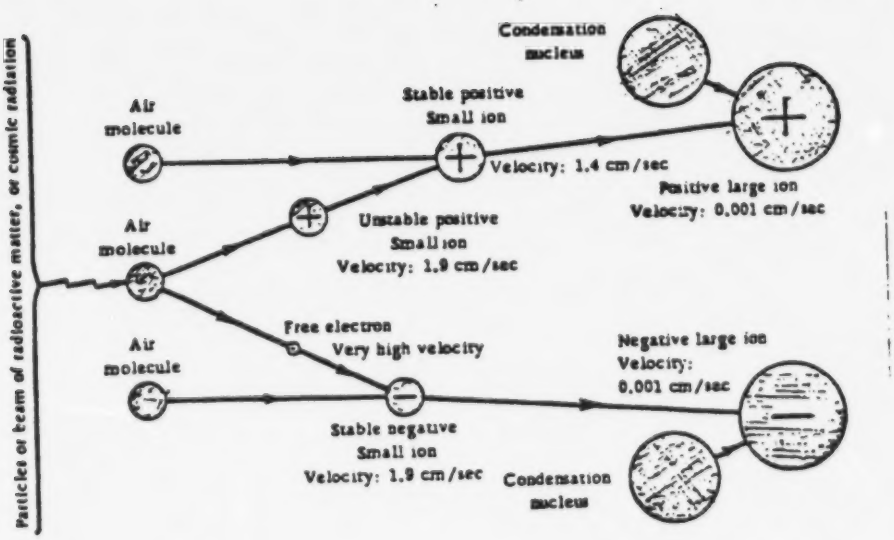

Fig. 7.1. Schematic representation of ion formation in the atmosphere (Is71).

mary ions become hydrated, resulting in a lower diffusion coefficient and a lower ion-ion recombination coefficient. Atmospheric ions can be classified into five categories as shown in Table 7.2.

An overall representation of the ions and natural aerosols in the atmosphere is given in Fig. 7.2.

Atmospheric radioactivity plays a significant role in ionization close to the earth's surface. Because of the constant emanation of the radioactive gases radon and thoron from the soil, radioactivity is present in the atmosphere close to the ground. The average concentration of radon in the atmosphere near ground level is estimated to be in the range 10^{-16} to 10^{-15} Ci/cm^3. At a height of a few metres above ground under normal conditions, there are formed of the order of 10 pairs of ions/cm^3, of which 20% are attributable to cosmic rays and the remainder to radioactivity of the air and soil (Br70). The most significant contribution is due to α-disintegrations in the air, which result in about 2 x 10^5 ion pairs compared to about 2 x 10^4 ion pairs from β and γ disintegrations combined. The radioactivity in the soil which contributes to ion production in the atmosphere near the ground consists only of β- or γ-radiation.

Of the 300-500 small ion/cm^3 normally present in air at ground level, <10% may survive in polluted atmosphere. The concentration of positive small ions is in general approximately 20% greater than that of negative ions. Small radioactive ions are generated from the decay of radon and thoron. These ions are almost exclusively the positively charged ^{218}Po (RaA) and ^{212}Pb (ThB) atoms, the decay products of radon (^{222}Rn) and thoron (^{220}Rn). Orbital elections of radon and thoron are

TABLE 7.2

Mobility and Size Limits of Individual Ion Types in the Atmosphere (Is71)

	Designation	Mobility limits	Size limits
Primary atmospheric ions	Small ions	$k > 1.0$ cm^2/(volt.sec)	$r < 6.6 \times 10^{-8}$ cm
Secondary atmospheric ions	Small intermediate ions	$1.0 > k > 0.01$	$6.6 < r < 78$
	Large intermediate ions	$0.01 > k > 0.001$	$78 < r < 250$
	Langevin ions	$0.001 > k > 0.00025$	$250 < r < 570$
	Ultra-large	$k < 0.00025$	$r > 570$ (up to $r = 10^{-5}$ cm)

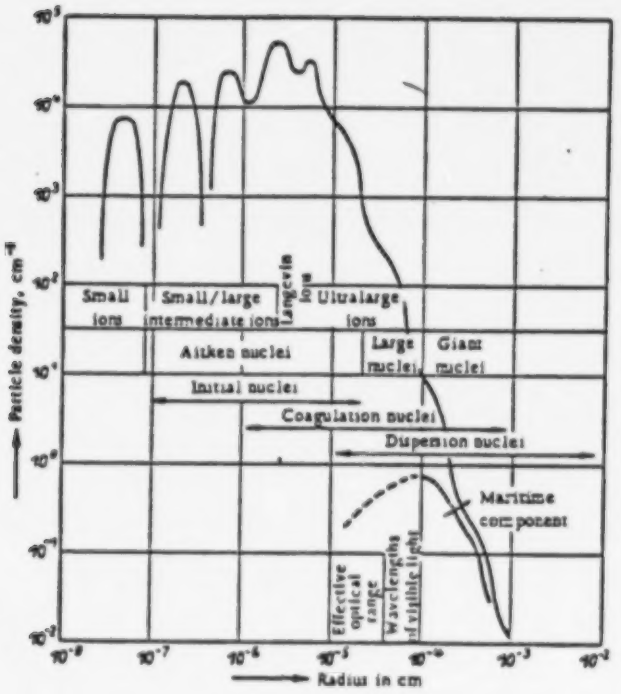

Fig. 7.2. Graphic survey of natural aerosols in air with a high nuclei concentration. The ordinate gives particle density relative to the unit of the logarithmic abscissa. The ion classification (Is71) and the particle sizes, as well as the ranges of the individual types of nuclei with regard to their formation, are plotted.

stripped from the outermost shell by the departing alpha particle. It should be noted that since the respective decay products ^{218}Po and ^{212}Pb are alpha emitters, they are capable of producing further ionization in the atmosphere surrounding them. The mean concentrations of ^{218}Po and ^{212}Pb in the atmosphere near the ground are ~1-2 x 10^{-4} atoms/cm^3 and ~7.5 x 10^{-6} atoms/cm^3, respectively (Br70).

A large ion of radius between 0.01 and 1 μm may carry one or more charges. Generally the concentrations of positive and negative large ions are similar. However, these concentrations may differ where the large ions are produced as a result of human activities. Junge (Ju54) represented the size distribution of large ions near the ground by the equation:

$$\frac{dN}{d(\log R)} = \frac{C}{R^3} \tag{45}$$

where R is the particle radius, dN is the number of ions contained in the range d log R and C is a constant. This equation was later modified for the small ion size distribution to

$$\frac{dN}{dR} = \frac{C}{R^3} \tag{46}$$

The mobility distribution of small radioactive ions in the atmosphere is shown in Fig. 7.3.

Since radioactive ions may become attached to neutral aerosols, be neutralized by ions of opposite charge, and become attached to large ions of opposite charge, it is not simple to estimate theoretically the number of ions remaining free. The number of free ions will depend upon the concentration of aerosols (neutral or charged), the number of charges carried by each particle, and the sizes of free ions and aerosols. From

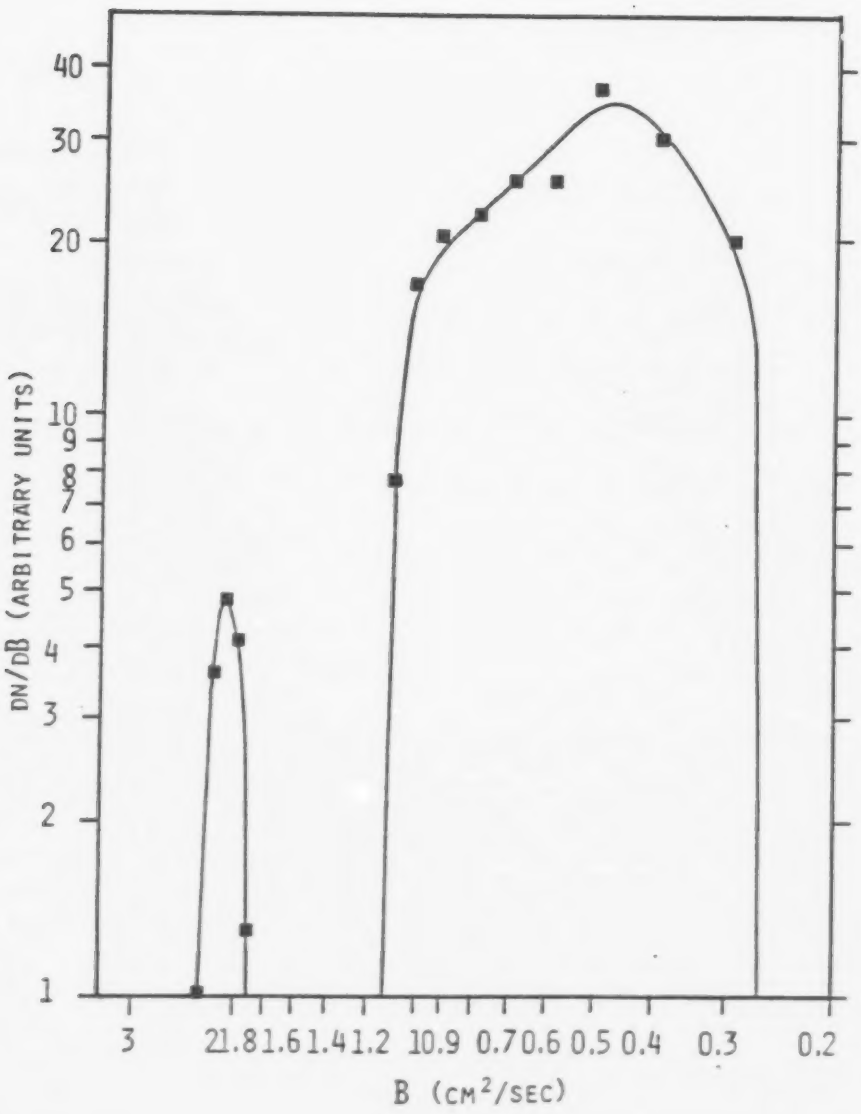

Fig. 7.3. The mobility distribution of small radioactive ions (Br70).

experimental observations, it has been found (Br62, La61, Mo63, Wi52, Re65) that medium condensation nuclei ($R < 0.02$ μm) collect 45-50% of the small ions formed at a minimum radius of 0.01 μm, and 70-75% at a minimum radius of 0.05 μm. Bricard (Br70) has suggested the following mean ratios of concentrations of large radioactive ions (N_{Ra}^{-}, N_{Ra}^{+} or N_{Ra}^{0}) in the atmosphere:

$$\text{For } {}^{218}\text{Po}, \quad \frac{N_{Ra}^{-}}{N_{Ra}^{+}} = 0.4 , \qquad \frac{N_{Ra}^{0}}{N_{Ra}^{+}} = 4 \tag{47}$$

$$\text{For } {}^{212}\text{Pb}, \quad \frac{N_{Ra}^{-}}{N_{Ra}^{+}} = 0.5 , \qquad \frac{N_{Ra}^{0}}{N_{Ra}^{+}} = 5 ,$$

where the superscripts −, + and ^{0} indicate negatively charged, positively charged and neutral, respectively. Wilkening et al. (Wi66) have shown experimentally that radon progeny ions are subject to the same fluctuation that is observed for the total positive small ion content of the atmosphere. Styro and Peston (St68) carried out detailed experimental studies on radioactive ions at different heights above the ground. Their results are shown in Tables 7.3 and 7.4.

An interesting aspect of the presence of ionizing radiation in the atmosphere is its role in the formation of condensation nuclei. The probability of nuclei production from ionization was estimated by Vohra et al. (Vo69) to be $\sim 10^{-5}$ nuclei/ion pair. Their experiments were carried out in a dark room to prevent any possible nuclei formation by photochemical reactions. They used atmospheric air filtered through successive grades of membrane filters to completely remove nuclei and ions from the air. Nuclei formation as a function of absorbed dose is shown in Fig.

TABLE 7.3

Concentration of Radioactive Matter, Rn Decay Products, on Ions of Different Sign and Varying Mobility (St68)

Height above ground, m	Positive ions, 10^{-16} curie/cm^3, %			Negative ions, 10^{-16} curie/cm^3,		
	light	medium	heavy	light	medium	heavy
0.01	0.18 (6)	1.24 (39)	1.79 (55)	0 (0)	0.39 (41)	0.56 (59)
0.5	0.11 (4)	1.06 (40)	1.54 (56)	0 (0)	0.42 (37)	0.72 (63)
2.5	0.05 (3)	0.45 (33)	0.89 (60)	0 (0)	0.20 (27)	0.55 (73)
12.5	0 (0)	0.24 (23)	0.80 (77)	0 (0)	0.13 (15)	0.74 (85)

TABLE 7.4

Radioactivity (%) due to Positive and Negative Ions and Neutral Carriers (St68)

Height above ground, m	Positive ions	Negative ions	Neutral particles	
			%	10^{-16} curie/cm^3
0.01	31.3	9.2	59.5	6.22
0.5	29.1	12.3	58.6	4.77
2.5	27.5	15.0	57.5	2.91
12.5	24.9	21.9	54.2	2.24

7.4.

In more recent experiments, Vohra et al. (Vo84) found considerable enhancement in aerosol formation on introducing radon into an SO_2-O_3-C_2H_2-H_2O (vapour) system. The aerosol concentration was found to increase by a factor of 4 on introducing 100 pCi/m^3 of radon into the reaction vessel. The authors postulate that atmospheric radon and its progeny play important roles in the formation of sulphate and nitrate particles in the atmosphere. These roles are likely to be subject to much research in the future.

7.2 Nucleation on Ions

The role of ions in the process of nucleation was recognized in the early experiments of Wilson in 1897 (Wi97) in which he found that an aerosol cloud can be produced relatively easily in the presence of ions. Wilson carried out these experiments in a chamber in which air was first saturated with water vapour. The chamber contents were then rapidly expanded to produce supersaturation due to the drop in temperature and pressure. Condensation occurred on small particles present in the air inside the chamber. The chamber was then cleared of all particles by repeated expansion and allowing the drops to settle. In the absence of particles, it was observed that droplets formed only at or above a saturation ratio of about four. In subsequent experiments, it was found that at a second critical saturation ratio of about eight, a dense cloud of drops formed. Wilson discovered that condensation could be induced between the two saturation ratios only by introducing air ions. Wilson confirmed this conclusion by exposing the chamber to X-rays between the

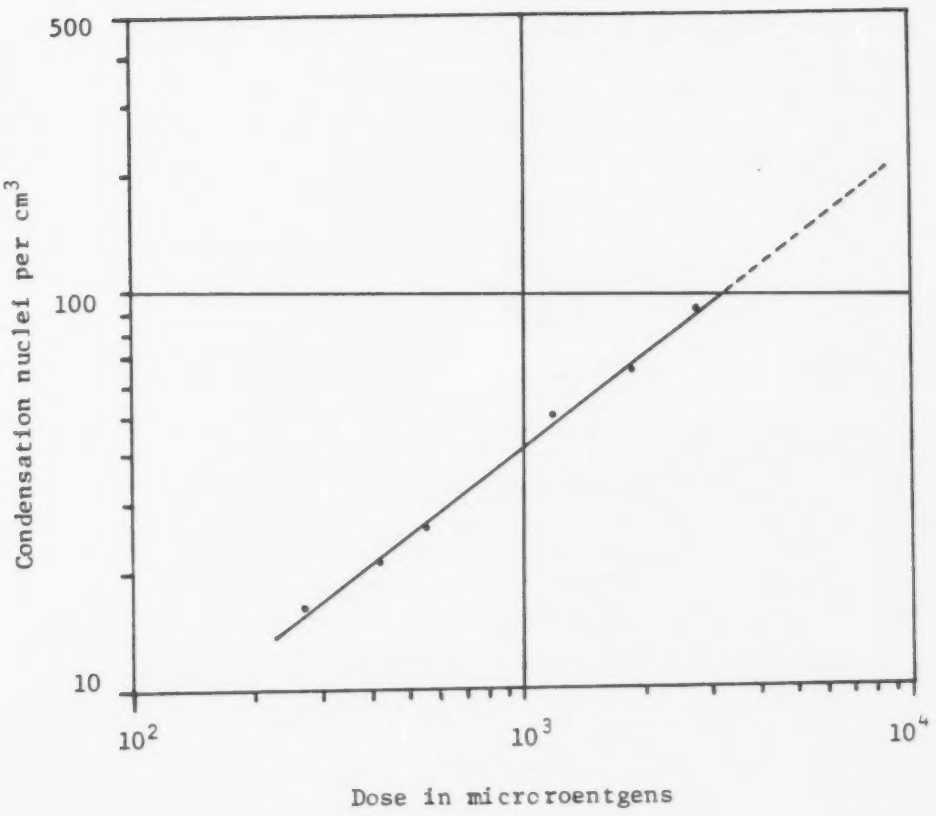

Fig. 7.4. Graph showing increase in nuclei concentration with absorbed dose of natural ionizing radiation (Vo69).

two saturation limits. These experiments proved that the presence of air ions lowers the saturation ratio required for condensation. In Wilson's later experiments, positive and negative ions were separated by an electric field. Positive and negative ions were found to have different nucleating properties for water vapor. At the same temperature ($\sim -6°C$), negative ions were observed to promote condensation at a lower supersaturation than positive ions. Many investigators have confirmed Wilson's experimental results for nucleation on ions. These observations are listed along with Wilson's observations in Table 7.5.

Further insight into the mechanism of nucleation on ions can be gained from Figs. 7.5 and 7.6. Fig. 7.5 is a plot of equilibrium conditions. Droplets grow in the area above the curve and evaporate in the area below the curve. Three cases for condensation and evaporation on an ion are represented by lines A, B and C in the diagram. Reference to Fig. 7.6, which is a free energy plot for cases A, B and C, is helpful in understanding the situation.

Droplets whose saturation ratio, S, places them along line A will either grow or evaporate toward the equilibrium curve, which represents a stable position. Along the line A, at first a growth in size of the particle corresponds to a decrease in the free energy of the particle. However, when the droplet diameter crosses the equilibrium line (the position corresponding to the minimum in the free energy curve for case A in Fig. 7.6), the free energy starts increasing with further increase in the droplet diameter. In order for the free energy to decrease, evaporation must therefore occur. In case B, the equilibrium curve is not intersected at all, which means that at saturation ratios higher than the

TABLE 7.5

Critical Saturation Ratios for Spontaneous Condensation on Ions based on Data from Expansion Cloud Chambers (from (Hi70))

Investigator	Sign of charge	Final temperature (°K)	Ratio of final to initial chamber volume	S_p (crit)
(Wi97)	(-	265	1.25	4.1
	(+		1.31	6.0
(Pr06)	(-		1.24	3.7
	(+		1.31	6.0
(La08)	-	268	1.26	4.2
(An17)	-	268	1.25	4.1
(Po28)	-	267	1.25	3.98
(F134)	-	265	1.25	4.1
(Sc39)	(-		1.25	4.14
	(+		1.28	4.87
(Sa43)	-	265		3.9

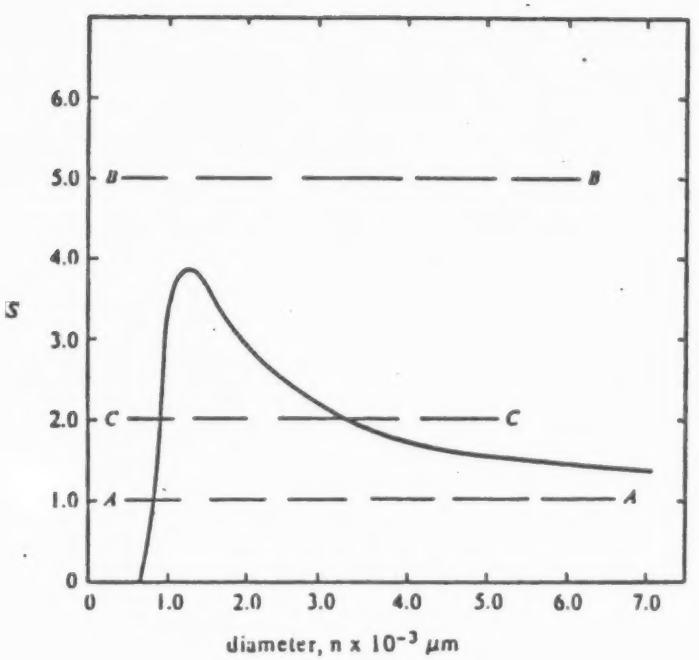

Fig. 7.5. Saturation ratio for water as a function of critical particle diameter, single ion, atmospheric pressure: T = 273°C (Ra84).

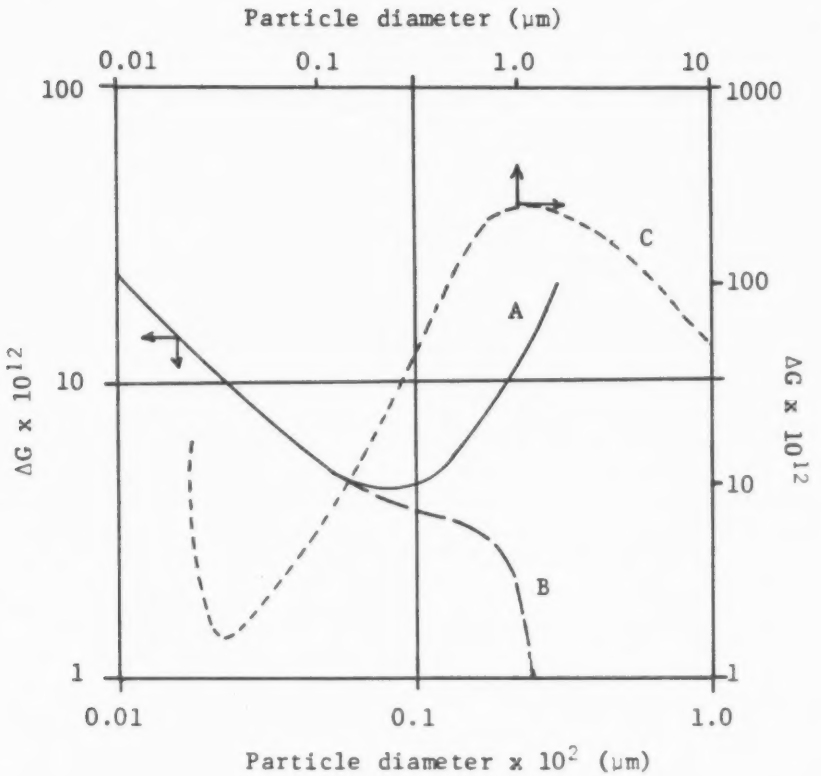

Fig. 7.6. Free energy change as a function of drop diameter for droplet containing single ion (lines A, B and C of Fig. 7.5). Curves A and B follow the left and bottom scale; curve C follows the right and top scale (Re84).

maximum for the curve in Fig. 7.5, charged droplets of any size will grow. Case B explains the formation of cloud in a cloud chamber at a saturation above a critical value. The free energy is always decreasing with increasing droplet size in this case, as shown in Fig. 7.6. Case C is a combination of Case A and Case B. The free energy shows a minimum and then a maximum in Fig. 7.6. Case C represents a growth-evaporation-growth sequence corresponding to the portions of line C outside, below and outside the curve, respectively.

The theoretical aspects of nucleation on ions are not very well understood. Many theories have been proposed but there are still discrepancies between experimental results and theoretical predictions. Many shortcomings in theory have been pointed out. Hidy (Hi70) considers the main shortcoming to be the lack of separate treatment of positive and negative ions. This lack is important because water is polar and may be preferentially oriented in surface layers. Since the water molecule dipole is considered to have its negative end oriented outward in the layers nearest to the surface, the free energy of the surface dipoles is lowered for condensation to occur on negative ions. For positive ions, the molecules would have to turn themselves around and condensation would therefore be more difficult (Re84).

Reviews of the theory of nucleation on charged particles appear in the monographs by Wilson (Wi51) and Fletcher (Fl62). Budd et al (Bu85) have recently described the physical processes involved in the initial growth from an ion to a small droplet.

8. BEHAVIOUR OF AEROSOLS IN A HUMID ATMOSPHERE

8.1 Summary of Previous Investigations

The present state of knowledge in the area of aerosol growth and respiratory deposition in humid atmospheres can be summarized as follows:

1. The nature of airborne aerosols varies greatly according to local conditions. Complex reactions involving chemical and/or photochemical reactions and ionization can result in the formation of new products in the form of trace gases or aerosols. The role of ionization in aerosol formation is poorly understood.

2. The deposition dynamics of aerosols in the respiratory tract is determined by the nature of the particles (size, shape, chemical nature, solubility, etc.) and the anatomy of the lung. Hygroscopic particles deposit according to their actual diameter after growth. Particles smaller than 0.5 μm are largely deposited by diffusion whereas particles larger than 1.0 μm are largely deposited by gravitational sedimentation and inertial impaction. Straight fibres are largely deposited by interception.

   Particle charge leads to enhanced respiratory deposition when the number of charges/particle is greater than ten.

3. The growth of hygroscopic particles in humid atmospheres is appreciable (a factor of 3 - 7) and is strongly dependent upon humidity. The relative humidity in the human respiratory tract has been reported to be in the range 95-100%. In this range, knowledge of the exact value of the humidity is critical in making predictions about the growth of hygroscopic particles.

4. Soluble nuclei become droplets at considerably less than 100% R.H and may already be in droplet form before being inhaled.

5. The growth of insoluble particles has not been studied extensively.

Although published results are not consistent, growth on insoluble particles at less than 100% R.H. appears to occur, although less than on soluble particles. The wettability of the surface of an insoluble particle seems to be important in determining whether or not such a particle will grow.

6. Supersaturation may be produced in the respiratory system as a function of the ambient climatic conditions. At low ambient temperatures, supersaturation may be achieved by mixing hot and cold air in the lung. This mixing may result in the growth of inhaled particles.
7. Chemical reactions which lead to the formation of condensable species are poorly understood.
8. Theories of nucleation, especially nucleation on ions, are not satisfactory at present.
9. The growth of particles is enhanced by the presence of ions because the required degree of supersaturation is less. The presence of ionizing species such as radon/thoron and their progeny may therefore affect the growth of particles in the respiratory tract.

8.2 Scope of the Present Investigations

Studies have previously been conducted to determine the growth factor of NaCl aerosols (hygroscopic) and kerosene aerosols (hydrophobic) on inhalation (Be81,Tu84). However, none of the previous studies has been conducted in the presence of radon progeny. Because radon progeny are present in uranium mines, the present study was undertaken. The purpose of the study was to measure changes in aerosol and activity size

distributions following exposure to humidity and temperature conditions similar to those in the respiratory tract.

Many uranium mines are diesel operated and have high concentrations of diesel aerosols. Since it is difficult to generate diesel aerosols on a steady state basis under laboratory conditions, the very similar kerosene heater aerosols were used.

The properties of kerosene aerosols (from burning a kerosene heater) have been studied in detail by Tu and Hinchliffe (Tu83). These aerosols were found to consist of mainly carbon black with trace amounts of chromium and nickel. The aerosols consisted of mixtures of individual solid and hollow spheres with sizes up to 0.3 μm and clusters and chain aggregates in the range of 0.1-3 μm. Carbon chain aggregates were found to be dominant. The mass median diameter of the kerosene aerosols was found to be 0.092 μm with a geometric standard deviation of 1.86. Tu and Knutson (Tu84) reported generation of 0.03-0.4 μm aerosols from a kerosene heater.

Diesel aerosols are mainly clusters or chains (~ 10 μm) formed by aggregates of spherical primary particles. The primary particles are basically combustion generated soot particles from 0.01-0.08 μm with most in the range 0.01-0.03 μm (Am82). Diesel particles may contain trace metals from fuel additives, hydrocarbons, sulphate and water. However, 90% of diesel particles generally consist of soot.

The aerosol and activity size distributions were observed under ambient conditions and under simulated respiratory tract conditions with respect to humidity and temperature (100% R.H., 37°C) following exposure to a radon chamber in which radon progeny atoms attach to the aerosols.

Initial conditions of temperature and relative humidity for the aerosol were 20°C and 35% R.H. The growth factors for count median aerosol and activity diameters were determined for both NaCl aerosols and kerosene aerosols.

9. MEASUREMENT OF THE GROWTH FACTORS OF AEROSOL AND ACTIVITY SIZE IN A HUMID ATMOSPHERE

9.1 Experimental Technique

The experiments consisted of aerosol generation (described in detail in Appendix A), mixing of aerosols with radon progeny in a radon chamber, sampling of aerosols both directly and through a humidification system, and measurement of aerosol and activity size distributions. Subsequent data analysis is required in order to determine growth factors. Only the humidification system and the sampling technique are discussed in this section. The aerosol and activity size distribution measurements are described in the two subsequent sections.

Conditions similar to those in the respiratory tract (37°C, 100% R.H.) were created inside a 1 metre long glass cylinder of 3 cm diameter. An absorbent material was wrapped around a 1 cm diameter wire screen (3 openings per inch) cylinder and placed inside the glass cylinder. The length of the wire screen cylinder was 95 cm. In order to prevent air leakage from the wire screen cylinder, plastic tape was wrapped tightly on the absorbent material. Finally, electrical heating tape was wrapped around the wire screen cylinder and it was placed inside the glass cylinder. The cylinder was closed with a rubber stopper through which holes were made for an air-inlet tube (4 mm I.D.), a similar tube with capillary end for water inlet and electrical leads from the heating tape. The rubber stopper was put in place and sealed off with silicone sealant. A similar glass cylinder with similar wire screen cylinder wrapped with absorbent material and plastic tape, but without the heating tape, was

also prepared to act as the dry tube for sampling aerosols at ambient temperature and humidity. Such an arrangement has been used previously to humidify air (Hi85).

The two cylinders were installed on a table through which two 1 cm diameter holes had been drilled to correspond to the wire screen cylinder diameter. Both cylinders were held in place by short cylindrical supports made from steel. Short protruding glass tubes inserted through the holes drilled in the table top ensured correct positioning of the wire screen cylinders on top of these holes. The glass cylinders were further secured and sealed in position with silicone sealant. One 15 cm x 18 cm rectangular wooden chamber was secured under the table for each glass cylinder, with a hole in the centre to correspond to the hole under each wire screen cylinder. Each sampling chamber was 10 cm deep. The purpose of these sampling chambers was to facilitate the aerosol and activity size distribution measurements. Affixed to each side of each sampling chamber were steel strips having threaded holes so that diffusion batteries (specially modified for these experiments by fixing rectangular steel plates around the inlets) could be mounted under the boxes with the help of screws. The arrangement is shown in Fig. 9.1. Diffusion batteries are described in detail in the next section.

At the top end of each glass cylinder, each air inlet tube is connected by rubber tubing to an outlet tube from the radon chamber. The radon chamber used for these experiments is described in detail elsewhere (Bu78). The water inlet tube in the humidifying tube is connected to a water reservoir via plastic tubing with a screw clamp to control the flow of water to the absorbent material. The heating tape is plugged into a

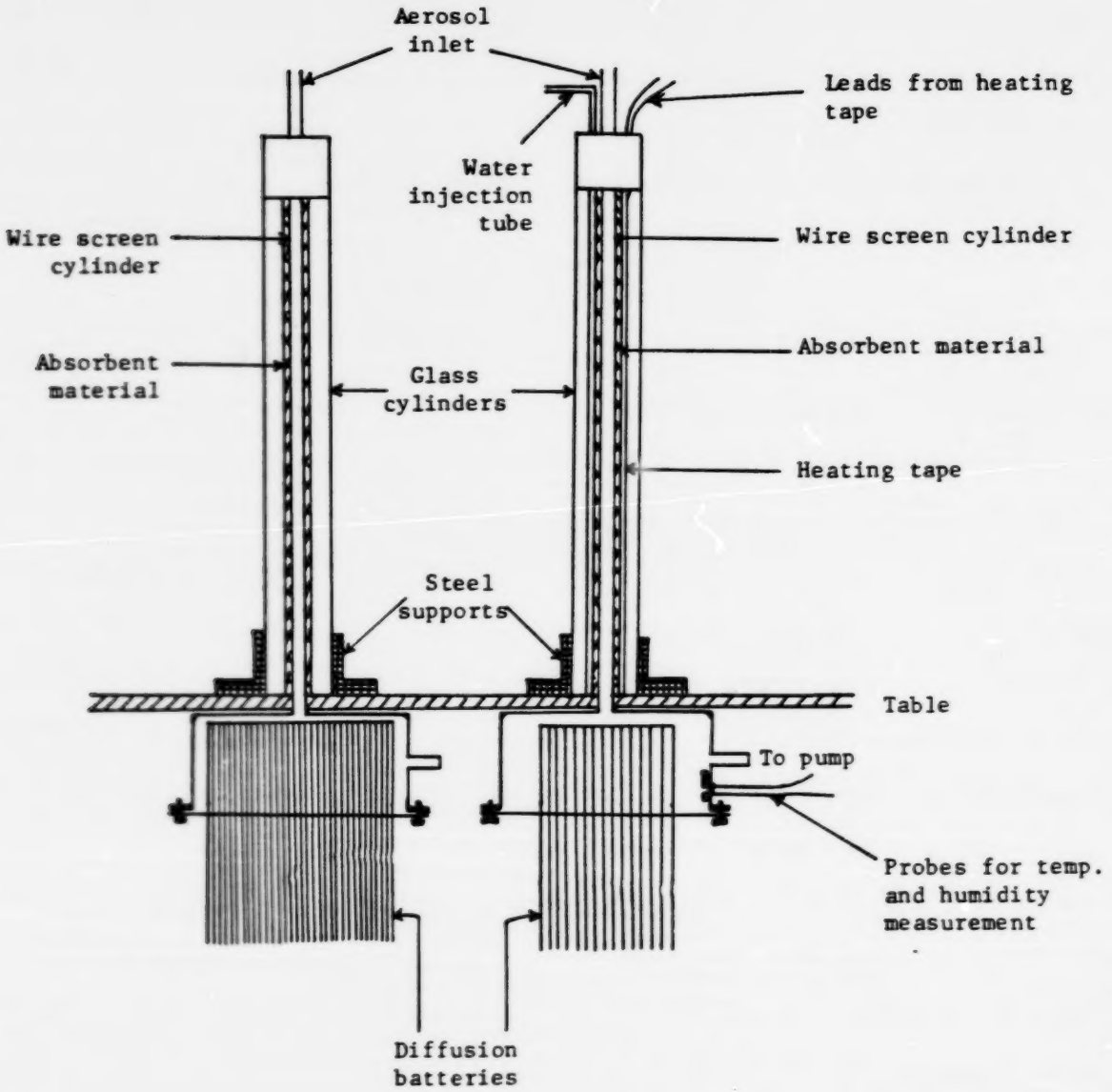

Fig. 9.1. Experimental arrangement for inhaled aerosol measurements.

variable transformer in order to control the temperature. The humidity and temperature measuring probes are located inside the sampling chamber under the humidifying tube. The probes were installed by passing their leads through a rubber stopper placed in a hole cut on one side of the sampling chamber. The rubber stopper is sealed with silicone sealant to prevent air leakage. The temperature and humidity probes are held against the inside sampling chamber wall. The probes could be pulled out in order to measure humidity or temperature at the exit end of the humidified tube. Rubber gaskets were glued on the edges of each sampling chamber for minimizing leakage during diffusion battery measurements.

Hicks and Megaw (Hi85) have taken the time for inspired air to pass from the nose to the terminal bronchioles to be 1 sec. Various other times have been used for the residence times of inspired air (Table 10.3). For this work, the residence time of the air through the humidification tube was chosen to be 1 sec.

The volume available inside the wire screen cylinder was used for residence time determination. A flowrate of 4.2 L/min corresponds to 1 sec residence time in the wire screen cylinder. A flowrate of 4.2 L/min was therefore constantly maintained through the humidified tube in order to keep conditions inside the tube similar to those in the respiratory tract. The temperature and relative humidity was checked between measurements using a YSI Model 91 Dew point hygrometer.

Since aerosol concentrations were monitored with a condensation nuclei counter (Model RICH 200, Environment One) with a sampling flowrate of 2.5 L/min, the sampling pump (Model P-4000, Dupont) for the activity size distribution was also adjusted for a flowrate of 2.5 L/min. However,

a make-up pump was run at all times, during both aerosol and activity size distribution measurements, at a flowrate of 1.7 L/min in order to deliver a total 4.2 L/min flowrate to produce a 1 sec residence time. The inlet for this pump was connected by rubber tubing to a small outlet at one side of each sampling chamber.

For each experiment, aerosol generation was started at least one hour ahead and aerosols were allowed in the radon chamber in order to let radon progeny attach to the aerosols. For NaCl aerosols, compressed air at about 300 kPa absolute pressure was used to drive the aerosols into the radon chamber. For kerosene aerosols, a negative pressure equivalent to about 1 cm of water was created inside the radon chamber by using a suction pump at the exhaust end of the chamber. Kerosene aerosols were led into the radon chamber through a system described in detail in Appendix A.

Initially atmospheric aerosols were also to be studied. An arrangement was made to lead the atmospheric aerosols from the adjoining street into the radon chamber. However, due to heavy traffic on the street, the aerosol concentrations inside the radon chamber were found to fluctuate in the range 40,000-90,000/cm^3 within minutes. These fluctuations were considered unacceptable for the experiments which spanned a time period of about 1 hour. No measurements for atmospheric aerosols were therefore obtained.

The experimental schedule is presented in Appendix C.

9.2 Aerosol Size Distribution Measurement

The aerosol size distribution measurements were carried out with

three diffusion batteries, a reference and a condensation nuclei counter. Each diffusion battery used for these experiments is an assembly of rectangular aluminum plates with spacings and dimensions as specified in Table 9.1. The three diffusion batteries were fitted with adapter plates so that the diffusion batteries could be mounted at the exit end of the glass cylinders. The diffusion battery placement under each tube is shown in Fig. 9.1.

The reference was an open face magnetic filter holder fixed at the centre of a rectangular steel plate by cutting an opening through the plate. The assembly of the filter holder, cylinder and plate could be secured under each sampling chamber with the help of screws in the same manner as the diffusion batteries with their adapter plates.

By connecting the reference and the exit end of the diffusion batteries to the condensation nuclei counter through rubber tubing and recording aerosol concentrations according to the experimental protocol given in Appendix C, penetrations of aerosols through the diffusion batteries were determined.

The size distribution of aerosols can be described by a lognormal size function (Da74):

$$C(d) = \frac{1}{d\sqrt{2\pi}\ \ln \sigma_g} \exp\left(-\frac{1}{2}\left(\frac{\ln(d/\bar{d})}{\ln \sigma_g}\right)^2\right) \qquad (48)$$

where $dC(d)$ = number size distribution function, $n(d)$

$\bar{d}$ = count median diameter of the distribution

σ_g = geometric standard deviation of the distribution

d = particle diameter

TABLE 9.1

Dimensions of Diffusion Batteries

D.B. no.	No. of channels	Width (cm)	Length (cm)	Spacing between plates (cm)
3	25	10	19	0.08
4	50	10	30	0.04
5	140	10	43	0.04

The count median diameter and the geometric standard deviation can be determined using equation (48) and the experimentally obtained diffusion battery penetrations as outlined below. The calculation technique used is based upon an iterative, direct search optimization technique utilizing random numbers and reduction of the size of the search region developed by Luus and Jaakola (Lu73). An optimal fit is obtained of the kth approximation of the size distribution $n^{(k)}(d)$ to the actual distribution n(d) using the experimental diffusion battery data.

The probability of a particle passing through a diffusion battery is

$$P = \sum_{i=1}^{\infty} a_i e^{-b_i \mu} \qquad (49)$$

where μ = 2 WLD/FH for a diffusion battery composed of rectangular plates

W = width of each rectangular plate (cm)

L = length of each rectangular plate (cm)

D = diffusion coefficient of the particle (cm^2/s)

F = volume flowrate through a single channel in the diffusion battery (cm^3/s)

2H = height of a plate in the diffusion battery (cm) (2H << W).

The penetration constants a_i and b_i for parallel plate diffusion batteries are:

$a_1 = 0.91035$, $a_2 = 0.5314$, $a_3 = 0.01529$, $a_4 = 0.0068$,

$b_1 = 1.88517$, $b_2 = 21.4317$, $b_3 = 62.3166$, $b_4 = 124.5$

The experimentally measured penetration, g, of aerosols through a diffusion battery is related to the theoretically calculable penetration

probability, $P_j.(d)$ by

$$g_j = \int_0^\infty P_j.(d)\ n(d)\ d(d) \qquad (50)$$

where n(d) is the required aerosol size distribution.

The aim of the optimization calculation therefore is to minimize the difference between g_j as given by eqn. (50) and the approximation $g_j^{(k)}$ where $g_j^{(K)} = \int_0^\infty P_j(d)\ n^{(k)}(d)\ d(d)$

Some constraints on the values of d and σ_g are required to ensure a reasonable solution.

The count median diameter, d, and the geometric standard deviation, σ_g, were calculated by using the experimental diffusion battery penetrations, g_j, as input for a computer program based on the optimization procedure described earlier.

9.3 Activity Size Distribution Measurement

For the activity size distribution measurements, 25 mm Millipore Type AA membrane filters were used in in-line filter holders placed between the diffusion batteries (or the reference) exit end and the sampling pump inlet. The sampling pump was run for 5 minutes for each sample. The filter was then removed and counted according to the experimental protocol in Appendix C. A sampling time of 5 minutes was used with counting from 40-45 minutes after sampling, in accordance with the Kusnetz method for determining radon progeny Working Level (Ku56). The ratio of the alpha activity on each filter from a diffusion battery sample to the alpha activity on the reference filter gave the experimental penetrations for activity size distributions. These experimental

penetrations were then used in a computer program, as outlined in the previous section, to determine the count median diameter and the geometric standard deviation for the activity size distribution in each case.

The reference filters for both the dry tube and the wet tube were counted according to a three counting interval scheme of 2-5, 9-25 and 40-45 minutes after sampling. These counts were used to determine the radon progeny concentrations in the radon chamber, and, from these, the age of the air.

The following equations were used to determine the concentrations C_1 of ^{218}Po, C_2 of ^{214}Pb and C_3 of ^{214}Bi in pCi/L:

$$V\eta C_1 = 0.128292\ I_1 - 0.053882\ I_2 + 0.124626\ I_3$$

$$V\eta C_2 = -0.012199\ I_1 - 0.003780\ I_2 + 0.058870\ I_3$$

$$V\eta C_3 = -0.005391\ I_1 + 0.019719\ I_2 - 0.056330\ I_3$$

In the above set of equations, V is the sampling flowrate, η is the alpha counter efficiency and I_1, I_2, I_3 represent the counts observed over the counting intervals 2-5, 9-25 and 40-45 minutes after sampling, respectively. The relative standard deviations for concentration measurement using eqns. (51) were 0.23, 0.09 and 0.19 for ^{218}Po, ^{214}Pb and ^{214}Bi, respectively.

10. RESULTS AND DISCUSSION

10.1 Results

The raw data for aerosol and activity size distributions including the experimentally obtained penetration fractions for the diffusion batteries, are given in Appendix B. Derived data for aerosol and activity size distributions together with the growth factors are presented in Table 10.1. The mean growth factor for the aerosol size distribution of NaCl aerosols was found to be ~ 1.9 ± 0.4 (standard deviation) and for kerosene aerosols ~ 1.3 ± 0.2 (standard deviation. For the activity size distribution, the mean growth factor for NaCl aerosols was ~ 1.2 ± 0.1 (standard deviation), and for kerosene aerosols ~ 1.3 ± 0.2 (standard deviation). The last column in Table 10.1 gives the activity median diameter of a size distribution resulting from the attachment of radon progeny (diffusion coefficient = 0.05, thermal diffusion velocity = 1.38 x 10^4 cm/s) to the aerosol size distribution in the first column, as calculated from the hybrid theory of attachment (Ba87).

The NaCl aerosols ranged in count median diameter from 0.035 μm to 0.068 μm. The kerosene aerosols were smaller, namely 0.015-0.024 μm. The aerosol concentration range was 25,000-100,000/cm^3 for NaCl aerosols, and 75,000-100,000/cm^3 for kerosene aerosols. The radon progeny concentrations are given in Table 10.2.

The results of the present study are compared with previous investigations on growth factor of aerosols in Table 10.3.

10.2 Discussion

Growth of NaCl aerosol at 20°C and 35% R.H. on being subjected to 37°C at 100% R.H. for 1 second was greater than for kerosene aerosol, as

TABLE 10.1

Aerosol and Activity Size Distribution Data and Growth Factors

Date	Input aerosol concn. #/cm^3	Aerosol size distribution*				Activity size distribution*				Theoretical Model** AMD (μm)
		CMD (μm)	G.F.	GSD	P.I.	CMD (μm)	G.F.	GSD	P.I.	
1. NaCl Aerosols										
Nov 28/86	~ 40,000	0.057 (D.T.)*	1.60	1.94	0.1	0.086 (D.T.)	1.08	1.54	0.01	0.123
		0.091 (H.T.)*		1.45	0.07	0.093 (H.T.)		1.83	0.09	0.116
Dec 2/86	~ 90,000	0.057 (D.T.)	1.98	1.96	0.07	0.075 (D.T.)	1.11	1.91	0.01	0.125
		0.113 (H.T.)		1.63	0.01	0.083 (H.T.)		1.55	0.04	0.167
Dec 3/86 (1st expt.)	~ 25,000	0.036 (D.T.)	1.97	2.11	0.006	0.100 (D.T.)	1.18	1.27	0.08	0.098
		0.071 (H.T.)		1.57	0.03	0.118 (H.T.)		1.26	0.12	0.102
Dec 3/86 (2nd expt.)	~ 100,000	0.049 (D.T.)	2.59	2.61	0.06	0.075 (D.T.)	1.24	1.32	0.10	0.209
		0.127 (H.T.)		2.41	0.02	0.093 (H.T.)		2.59	0.05	0.371
Dec 4/86 (1st expt.)	~ 25,000	0.035 (D.T.)	1.31	1.95	0.06	0.074 (D.T.)	1.09	1.32	0.10	0.080
		0.046 (H.T.)		1.62	0.02	0.081 (H.T.)		1.59	0.01	0.071
Dec 4/86 (2nd expt.)	~ 70,000	0.048 (D.T.)	1.69	1.5	0.03	0.062 (D.T.)	1.34	1.87	0.03	0.065
		0.081 (H.T.)		1.48	0.06	0.083 (H.T.)		1.43	0.06	0.106
Feb 16/87 (1st expt.)	~ 80,000	0.051 (D.T.)	2.04	2.06	0.05	0.050 (D.T.)	1.40	2.32	0.07	0.126
		0.104 (H.T.)		1.73	0.004	0.070 (H.T.)		2.34	0.03	0.170
Feb 16/87 (2nd expt.)	~ 80,000	0.068 (D.T.)	1.72	2.09	0.09	0.060 (D.T.)	1.17	2.49	0.09	0.167
		0.117 (H.T.)		2.51	0.08	0.070 (H.T.)		2.14	0.09	0.377

TABLE 10.1 (cont'd)

Date	Input aerosol concn. #/cm^3	Aerosol size distribution*				Activity size distribution*				Theoretical Model** AMD (μm)
		CMD (μm)	G.F.	GSD	P.I.	CMD (μm)	G.F.	GSD	P.I.	
2. Kerosene Aerosols										
Feb 3/87	~ 80,000	0.024 (D.T.)	1.21	1.73	0.02	0.023 (D.T.)	1.56	2.78	0.03	0.043
(1st expt.)		0.029 (H.T.)		1.76	0.09	0.036 (H.T.)		1.92	0.01	0.053
Feb 3/87	~ 70,000	0.017 (D.T.)	1.18	2.30	0.02	0.038 (D.T.)	0.89	2.13	0.03	0.063
(2nd expt.)		0.020 (H.T.)		2.25	0.02	0.034 (H.T.)		1.78	0.02	0.069
Feb 4/87	~ 85,000	0.017 (D.T.)	1.18	1.98	0.03	0.026 (D.T.)	1.42	2.22	0.003	0.042
(1st expt.)		0.020 (H.T.)		2.07	0.01	0.037 (H.T.)		1.64	0.005	0.055
Feb 4/87	~ 85,000	0.015 (D.T.)	1.27	1.95	0.11	0.026 (D.T.)	1.27	2.41	0.009	0.036
(2nd expt.)		0.019 (H.T.)		2.00	0.03	0.033 (H.T.)		2.28	0.03	0.048
Feb 12/87	~ 100,000	0.015 (D.T.)	1.47	2.05	0.02	0.024 (D.T.)	1.33	1.98	0.007	0.041
(1st expt.)		0.022 (H.T.)		1.83	0.004	0.032 (H.T.)		1.84	0.02	0.045
Feb 12/87	~ 80,000	0.019 (D.T.)	1.16	1.96	0.02	0.029 (D.T.)	1.38	2.29	0.02	0.046
(2nd expt.)		0.022 (H.T.)		1.96	0.01	0.040 (H.T.)		1.75	0.02	0.052
Feb 18/87	~ 75,000	0.016 (D.T.)	1.50	2.08	0.02	0.027 (D.T.)	1.22	2.00	0.1	0.045
		0.024 (H.T.)		1.63	0.02	0.033 (H.T.)		1.81	0.008	0.038
Feb 19/87	~ 80,000	0.015 (D.T.)	1.53	2.12	0.03	0.022 (D.T.)	1.59	2.16	0.005	0.045
		0.023 (H.T.)		1.93	0.04	0.035 (H.T.)		1.77	0.01	0.053
Feb 23/87	~ 80,000	0.014 (D.T.)	1.64	1.99	0.03	0.033 (D.T.)	1.33	2.22	0.03	0.035
		0.023 (H.T.)		1.91	0.02	0.044 (H.T.)		2.16	0.02	0.051

TABLE 10.1 (cont'd)

Date	Input aerosol concn. #/cm^3	Aerosol size distribution*				Activity size distribution*				Theoretical Model** AMD (μm)
		CMD (μm)	G.F.	GSD	P.I.	CMD (μm)	G.F.	GSD	P.I.	
Feb 24/87 (1st expt.)	~ 89,000	0.014 (D.T.) 0.018 (H.T.)	1.29	2.29 1.96	0.03 0.02	0.021 (D.T.) 0.028 (H.T.)	1.33	2.34 2.23	0.01 0.02	0.052 0.043
Feb 24/87 (2nd expt.)	~ 65,000	0.017 (D.T.) 0.020 (H.T.)	1.18	2.26 1.99	0.07 0.02	0.024 (D.T.) 0.031 (H.T.)	1.29	2.23 2.08	0.007 0.02	0.060 0.050
Feb 25/87 expt.)	~ 85,000	0.014 (D.T.) 0.016 (H.T.)	1.14	1.92 2.19	0.03 0.03	0.022 (D.T.) 0.031 (H.T.)	1.41	2.23 1.91	0.05 0.02	0.032 0.052

* CMD - Count median diameter; G.F. - Growth factor; GSD - Geometric standard deviation; P.I. - Performance index. The P.I. is a measure of the goodness of fit to the theoretical size distribution. For a perfect fit, P.I. = 0; D.T. - Dry tube; H.T. - humid tube.

** The theoretical model gives the activity median diameter (AMD) calculated from the hybrid theory of attachment (Ba87). Attachment of radon progeny (diffusion coefficient of 0.05 cm^2 s^{-1} and thermal diffusion velocity of 1.38 x 10^4 cm/s) to the aerosol of specific CMD and GSD is calculated. The calculation gives the AMD of the attached activity as shown in the table.

Statistical analysis:

NaCl: Aerosol size distribution:

Mean growth factor = 1.86

Best esimate of s.d. (σ_{n-1}) = 0.38

Aerosol growth factor ≅ 1.9 ± 0.4

Activity size distribution:

Mean growth factor = 1.20

σ_{n-1} = 0.12

Activity growth factor ≅ 1.2 ± 0.1

Kerosene: Aerosol size distribution:

Mean growth factor = 1.31

σ_{n-1} = 0.17

Aerosol growth factor ≅ 1.3 ± 0.2

Activity size distribution:

Mean growth factor = 1.33

σ_{n-1} = 0.18

Activity growth factor ≅ 1.3 ± 0.2

TABLE 10.2

Radon Progeny Concentrations in (pCi/L) during Experiments

Date	Dry tube			Wet tube		
	^{218}Po	^{214}Pb	^{214}Bi	^{218}Po	^{214}Pb	^{214}Bi
Nov 28/86	8495	3900	1479	8757	3976	1523
Dec 2/86	113	71	49	113	67	45
Dec 3/86	186	83	32	186	97	41
Dec 3/86 (2nd expt.)	143	90	58	111	80	60
Dec 4/86	95	67	43	145	76	47
Dec 4/86 (2nd expt.)	88	62	39	90	56	42
Feb 16/87	2218	2010	1678	1821	1638	1367
Feb 16/87 (2nd expt.)	482	382	306	404	328	278
Feb 3/87	1136	1093	968	999	974	931
Feb 3/87 (2nd expt.)	316	251	194	218	189	176
Feb 4/87	First two counts could not be obtained					
Feb 4/87 (2nd expt.)	462	490	460	420	408	378
Feb 12/87	2460	2293	1752	2269	2027	1500
Feb 12/87 (2nd expt.)	615	622	610	480	491	480
Feb 18/87	901	899	840	748	747	686
Feb 19/87	1004	967	1018	930	923	809
Feb 23/87	371	286	220	285	247	207
Feb 24/87	758	773	717	719	636	598
Feb 24/87 (2nd expt.)	191	186	158	192	160	134
Feb 25/87	714	719	642	575	575	518

TABLE 10.3

Comparison of the Present Study with Previous Experimental Investigations on Growth of Particles in a Humid Atmosphere

Reference	Aerosol material	R.H. (%) (Temp °C)		Growth factor	Particle radius (μm)	Residence time (s) (breathing frequency/ min)
		Initial	Final			
Ci68	cigarette smoke	NA	99 (-)	1.3-1.5	4-10	NA
Ge69	radon progeny attached to atmospheric aerosols	35-40 (21)	95-100 (35)	2.0	0.02-0.045	(8-20)
Po71	NaCl	NG	100 (20-22)	3.0	0.06	>1.5
	SiO_2			~ 1	0.12	
	latex			1.35	0.05	
	cigarette smoke			1.55	0.011	
	atmospheric aerosols			2.0	0.028	
Be81	NaCl	NG	95 (34-38)	3-4.5	1-3	0.05-1
Tu84	NaCl	NG	98-99 (32-33)	3.5-4.5	0.06-0.1	(10,15)
This study	NaCl	35 (20)	100 (37)	1.9	0.03-0.07	1
	Kerosene			1.3	0.015-0.024	

NA Not available
NG Not given in reference

is expected based on the hygroscopicity of NaCl. NaCl has been reported to grow by a factor of 2-6 (Be81,Da61,Ci71,Ze56) in the respiratory tract. The growth factor found in the present work is lower, possibly a result of a residence time of 1 sec. A longer residence time would increase the growth factor. Residence times used previously in the literature are generally in the range 1-4 secs (Po71,Fe77,Ro84,Hi85). A schematic representation of the respiratory tract showing the residence time at various pulmonary levels is given in Fig. 10.1a. The residence time in the three compartments of the lung used in the lung model of the Task Group (Ta66) is shown in Table 10.3a. For kerosene aerosols, a growth factor of 1.3 is consistent with the non-hygroscopic character of the aerosol. Growth of insoluble particles can occur to some extent, depending upon the wettability of the surface of the particles.

The interaction of radon and aerosols in a warm and humid environment seems to be complicated. The growth factor for the activity size of NaCl was found to be lower (1.2) than the size growth factor (1.9). This result is consistent for the entire NaCl experimentation period. The presence of wire screen cylinders inside the dry and humid tubes may have caused removal of unattached activity and the small end of the activity size distribution. It is interesting to note that in the dry tube the activity median diameters were found to be consistently larger than the aerosol median diameters.

Further analysis of data was undertaken in order to find an explanation for this behaviour. Unattached fractions corresponding to each experimental data set were determined theoretically. The method used for this further analysis is described in detail by Phillips, Khan and Leung

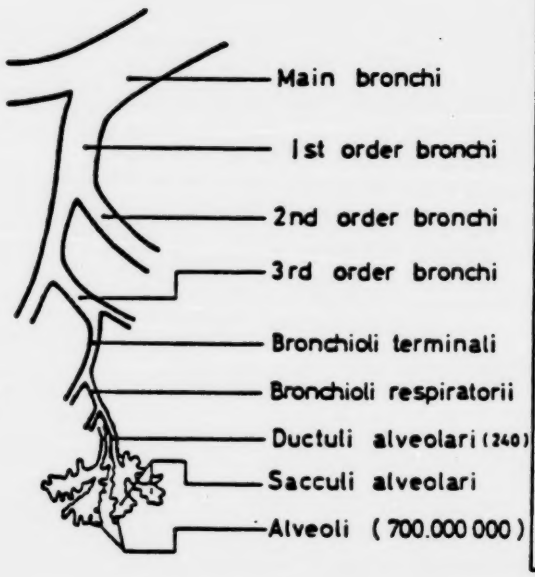

	Inner diameter (cm)	Air velocity (cm/sec)	Time for passage (sec)
Main bronchi	0.75	180	0.04
1st order bronchi	0.40	130	0.02
2nd order bronchi	0.20	65	0.02
3rd order bronchi	0.15	14	0.04
Bronchioli terminali	0.06	1.3	0.22
Bronchioli respiratorii	0.05	0.9	0.17
Ductuli alveolari (240)	0.02	0.025	0.82
Sacculi alveolari	0.03	0.0	1.2
Alveoli (700.000 000)			

Fig. 10.1.a. Schematic representation of the respiratory tract in connection with airflow characteristics at various pulmonary levels. From (Da64).

TABLE 10.3a

Residence Time of a Particle during a Respiration Cycle in the Three Compartments of the Lung (Ta66). The Residence Time of a Particle in the Pulmonary Region is Counted from the Time the Particle Enters the Alveolated Airways.

Tidal vol. (cm^3)	Mean Residence Time in a Compartment (sec)						
	Inspiration			Pause	Expiration		
	NP*	TB*	P*	P	P	TB	NP
750	0.116	0.308	0-1.32	0.20	0-1.56	0.365	0.137
1450	0.060	0.160	0-1.52	0.20	0-1.80	0.189	0.071
2150	0.040	0.108	0-1.59	0.20	0-1.89	0.128	0.047

* NP - Nasopharyngal region; TB-Tracheobronchial region; P - pulmonary region.

(Ph87). The attachment rate, λ_s, is determined by using the kinetic theory according to the following relation (Ba87):

$$\lambda_s = \frac{\pi}{4} \bar{v} \bar{d}^2 \exp(2(\ln \sigma_g)^2) \qquad (51)$$

where $\bar{v}$ = mean thermal diffusion velocity of radon progeny atoms

$\bar{d}$ = count median diameter of the distribution

σ_g = geometric standard deviation of the distribution.

The unattached fractions are listed in Table 10.4. The dry tube aerosol size distribution data used for these calculations are also listed in Table 10.4.

Further, the deposition of activity inside the 3.65 m long tubing (used for drawing the aerosols-radon progeny from the radon chamber into the dry and humid tubes) and on the wire screen cylinders in the dry and humid tubes was also investigated. Deposition along the walls of the inlet tube was calculated using the Gormley and Kennedy equation (Go49) for penetration through a cylindrical tube, namely,

$$P = 0.819 \exp(-3.65\ \phi) + 0.097 \exp(-22.3\ \phi) \quad \text{for } \phi > 0.04$$

$$P = 1 - 2.56\ \phi^{2/3} + 1.2\ \phi + 0.177\ \phi^{4/3} \quad \text{for } \phi < 0.04 \qquad (52)$$

where $\phi = \frac{\pi DL}{Q}$, D = diffusion coefficient
L = length of the tube (3.65 m)
Q = flowrate (4.2 L/min = 70 cm^3/s)

The deposition efficiency is given by E = 1 - P. For calculating the deposition inside the wire screen cylinder, eqn. (52) was used with L = 95 cm. The results of these calculations for deposition in the tubing and the wire screen cylinder as a function of diffusion coefficient are shown in Fig. 10.1. The relationship between aerosol diameter and dif-

TABLE 10.4

Theoretically Determined Unattached Fractions

Date	$(CMD)_{Aerosol}$	$(\sigma g)_{Aerosol}$	$\frac{(CMD)_{Activity}}{(CMD)_{Aerosol}}$	Unattached fractions of ^{218}Po
NaCl				
Nov 28*	0.057	1.94	1.5	0.10
Dec 2	0.057	1.98	1.3	0.05
Dec 3	0.036	2.11	2.8	0.26
Dec 3*	0.049	2.61	1.53	0.02
Dec 4*	0.035	1.95	2.11	0.32
Dec 4	0.048	1.5	1.3	0.13
Feb 16	0.051	2.06	1	0.06
Feb 16	0.068	2.09	1	0.03
Kerosene				
Feb 3	0.024	1.73	1	0.29
Feb 3	0.017	2.30	2.23	0.30
Feb 4*	0.017	1.98	1.5	0.36
Feb 4	0.015	1.95	1.73	0.43
Feb 12	0.015	2.05	1.6	0.36
Feb 12	0.019	1.96	1.53	0.33
Feb 18	0.016	2.08	1.7	0.38
Feb 19	0.015	2.12	1.5	0.39
Feb 23	0.014	1.99	2.36	0.46
Feb 24	0.014	2.29	1.5	0.34
Feb 24	0.017	2.26	1.4	0.33
Feb 25	0.014	1.92	1.6	0.47

* These size distributions are plotted in Fig. 10.3.

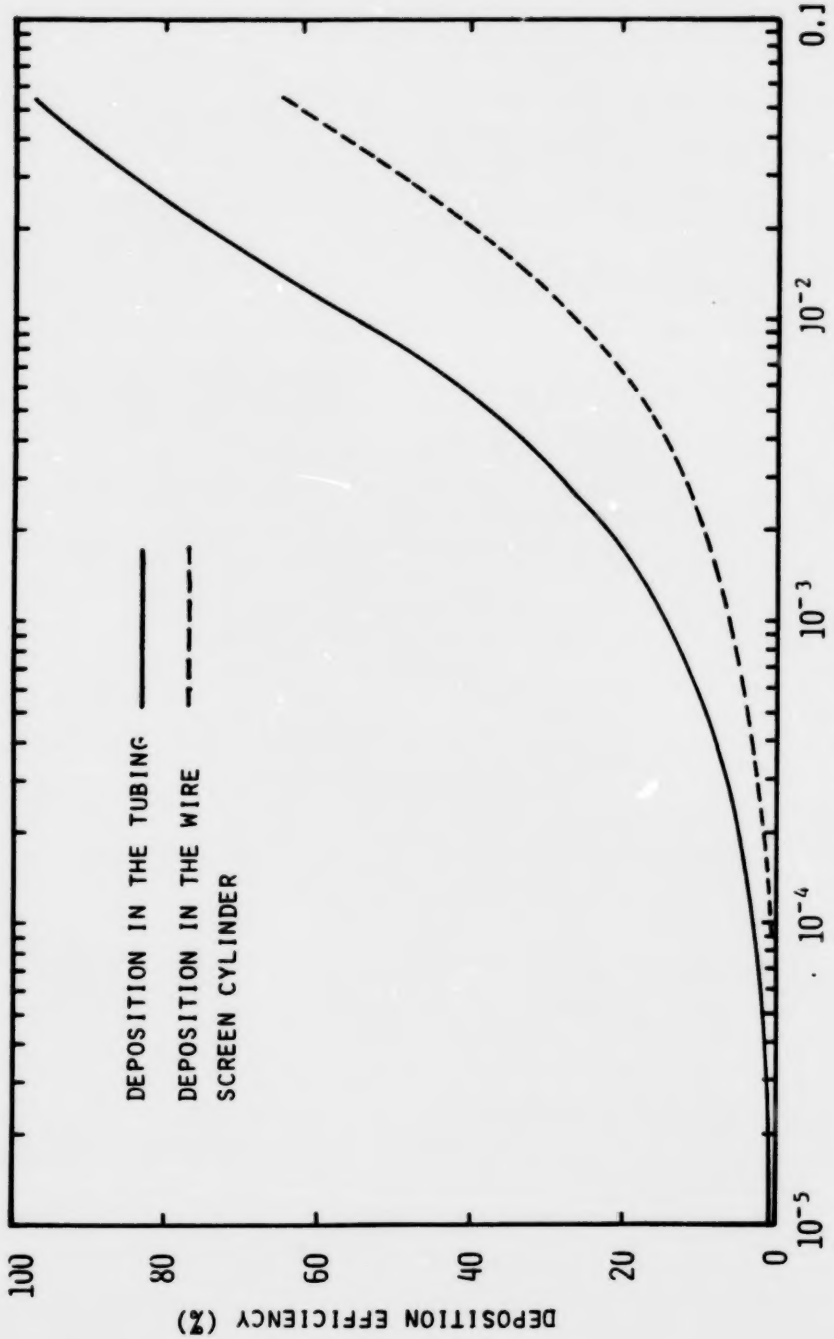

Fig. 10.1. Deposition efficiency vs diffusion coefficient.

fusion coefficient is shown in Fig. 10.2 (Fr77). Unattached radon progeny are generally believed to have size distributions with the median at ~ 0.002 μm or less. Passage through the tubing results in the removal of ~ 60% or more of the unattached fraction (Fig. 10.1). Of the unattached fraction, therefore, only about 40% or less would reach the wire screen cylinders. Of the unattached activity reaching the wire screen cylinder, about 65% is removed by the cylinder. However, aerosols at the lower end of the attached size distribution are also removed with an efficiency which decreases as the particle size increases. The overall effect of the removal of smaller aerosols by the wire screen can be seen by examining the actual size distributions (chosen randomly from Table 10.4) plotted in Fig. 10.3.

For kerosene aerosol of count median diameter 0.017 μm, it is evident from Fig. 10.3 that a large part of the size distribution curve is removed if removal of 0.01 μm or smaller particles takes place. Such removal would shift the count median diameter of the size distribution to a larger size. Even removal of aerosols up to 0.005 μm would affect this particular size distribution noticeably. However the growth factor would not be reduced in this case because the size distribution in the humid tube is affected in the same manner (because of the non-hygroscopicity of the aerosol combined with a small count median diameter) and the overall effect approximately cancels out in the ratio of humid tube aerosol size to the dry tube aerosol size (growth factor).

Each size distribution of the NaCl aerosol is affected differently by the removal of certain size particles. For the smaller (0.036 μm count median diameter) distribution, it can be seen from Fig. 10.3 that

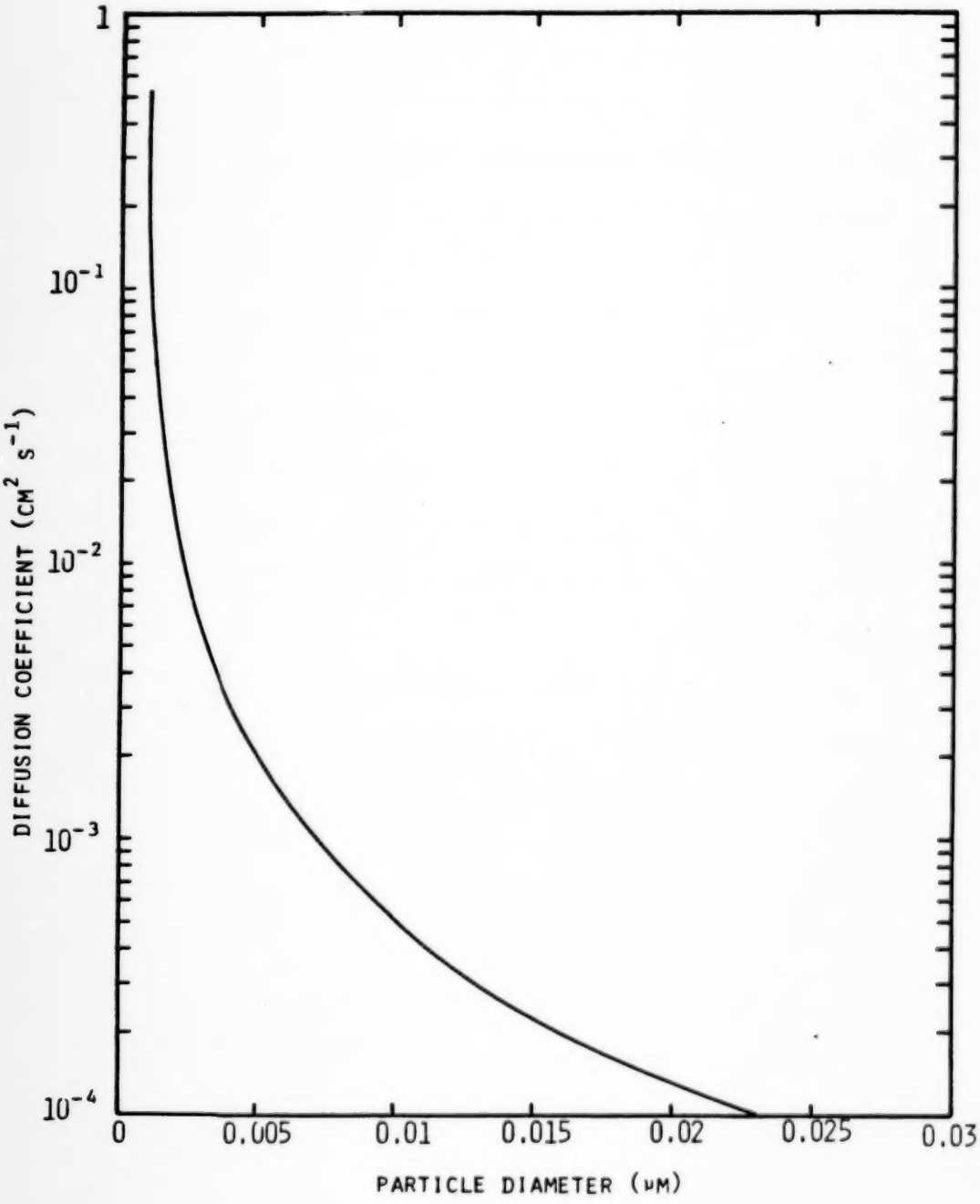

Fig. 10.2. Diffusion coefficient vs particle diameter (Fr77).

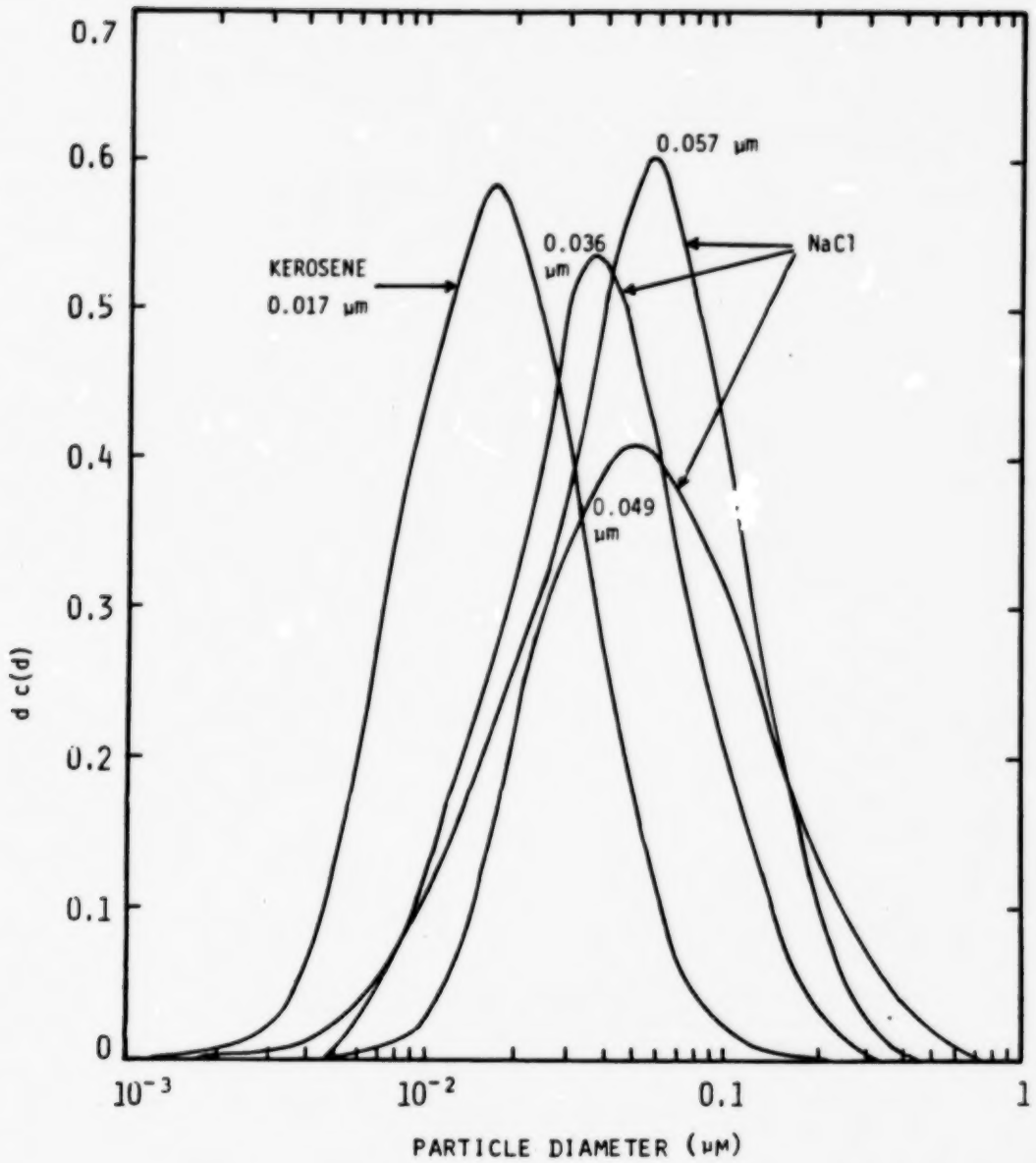

Fig. 10.3. Aerosol size distributions for some experimental data in Table 10.1.

removal of particles up to 0.005 μm does not affect the size distribution, whereas removal of particles up to 0.01 μm causes a loss of portion of the size distribution, resulting in a shift in the count median diameter. The larger aerosol (0.057 μm count median diameter) is only very slightly affected by the removal of up to 0.01 μm particles because only the tail end of its size distribution falls in that region. However the smaller 0.049 μm distribution with a larger geometric standard deviation is sensitive to the removal of particles as small as 0.005 μm. In the humid tube, the NaCl aerosol distribution shifts towards larger sizes owing to growth and becomes insensitive to the removal of particles up to 0.01 μm. The growth factor is thus smaller because of the increase in the denominator of the size ratio for the humid and the dry tube. Similar behaviour occurs for the activity size distribution. However, the effect is more pronounced for the activity size distribution, perhaps because of the fact that unattached activity exists in the form of a size distribution rather than a single size. The removal of the larger end of the unattached activity size distribution in the dry tube (but not in the humid tube owing to growth) could also cause a slight shift in the activity size distribution.

The calculated activity size in Table 10.1 reflects a tendency of the size distribution to shift to a larger diameter after attachment of radon progeny. However, no direct comparisons can be made based on these results because attachment theories are based on many assumptions and do not describe the complex process of attachment perfectly.

The humidity and temperature conditions created inside the humi-

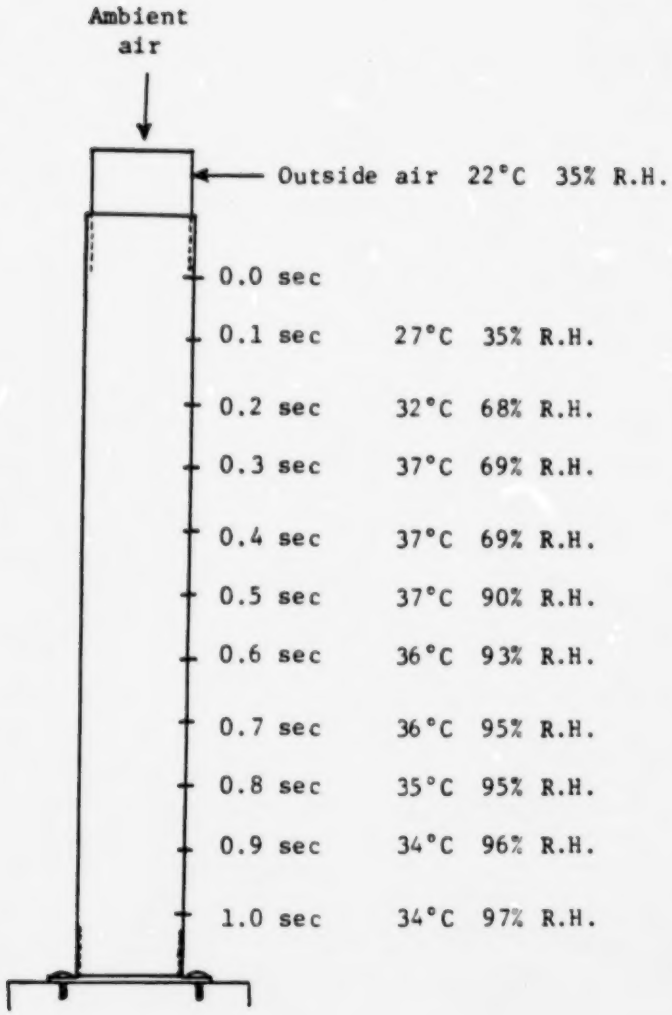
Ambient air
Outside air 22°C 35% R.H.
0.0 sec
0.1 sec 27°C 35% R.H.
0.2 sec 32°C 68% R.H.
0.3 sec 37°C 69% R.H.
0.4 sec 37°C 69% R.H.
0.5 sec 37°C 90% R.H.
0.6 sec 36°C 93% R.H.
0.7 sec 36°C 95% R.H.
0.8 sec 35°C 95% R.H.
0.9 sec 34°C 96% R.H.
1.0 sec 34°C 97% R.H.

Fig. 10.4. Temperature and humidity profile in Hicks and Megaw's (Hi73) column.

difying tube may not ideally represent the respiratory tract conditions because these conditions were not uniform through the entire length of the tube as they are expected to be in the respiratory tract. Hicks and Megaw (Hi73) have determined the temperature and humidity profile of a column similar to the one used in this work (for a residence time of 1 sec) (Fig. 10.4).

The aerosols from burning the kerosene heater could not be controlled at specific aerosol sizes. However a size range of 0.015-0.024 μm count median diameter was obtained for kerosene aerosols. The aerosol concentrations for kerosene heater were generally in the range 70,000-85,000/cm^3. For NaCl aerosols, however, the size of aerosol could be controlled by increasing or decreasing the salt concentration in the solution. This is detailed in Appendix B.1. The aerosol concentration was also easy to control for NaCl aerosols and a range of 25,000-100,000/cm^3 was obtained.

It is important to note that all measurements presented here are subject to uncertainties. Using standard statistical procedures, the uncertainty for activity measurement was calculated as 7%, based on 5% flow fluctuation and 5% concentration fluctuation. The uncertainty in size distribution measurement is estimated as ~10% (Bu81). The uncertainty arising from flow fluctuations (which lead to uncertainties in residence time) is estimated as <5%.

11. CONCLUSIONS AND RECOMMENDATIONS

11.1 Conclusions

Conclusions based on published knowledge of the behaviour of inhaled aerosols are summarized in Section 8.1.

Conclusions from the experiments are as follows:

1. The growth factor for NaCl aerosols under the respiratory tract conditions of humidity and temperature was found to be 1.9 ± 0.4 (standard deviation) for a residence time of 1 sec. For activity size, the growth factor for NaCl aerosols was 1.2 ± 0.1 (standard deviation).
2. The growth factor for kerosene heater-generated aerosols under inhalation conditions was found to be 1.3 ± 0.2 (standard deviation). A similar growth factor was found for the activity size distribution.
3. The use of a wire screen cylinder to support the humidification surface seems to be responsible for a low aerosol and activity size growth factor for NaCl aerosols. (Rough cylinder walls such as walls made of a screen material form an efficient medium for removing unattached radon progeny atoms and small aerosol particles with high diffusion coefficients.)

   Although significant removal occurred for kerosene aerosols, the overall effect was negligible because removal occurred in both dry and humid tubes.
4. The residence time is important for studies such as the present work. A longer residence time would be expected to correspond to a larger growth factor.

11.2 Recommendations

The following recommendations are made based on the review of present knowledge about the behaviour of inhaled aerosols:

1. The role of ionization in the formation of new aerosols by both reaction and condensation may be significant in areas such as underground uranium mines in which uranium and thorium and radon/thoron and their progeny are present. The effect on aerosol concentration of the presence of ionizing radiation or ionizing species, therefore, requires further study in both the presence and the absence of light. (In the presence of light, photolytic nucleation reactions occur.)
2. The humidity in the human respiratory tract should be estimated or determined for various ambient humidities and temperatures. Cold winter conditions are of particular interest.
3. The growth and deposition of charged particles should be investigated since only limited data are available.
4. Chemical reactions which lead to the formation of condensable species in the atmosphere should be studied.
5. Nucleation theories, especially the theory for nucleation on ions, should be improved so that they can explain experimental results satisfactorily.
6. The growth of inhaled particles in the presence of ions should be studied further to determine whether charged and neutral particles grow at the same rate and to the same extent.

Based on the experimental study undertaken in this work, the following recommendations can be added to the above list:

1. Further studies on the growth of aerosols in a radon atmosphere under

1. Further studies on the growth of aerosols in a radon atmosphere under respiratory tract conditions are desirable in order to investigate differences between aerosol growth and activity size growth. Residence times of 1 sec, 1.5 sec and 2 sec should be used to investigate the effect of residence time on growth factors.
2. A humidification configuration having few surfaces which are efficient for removal of unattached radon progeny and lower end of aerosol size distribution (such as a wire screen) should be used for future studies on aerosol and activity size growth on inhalations. However, the objective of having minimum surface area (to minimize removal of unattached radon progeny and small aerosols) is in conflict with the requirement for surface area for humidification purposes. A compromise solution is probably the only resolution to these conflicting requirements.
3. Other insoluble aerosols should be studied in order to draw generic conclusions about growth of insoluble particles. The wettability of the aerosol surface is likely to be of importance.
4. Use of monodispersed aerosols for further studies on growth of inhaled aerosols would give more readily interpretable information on the behaviour of different size particles in the respiratory tract.
5. The effect of the age of the air and radon progeny concentrations on activity size under humid conditions should be investigated in more detail.

REFERENCES:

Ai80 Aitken (1880-1) Collected papers 1923, p.34, Cambridge.

Am82 Amann, C.A. and Siegla, D.C., 1982. Diesel particulates - what they are and why, Aeros. Sci. & Tech. 1, 73.

An17 Andren, L., 1917. Ann. Physik (Leipzig) 52, 1.

Ba23 Baumberger, J.P., 1923. J. Pharmacol. 21, 47.

Ba87 Bandi, F., Khan, A. and Phillips, C.R., 1987. Effects of aerosol polydispersity on theoretical calculations of unattached fractions of radon progeny. In ACS Symp. Series 331, Radon and Its Decay Products, Occurrence, Properties and Health Effects (Ed. P. Hopke), American Chemical Soc., Washington, D.C., 137.

Be78 Bell, K.A, Martonen, T.L. and Ho, A., 1978. Growth rate measurements and deposition modelling of hygroscopic medicinal aerosols in the respiratory tract, Pap. 71st AIChE Meet.

Be81 Bell, K.A. and Ho, A.T., 1981. Growth rate measurements of hygroscopic aerosols under conditions simulating the respiratory tract, J. Aeros. Sci., 12(3), 247.

Bl83 Blanchard, J.D. and Witleke, K., 1983. An inhalation system for characterizing total lung deposition of ultrafine particles, Am. Ind. Hyg. Assoc. J., 44(11), 846.

Br62 Bricard, J., Pradel J. and Renoux, A., 1962. Ann de Geophys. 18, 384.

Br70 Bricard, J. and Pradel, J., 1970. Electric charge and radioactivity of naturally occurring aerosols, in Aerosol Science, C.N. Davies, Ed.

Br75 Brock, J.R. and Marlow, W.H., 1975. Charged aerosol particles and air pollution, Env. Lett. 10(1), 53.

Br31 Brown, C.E., 1931. J. Industr. Hyg. 13, 285, 293.

Bu78 Busigin, A., van der Vooren, A. and Phillips, C.R., 1978. Attached and unattached radon daughters: Measurements and Measurement Techniques in Uranium Mines and in the Laboratory, report to the Atomic Energy Control Board, AECB-1169.

Bu81 Busigin, A., van der Vooren, A. and Phillips, C.R., 1981. Measurement of the total and radioactive aerosol size distributions in a Canadian uranium mine, Amer. Ind. Hyg. Assoc. J., 42, 310.

Bu85 Budd, T., Marshall, M. and Kewok, C.S., 1985. Droplet growth and diffusion in low-pressure cloud chamber, J. Aeros. Sci., 16(2), 145.

Ca74 Castleman, A.W., 1974. Space Sci. Rev. 15, 147.

Ca79 Carpenter, K. and Johnson, J.H., 1979. Analysis of the physical characteristics of diesel particulate matter using transmission electron microscope techniques, SAE Trans. 88, 2743.

Ch78 Chan, T.L., Schreck, R.M and Lipmann, M., 1978. Effect of turbulence on particle deposition in the human trachea and bronchial airways, Symp. Transp. Processes Biol. Syst. AIChE Meeting, Paper No. 124d.

Ch78a Chan, T.C., Lippman, M., Cohen, V.R. and Schlesinger, R.B, 1978. Effect of electrostatic charges on particle deposition in a hollow cast of the human larynx-tracheobronchial tree, J. Aeros. Sci., 9, 463.

Ci68 Cinkotai, F.F., 1968. Beitr. Tabakforsch. 4, 189.

Ci71 Cinkotai, F.F., 1971. The behaviour of sodium chloride particles in moist air, Aeros. Sci. 2, 325.

Cl84 Clarke, S.W. and Pavia, D., 1984. Aerosols and the Lung: Clinical and Experimental Aspects, Butterworths, Toronto.

Co73 Cooper, D.W., Byers, R.L. and Davis, J.W., 1973. Measurements of laser light backscattering vs. humidity for salt aerosols. Environ. Sci. Technol. 7, 142.

Co75 Coulier, 1875. J. Pharm. Chem., Paris 22, 165.

Da61 Dautrebande, L. and Walkenhorst, W., 1961. In Inhaled Particles and Vapours, Ed. C.N. Davies, Pergamon Press, Oxford.

Da64 Dautrebande, L. and Walkenhorst, W., 1964. Deposition of microaerosols in human lung with special reference to the alveolar spaces. Health Phys. 10, 981.

De67 Derry, R., Pelletier, J., Jacques, A., Clarret, M. and Houde, J.J. Can. Anaes. Soc. J. 14, 287.

Dr28 Drinker, P., Thompson, R.M. and Finn, J.L., 1928. J. Industr. Hyg. Toxicol. 10, 13.

Fe75 Fennelly, P.F., 1975. Primary and secondary particles as pollutants, J. Air Pollution Control Assoc. 25, 697.

Fe77 Ferron, G.A., 1977. The size of soluble aerosol particles as a function of the humidity of the air. Applications to the human respiratory tract, J. Aeros. Sci. 8, 251.

Fe84 Ferron, G.A. and Hornik, S., 1984. Influence of different humidity profiles on the deposition probability of soluble particles in the human lung, J. Aeros. Sci. 15(3), 209.

F134 Flood, H.Z., 1934. Phys. Chem. A. 170, 286.

F162 Fletcher, N.H., 1962. The Physics of Rain Clouds, Cambridge Univ. Press, London.

Fr77 Friedlander, S.K., 1977. Smoke, Dust and Haze, John Wiley & Sons, Inc., New York.

Fu65 Fuchs, N.A., 1965. The Mechanics of Aerosols, Pergamon Press, Oxford.

Ga75 Gartrell, G. Jr. and Friedlander, S.K. 1975. Atmos. Environ. 9, 279.

Ge69 George, A. and Breslin, A.J., 1969. Deposition of radon daughters in humans exposed to uranium mine atmosphere, Health Phys. 17, 115.

Go49 Gormley, R.G. and Kennedy, M., 1949. Proc. Roy. Irish Acad., 52A, 163.

Hi70 Hidy, G.M. and Brock, J.R., 1970. The Dynamics of Aerocolloidal Systems, Pergamon Press.

Hi82 Hinds, W.C., 1982. Aerosol Technology, John Wiley and Sons, Toronto.

Hi84 Hidy, G.M., 1984. Aerosols, an Industrial and Environmental Science, Academic Press Inc, Florida.

Hi85 Hicks, J.F. and Megaw, W.J., 1985. The growth of ambient aerosols in the conditions of the respiratory system, J. Aerosol Sci. 16(6), 521.

Is71 Israel, H., 1971. Atmospheric Electricity, Vol. I, Keter Press, Jerusalem, Israel.

Ju54 Junge, C., 1954. J. of Meteor. 11, 324.

Ju67 Junge, C.E., 1967. Mathematical interrelationships in the size distribution of atmospheric aerosols above the continent, NASA TT F-11,091.

Ka69 Kasten, F., 1969. Visibility forecast in the phase of precondensation, Tellus, 21, 631.

Ku56 Kusnetz, H.L., 1956. Radon daughters in mine atmospheres - A field method for determining concentrations, Am. Ind. Hyg. Assoc. Quart., 17, 87.

La08 Laby, T., 1908. Phil. Trans. Roy. Soc. (London) A 208, 445.

La60 Langer, G. and Liebermann, A., 1960. J. Colloid. Sci. 15, 357.

La61 Lassen, L., 1961. Zeit. fur Phys. 163, 363.

Li75 Lipmann, M. and Altshuller, B., 1975. In Air Pollution and the Lung (E.F. Abaronson, ed.) pp.25-48, Keter Publishing House, Israel.

Li77 Lipmann, M., 1977. In Handbook of Physiology, Sect. 9, Reactions to Environmental Agents (D.H.K. Lee, ed.), Am. Physiological Society, Bethesda, Maryland.

Li80 Lipman, M., Yeates, D. and Albert, R., 1980. Br. J. Ind. Med. 37, 337.

Li83 Lipmann, M., Gurman, J. and Schlesinger, R., 1983. In Aerosols in the Mining and Industrial Work Environments (V.A. Marple and B.Y.H. Liu, eds.) p.119, Ann Arbor Science Press, Ann Arbor, Michigan.

Lu73 Luus, R. and Jaakola, T.H.I., 1973. Optimization by direct search and system reduction of the size of the search region, A.I.Ch.E. J., 19(4), 760.

Ma61 Mason, B., 1961. Disc. Faraday Soc. 30, 20.

Ma73 May, K.R., 1973. The Collison nebulizer: Description, performance and application, J. Aerosol Sci., 4, 173.

Ma82 Martonen, T.B., 1982. Analytical model of hygroscopic particle behaviour in human airways, Bull. Math. Biol. 44, 425.

Me77 Melandri, C., Prodi, V., Tanoni, G., Formignani, M., Dezaiacomo, T., Borropane, C.F., Maestri, G. and Giacomelli-Maltoni, G., 1977. Inhaled Particles, Vol. 4. Proc. Int. Symp. 1975 (W.H. Walton, ed.) pp.193-200.

Me73 Mercer, T.T., 1973. Aerosol Technology in Hazard Evaluation, Academic Press, New York.

Mi56 Miller, R.C. and Kusch, P., 1956. J. Chem. Phys. 11, 860.

Mi67 Milne, T.A. and Greene, F.T., 1967. J. Chem Phys. 47, 4095.

Mi74 Mirabel, P. and Katz, J.L., 1974. J. Chem. Phys. 60, 1138.

Mo63 Mohnen, V and Stierstadt, K., 1963. Zeits. für Phys. 165, 1.

Mo69 Mohnen, V., 1969. On the nature of tropospheric ions. In Planetary Electrodynamics, Ed. S.C. Coroniti and J. Hughes, Gordon and Breach, New York.

Ph87 Phillips, C.R., Khan, A. and Leung, H., 1987. The Nature and Measurement of the Unattached Fraction of Radon and Thoron Progeny, Chapter in 'Radon and Its Decay Products in Indoor Air', Wiley Interscience, accepted for publication.

Po28 Powell, C., 1928. Proc. Roy Soc. (London) A119, 553.

Pr06 Przibam, K., 1906. Sitz. Akad Wiss. Wien. 115, 81.

Re50 Reiss, H., 1950. J. Chem. Phys., 18, 840.

Re84 Reist, P.C., 1984. Introduction to Aerosol Sicence, McMillan Publishing Company, New York.

Re65 Renoux, A., 1965. Thesis, Paris.

Ro75 Roberts, P.T. and Friedlander, S.K., 1975. Environmental Health

Perspectives, 10, 3.

Ro84 Rothenherg, S.J., Swift, D.L., 1984. Aerosol deposition in the human lung at variable tidal volumes: clculation of fractional deposition, Aerosol Sci Tech., 3, 215.

Sa43 Sander, A. and Damköhler, G., 1943. Naturwiss. 31, 460.

Sc39 Scharrer, L., 1939. Ann. Physik 35, 619.

Sc79 Scherer, P.W., Haselton, F.R., Hanna, L.M. and Stone, D.R., 1979. Growth of hygroscopic aerosols in a model of bronchial airways, J. Appl. Physiol.: Respir., Environ. Excercise Physiol. 47(3), 544.

Si69 Siksna, R., 1969. Role of the water substance in the structure and by production of ions in the ambient atmospheric air, in Planetary Electrodynamics, Ed. S.C. Coroniti and J. Hughes, Gordon and Breach, New York.

Si74 Sinclair, D., Countess, R.J. and Hoopes, G.S., 1974. Effect of relative humidity of the size of atmospheric aerosol particles, Atmos. Environ. 8, 1111.

Si78 Sinclair, D., George, A.C. and Knutson, E.O., 1978. Application of diffusion batteries to measurement of submicron radioactive aerosols, Proc. Am. Nucl. Soc. "Assessment of Airborne Radioactivity".

St73 Stuart, B.O., 1973. Deposition of inhaled aerosols, Arch. Intern. Med. 131, 60.

St68 Styro, B.I. and Pestov, V.S., 1968. Investigation of electrical carriers of natural atmospheric radioactivity, Izv. Atm. and Oc. Phys. 4(8), 850.

Ta66 Task Group on Lung Dynamics, 1966. Health Phys., 12, 173.

Th72 Thomas, J.W. and Hinchliffe, L.E., 1972. Filtration of 0.001 μm particles by wire screens, Aerosol Sci., 3, 387.

Tu83 Tu, K.W.. and Hinchliffe, L.E., 1983. A study of particulate emissions from portable space heaters, Am. Ind. Hyg. Assoc. J., 44(11), 857.

Tu84 Tu, K.W. and Knutson, E.O., 1984. Total deposition of ultrafine hydrophobic and hygroscopic aerosols in the human respiratory system, Aeros. Sci. & Tech. 453.

Vo69 Vohra, G., Subbea Ramu, M.C. and Vasudevan, K.N., 1969. Role of natural ionization in the formation of condensation nuclei in the atmospheric air. In Planetary Electrodynamics, Ed. S.C. Coriniti and J. Hughes, Gordon and Breach, New York.

Vo84 Vohra, K.G., Subbea Ramu, M.C. and Muraleedharan, T.S., 1984. An experimental study of the role of radon and its daughter products in the conversion of sulphur dioxide into aerosol particles in the atmosphere, Atmos. Env. 18(8), 1653.

Vu76 Vuk, C.T., Jones, M.A. and Johnson, J.H., 1976. The measurement and analysis of the physical character of diesel particulate emissions, SAE Trans. Paper No 760131, Feb. 1976.

Wa34 Wait, G.R., 1934. Ions in the Air - Carnegie Inst. of Washington. News Service Bulletin, III, No. 12, 87.

We64 Wegener, P.P. and Pouring, A.A., 1964. Physics of Fluids, 7, 352.

We63 Weibel, E.R., 1963. Morphometry of the Human Lung, Springer, Berlin.

Wi52 Wilkening, M.H., 1952. Rev. Sci. Instr. 23, 13.

Wi66 Wilkening, M.H., Kawano, M. and Lane, C., 1966. Radon daughter

ions and their relation to some electrical properties of the atmosphere, Tellus, 18, 2.

Wi97 Wilson, C.T.R., 1897. Philos. Trans. Royal Soc. (London) A 189, 265; A 193, 289 (1900).

Wi99 Wilson, C.T.R., 1899. Phil. Trans. 192, 403.

Wi51 Wilson, J.G., 1951. The Principles of Cloud Chamber Techniques, Cambridge Univ. Press, London.

Wi69 Winkler, P., 1969. Growth of natural aerosol particles with relative humidity. Suppl. Vol. of the 7th Int. Conf. on Condensation and Ice Nuclei, Prague and Vienna, pp.168-175.

Wi73 Winkler, P., 1973. The growth of atmospheric aerosol particles as a function of the relative humidity - II. An improved concept of mixed nuclei, J. Aerosol. Sci., 4, 373.

Xu84 Xu, G.B. and Yu, C.P., 1984. Theoretical lung deposition of hygroscopic aerosols. In Aerosols, Science, Technology and Industrial Applications of Airborne Particles, Ed. Liu, B.V.H., Pui, Y.H. and Fissan, H.J., Elsevier Press, New York.

Ye80 Yeh, H.C. and Schum. G.M., 1980. Bull. Math. Biol. 42(3), 461.

Yo76 Yoshida, T., Kouisaka, Y. and Okuyama, K., 1976. Growth of aerosol particles by condensation, Ind. Eng. Chem Fundam. 15(1), 37.

Yu78 Yu, C.P., 1978. Powder Tech., 21, 55.

Ze56 Zebel, G., 1956. Z. Aerosolforsh. Ther. 5, 263.

APPENDICES

APPENDIX A

AEROSOL GENERATION

A.1 The Collison Atomizer

NaCl aerosols were generated by using a Collison atomizer built according to the specifications given by May (Ma73). The reservoir capacity was 460 cm^3, larger than May's specified size. The details of the atomizer are shown in Fig. A.1. Air at 140 kPa was supplied as indicated in the diagram. As a result of the reduced pressure caused by the expansion of air from (1) to the nozzle (2), fluid is drawn into (3) from the reservoir. The fluid is broken into droplets by the jet resulting in a spray of droplets on the inside wall of the reservoir. Small droplets leave the atomizer through the top as a result of entrainment in the air flow. These droplets consist of a solution of NaCl. In order to produce a dry aerosol, the exit stream is dried and diluted. The aerosol is then passed to the radon chamber through a Kr-85 neutralizer.

The aerosol size is controlled by varying the salt concentration in water. The aerosol size, d_s is given by (Ma73)

$$d_s = 0.4732 \left(\frac{F}{\rho}\right)^{1/3} \qquad (A.1)$$

where F is the salt concentration in the solution in g/cc and ρ is the density of salt (2.2 g/cm^3 for NaCl).

A.2 Generation of Kerosene Aerosols

Kerosene aerosols were generated by burning a Toyoset Model CTA-1E-2 kerosene heater. The wick height was adjusted below the maximum in order to avoid undesirable smoke. The arrangement for leading kerosene aerosols into the radon chamber is shown in Fig. A.2.

Figure A.1.

COLLISON ATOMIZER

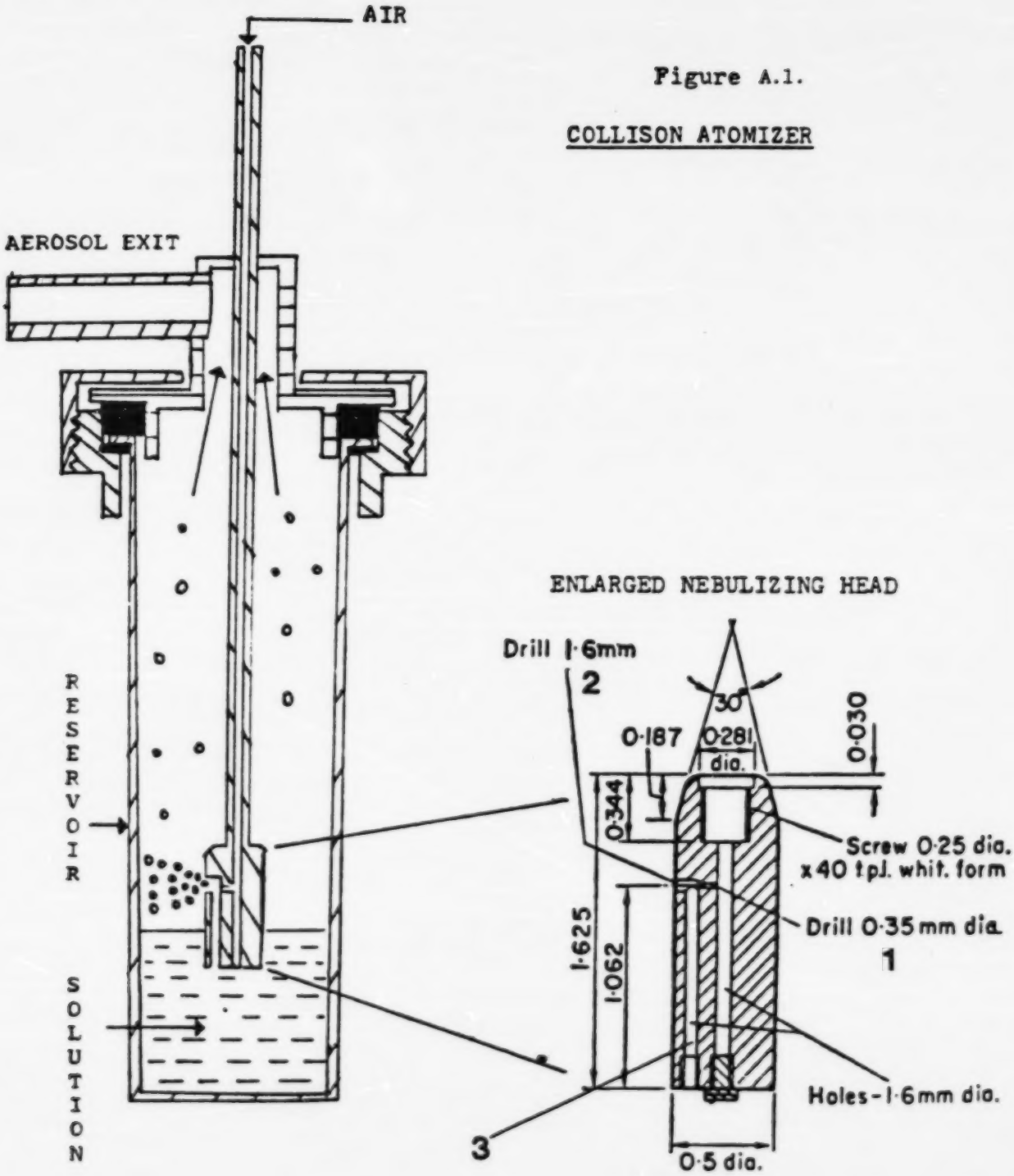

All measurements in inches unless otherwise specified

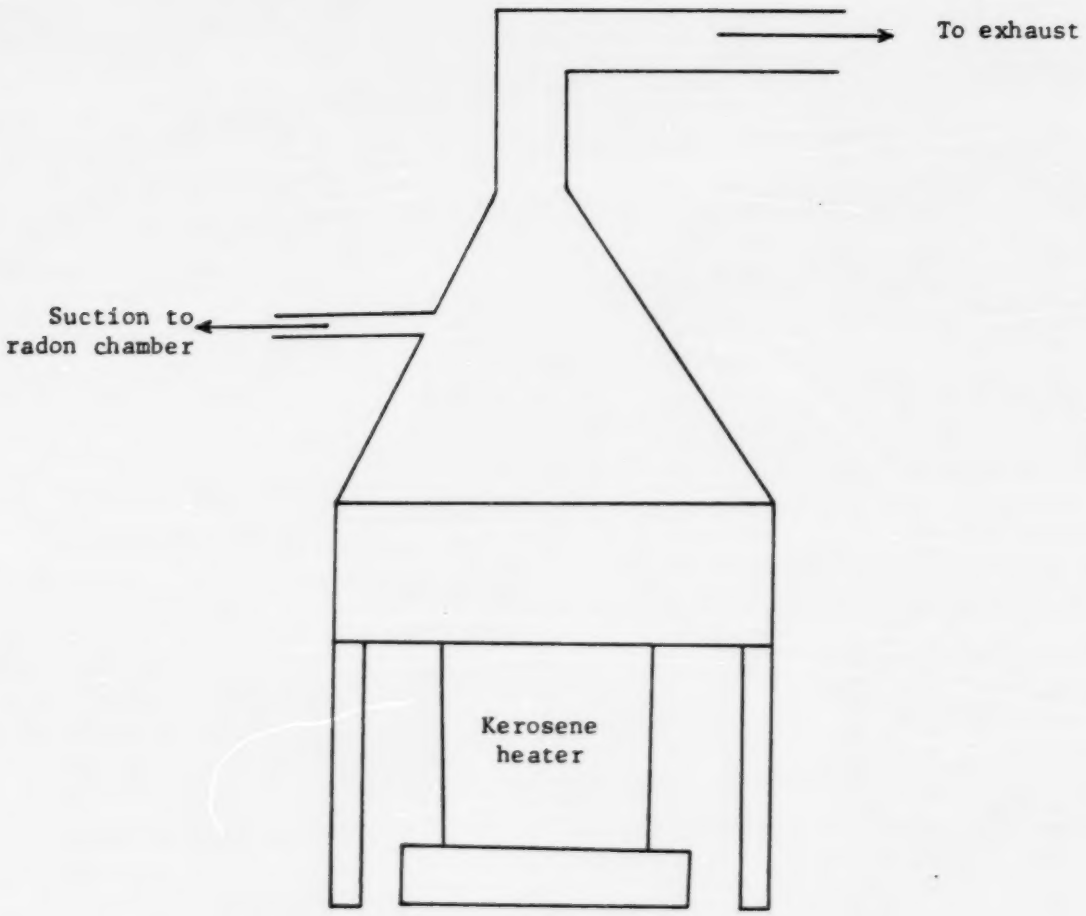

Fig. A.2. The arrangement for kerosene aerosols generation.

APPENDIX B

RAW DATA

B.1 Activity Size Distribution Data

Date	Mode	Wet tube		Dry tube	
		Counts†	Pene-tration	Counts†	Pene-tration
Nov 28/86 NACl aerosols	Ref.	159259		150875	
		526946		501321	
		139945		133350	
	D.B.3	110565	0.81	119980	0.90
	D.B.4	97065	0.71	83780	0.63
	D.B.5	40280	0.29	39113	0.29
Dec 2/86 NaCl aerosols	Ref	2906		2972	
		10414		10824	
		2495		2578	
	D.B.3	2119	0.87	2174	0.84
	D.B.4	1598	0.66	1467	0.57
	D.B.5	553	0.23	656	0.25
Dec 3/86 (1st expt.) NaCl aerosols	Ref	3720		3275	
		12938		10772	
		3382		2859	
	D.B.3	3132	0.95	3087	1.08 (~0.99)
	D.B.4	2923	0.88	2176	0.76
	D.B.5	1168	0.35	857	0.30
Dec 3/86 (2nd expt.) NaCl aerosols	Ref	3406		3627	
		12811		13292	
		2998		3225	
	D.B.3	2337	0.80	2590	0.80
	D.B.4	1894	0.65	1827	0.57
	D.B.5	961	0.33	840	0.26
Dec 4/86 (1st expt.) NaCl aerosols	Ref	3334		2585	
		11558		9744	
		2827		2359	
	D.B.3	2415	0.87	2298	0.97
	D.B.4	1704	0.62	1248	0.53
	D.B.5	709	0.26	487	0.21

Date	Mode	Wet tube		Dry tube	
		Counts†	Pene-tration	Counts†	Pene-tration
	Ref	2511		2389	
Dec 4/86		9094		9029	
(2nd expt.)		2132		2191	
NaCl aerosols	D.B.3	1758	0.84	1740	0.79
	D.B.4	1406	0.68	1120	0.51
	D.B.5	460	0.23	375	0.17
	Ref	43552		45607	
Feb 3/87		71398		80290	
(1st expt.)		37945		40619	
Kerosene aerosols	D.B.3	24018	0.65	18579	0.46
	D.B.4	10429	0.28	9502	0.23
	D.B.5	2415	0.06	2190	0.05
	Ref	8573		10227	
Feb 3/87		33111		39298	
(2nd expt.)		7387		9141	
Kerosene aerosols	D.B.3	4723	0.66	5853	0.64
	D.B.4	1633	0.23	3064	0.33
	D.B.5	233	0.03	681	0.07
	Ref	-		--	
Feb 4/87		-			
(1st expt.)		35264		40784	
Kerosene aerosols	D.B.3	23272	0.68	21769	0.53
	D.B.4	8911	0.26	7611	0.19
	D.B.5	1475	0.04	1892	0.05
	Ref	17928		20706	
Feb 4/87		70702		82791	
(2nd expt.)		15763		18389	
Kerosene aerosols	D.B.3	9083	0.59	9784	0.53
	D.B.4	4409	0.29	3674	0.20
	D.B.5	928	0.06	1219	0.07
	Ref	79833		90312	
Feb 12/87		315873		354303	
(1st expt.)		74099		82565	
Kerosene aerosols	D.B.3	44512	0.62	40896	0.49
	D.B.4	17356	0.24	12421	0.15
	D.B.5	2089	0.03	2008	0.02

Date	Mode	Wet tube		Dry tube	
		Counts†	Pene-tration	Counts†	Pene-tration
	Ref	10519		11722	
Feb 23/87		40926		44793	
		9346		10438	
Kerosene aerosols	D.B.3	6262	0.69	6026	0.58
	D.B.4	3458	0.38	2945	0.28
	D.B.5	1062	0.11	1047	0.10
	Ref	28846		32709	
Feb 24/87		111676		130094	
(1st expt.)		24836		28990	
Kerosene aerosols	D.B.3	13288	0.54	12724	0.44
	D.B.4	5503	0.23	4453	0.15
	D.B.5	957	0.04	1455	0.05
	Ref	6894		7545	
Feb 24/87		26616		30003	
(2nd expt.)		6078		6819	
Kerosene aerosols	D.B.3	3482	0.58	3419	0.50
	D.B.4	1470	0.25	1190	0.17
	D.B.5	261	0.04	322	0.05
	Ref	24651		29809	
Feb 25/87		97962		118703	
		21973		26683	
Kerosene aerosols	D.B.3	12705	0.59	12477	0.47
	D.B.4	4837	0.23	4021	0.15
	D.B.5	687	0.03	1086	0.04

† Wet tube reference counts, Trimet efficiency = 0.433;
All other counts, Trimet efficiency = 0.422

Date	Mode	Wet tube		Dry tube	
		Counts†	Pene-tration	Counts†	Pene-tration
	Ref	22045		27331	
Feb 12/87		87277		107931	
(2nd expt.)		19211		23734	
Kerosene aerosols	D.B.3	12916	0.69	13009	0.55
	D.B.4	5725	0.31	5678	0.24
	D.B.5	994	0.05	1169	0.05
	Ref	68911		82266	
Feb 16/87		270355		323203	
(1st expt.)		61765		73830	
NaCl aerosols	D.B.3	46854	0.78	49315	0.67
	D.B.4	33580	0.55	34263	0.46
	D.B.5	15151	0.25	12688	0.17
	Ref	14320		15879	
Feb 16/87		54965		60833	
(2nd expt.)		12535		14040	
NaCl aerosols	D.B.3	9146	0.75	9773	0.70
	D.B.4	7428	0.60	7569	0.54
	D.B.5	2360	0.19	2228	0.16
	Ref	32402		38444	
Feb 18/87		128520		152206	
		28709		33860	
Kerosene aerosols	D.B.3	17640	0.63	18243	0.54
	D.B.4	6674	0.24	6586	0.19
	D.B.5	1148	0.04	1016	0.03
	Ref	38961		44958	
Feb 19/87		155046		175032	
		35006		37891	
Kerosene aerosols	D.B.3	22020	0.65	17713	0.47
	D.B.4	8689	0.26	5347	0.14
	D.B.5	1329	0.04	1222	0.03

B.2. Aerosol Size Distribution Data

Date	Mode	Wet tube		Dry tube	
		Aerosol concentration (x 1000 cc)	Penetration	Aerosol concentration (x 1000 cc)	Penetration
NaCl aerosols					
Nov 28/86	Ref	39		38	
	D.B.3	38	0.97	27	0.71
	D.B.4	27	0.69	20	0.53
	D.B.5	10	0.26	4	0.10
Dec 2/86	Ref	88		82	
	D.B.3	82	0.93	60	0.73
	D.B.4	63	0.72	42	0.51
	D.B.5	35	0.40	10	0.12
Dec 3/86 (1st expt.)	Ref	24		23	
	D.B.3	20	0.83	15	0.65
	D.B.4	14	0.58	6.4	0.28
	D.B.5	4.5	0.19	2	0.09
Dec 3/86 (2nd expt.)	Ref	102		100	
	D.B.3	90	0.88	74	0.74
	D.B.4	70	0.69	36	0.36
	D.B.5	48	0.47	23	0.23
Dec 4/86 (1st expt.)	Ref	24		22	
	D.B.3	18	0.75	15	0.68
	D.B.4	9	0.37	4.6	0.21
	D.B.5	1.5	0.06	2.5	0.11
Dec 4/86 (2nd expt.)	Ref	70		62	
	D.B.3	65	0.93	47	0.76
	D.B.4	46	0.66	25	0.40
	D.B.5	15	0.21	3.6	0.06
Feb 16/87 (1st expt.)	Ref	82		76	
	D.B.3	74	0.90	55	0.72
	D.B.4	57	0.69	34	0.45
	D.B.5	30	0.37	9	0.12

B.2. Aerosol Size Distribution Data (cont'd)

Date	Mode	Wet tube		Dry tube	
		Aerosol concentration (x 1000 cc)	Penetration	Aerosol concentration (x 1000 cc)	Penetration
NaCl aerosols					
	Ref	85		71	
Feb 16/87	D.B.3	70	0.82	53	0.75
(2nd expt.)	D.B.4	63	0.74	42	0.59
	D.B.5	32	0.38	13	0.18
Kerosene aerosols					
	Ref	80		78	
Feb 3/87	D.B.3	53	0.66	40	0.51
(1st expt.)	D.B.4	8.5	0.11	7.5	0.10
	D.B.5	3	0.04	2.15	0.03
	Ref	66		68	
Feb 3/87	D.B.3	28	0.42	25.5	0.37
(2nd expt.)	D.B.4	7	0.11	5.4	0.08
	D.B.5	3.5	0.05	2.5	0.04
	Ref	85		70	
Feb 4/87	D.B.3	37	0.43	26	0.37
(1st expt.)	D.B.4	9	0.11	2.8	0.04
	D.B.5	2.6	0.03	2.2	0.03
	Ref	72		85	
Feb 4/87	D.B.3	30	0.42	25	0.29
(2nd expt.)	D.B.4	5.8	0.08	4.8	0.06
	D.B.5	2.8	0.04	3	0.03
	Ref	110		95	
Feb 12/87	D.B.3	51	0.46	31	0.33
(1st expt.)	D.B.4	12.5	0.11	5	0.05
	D.B.5	1.3	0.01	2.3	0.02
	Ref	82		66	
Feb 12/87	D.B.3	38	0.46	27	0.41
(2nd expt.)	D.B.4	9	0.11	5.6	0.08
	D.B.5	2.6	0.03	1.9	0.03

B.2. Aerosol Size Distribution Data (cont'd)

Date	Mode	Wet tube		Dry tube	
		Aerosol concentration (x 1000 cc)	Penetration	Aerosol concentration (x 1000 cc)	Penetration
Kerosene aerosols					
Feb 18/87	Ref	78		68	
	D.B.3	40	0.51	22	0.32
	D.B.4	7	0.09	3.8	0.06
	D.B.5	2.5	0.03	1.5	0.02
Feb 19/87	Ref	85		80	
	D.B.3	43	0.51	23	0.29
	D.B.4	8.8	0.10	3.5	0.04
	D.B.5	3	0.03	2.8	0.03
Feb 23/87	Ref	72		82	
	D.B.3	36	0.50	22	0.27
	D.B.4	9	0.12	4.5	0.05
	D.B.5	3.2	0.04	2.8	0.03
Feb 24/87 (1st expt.)	Ref	82		65	
	D.B.3	30	0.37	17.5	0.27
	D.B.4	6.5	0.08	3	0.05
	D.B.5	2.5	0.03	1.5	0.02
Feb 24/87 (2nd expt.)	Ref	64		66	
	D.B.3	28	0.44	19	0.29
	D.B.4	5.5	0.09	3.5	0.05
	D.B.5	2.5	0.04	2	0.03
Feb 25/87	Ref	85		70	
	D.B.3	30	0.35	17.5	0.25
	D.B.4	5.5	0.06	2	0.03
	D.B.5	3.2	0.04	1.5	0.02

APPENDIX C

EXPERIMENTAL SCHEDULE

Dated _____

hr	min	
		- Place reference under D.T. (dry tube). Note the aerosol concentration _____K (RD)
	00	- Start sampling in D.T.
		- Note temp. _____ amb. v.p. _____ dew pt. v.p. _____
	05	- Stop sampling in D.T.
		- Transfer filter to Trimet 1.
		- Place reference under H.T. (humid tube).
	07	- Start counting in Trimet 1.
	08	- Start sampling in H.T.
	10	- Stop counting in Trimet 1. Counts _____ (1D,1)
		- Place D.B.3 under D.T.
		- Note the aerosol concn. in D.T. _____K (3D)
	13	- Stop sampling in H.T. Transfer filter to Trimet 2.
	14	- Start counting in Trimet 1.
	15	- Start counting in Trimet 2.
	16	- Start sampling in D.T.
		- Note the aerosol concn. in H.T. _____K (RH)
		- Note the temp. _____ amb. v.p. _____ dew pt. v.p. _____
	18	- Stop counting in Trimet 2. Counts _____ (1,1)
	21	- Stop sampling in D.T. Store filter '3D'
		- Transfer D.B.3 to H.T.
	22	- Start counting in Trimet 2

24 - Start sampling in H.T.

- Place D.B.4 under D.T. and note the aerosol concentration _____K (4D)

29 - Stop sampling in H.T. Store filter '3'.

- Note the aerosol concn. in H.T. _____K (3H)

30 - Stop counting in Trimet 1. Counts _____ (1D,2)

32 - Start sampling in D.T.

- Remove D.B.3 from H.T.

- Note temp. _____

amb. v.p. _____ dew pt. v.p. _____

37 - Stop sampling in D.T. Store filter '4D'.

- Place D.B. 4 under H.T.

38 - Stop counting in Trimet 2. Counts _____(1,2).

41 - Start sampling under H.T.

- Place D.B.5 under D.T.

- Note the aerosol concn. _____K (5D)

45 - Start counting in Trimet 1.

46 - Stop sampling in H.T. Store filter '4'.

- Note the aerosol concn. _____K (4H)

49 - Start sampling in D.T.

- Remove D.B.4 from H.T.

- Note temp. _____

amb. v.p. _____ dew pt. v.p. _____

50 - Stop counting in Trimet 1. Counts _____ (1D,3)

53 - Start counting in Trimet 2.

54 - Stop sampling in D.T. Store filter '5D'.

- Place D.B.5 under H.T.

58 - Stop counting in Trimet 2. Counts _____ (1,3)

- Load filter '3D' in Trimet 1.

59 - Start sampling in H.T.

1 01 - Start counting in Trimet 1.

1 04 - Stop sampling in H.T. Store filter '5'.

- Note aerosol concn. in D.B.5 _____K (5H).

1 06 - Stop counting in Trimet 1. Counts _____ 3D.

- Load filter '3' in Trimet 1.

1 09 - Start counting in Trimet 1.

1 14 - Stop counting in Trimet 1. Counts _____ 3

- Load filter '4D' in Trimet 1.

1 17 - Start counting in Trimet 1.

1 22 - Stop counting in Trimet 1. Counts _____ 4D

- Load filter '4' in Trimet 1.

1 26 - Start counting in Trimet 1.

1 31 - Stop counting in Trimet 1. Counts _____ 4

- Load filter '5D' in Trimet 1.

1 34 - Start counting in Trimet 1.

1 39 - Stop counting in Trimet 1. Counts _____ 5D

- Load filter '5' in Trimet 1.

1 44 - Start counting in Trimet 1.

1 49 - Stop counting in Trimet 1. Counts _____ 5